Analysis of weather-related uncertainties in the formation of persistent contrails

Angela Hekker (4551575)
Aircraft Noise and Climate Effects (ANCE)

Delft University of Technology
Supervisor: F. Yin (Aircraft Noise and Climate Effects)

February 13, 2024

Abstract

The avoidance of the formation of persistent contrails and their resulting contrail cirrus is a promising strategy for the mitigation of aviation climate effects in the short term. However, there is still a high level of uncertainty associated with contrail formation, and in particular the regions containing suitable weather conditions for contrails to form, which makes contrail avoidance challenging in practice. This MSc thesis project aims to contribute to closing the research gap related to contrail formation regions, by investigating three associated topics where uncertainty is still high. First, the ability to accurately simulate contrail formation in a climate model is evaluated using data from atmospheric simulation model ECHAM5, and comparing this data to in-flight measurements from the IAGOS-CORE project. ECHAM5 shows a cold bias relative to the measurements. It is also shown to overestimate values of humidity relative to ice when compared to measurements that were below saturation level, while simultaneously having difficulty simulating (high) supersaturated values. The second part of the project investigates the ability of numerical weather forecast models to predict contrail formation conditions by using the ERA5 reanalysis data from ECMWF (European Center for Medium-Range Weather Forecasts) weather model prediction, again compared to IAGOS-CORE in-flight measurements. ERA5 shows good agreement in terms of temperature as well as humidity relative to ice for values below saturation, however it struggles with (high levels of) ice supersaturation. The third aspect of the research is related to the temporal evolution of ISSRs over the North Atlantic region, by using data from MOZAIC and IAGOS-CORE over the years 2010 until 2019. The ISSRs investigated show clear seasonality in terms of their temperature, altitude and pressure level. No clear trends are observed when looking at the temporal evolution of ISSR properties over the span of several years, however this may be due to limitations in the used data.

Contents

1 Introduction

The aviation sector is estimated to contribute about 3.5% of anthropogenic climate change, a figure which is expected to grow in the coming years, due to the growth of the sector as well as progress in other sectors towards more sustainability[16][38]. Technical innovations within aviation such as electric or hydrogen-powered aircraft, are promising to reduce aviation's climate impact but still far away from being implemented at a scale that suits the needs of the sector. In the meantime, operational measures to mitigate aviation climate effects are a promising option in the shorter term[17]. Particularly, the avoidance of persistent contrails and their resulting contrail cirrus is an interesting strategy, especially given that recent studies have shown that non-CO_2 effects, of which contrails and contrail cirrus are the largest contributor, may account for two thirds of all climate impacts of aviation[38]. However, in order to effectively use such a strategy, more certainty is required in the understanding of contrail formation. In particular, more knowledge is needed on the regions with suitable atmospheric conditions for persistent contrails and contrail cirrus to form[14].

This project aims to contribute to a better understanding of the characteristics of ice supersaturated regions (ISSRs), the regions in which contrails persist and spread into cirrus clouds. This is done by looking at the current level of weather-related uncertainty associated with ISSRs, by considering three different inputs. The first is the uncertainty associated with the simulation of ISSRs, which is evaluated by comparing in-situ data with data from the ECHAM5 atmospheric simulation model. The second part looks into reanalysis data from ERA5 based on weather data from ECMWF, to evaluate the current ability of weather models to recreate ISSRs through reanalysis, also by comparing the reanalysis data with in-situ observations. Finally, in-situ data is used to look into the temporal evolution of ISSR properties over a period of 10 years, from January 2010 to December 2019. The starting point for all three parts of the project is IAGOS in-situ observational data, which provide a valuable look into ISSR properties by taking high-quality, quasi-continuous measurements at flight level.

The report is structured as follows: a literature study is presented first, looking into the climate effects of aviation and then to (persistent) contrails in particular. It also touches on the current mitigation methods for aviation climate effects and in particular, the avoidance of contrail formation. A project description section presents the research objectives as well as the relevance of this project. It is followed by the sections on the analysis performed, first providing some background on the IAGOS project, as well as more information on the data gathered for the current project. The following chapter presents the analysis of the ECHAM5 atmospheric simulation model, featuring some background on the model, the methodology used, the analysis results as well as some sensitivity analysis. The next chapter investigates the ERA5 reanalysis data following a similar approach to the previous chapter. The section on the temporal evolution of ISSR properties in the North Atlantic comes next, featuring first the data selection approach and methodology, and then the results. Verification and validation of the overall results is presented throughout the report within the relevant sections. Finally, the report ends with a conclusion, a discussion on the project, and some recommendations for further research.

2 Literature review

2.1 Aviation and climate change

Anthropogenic climate change, i.e. climate change due to human influence, is a topic of ongoing debate and increasing urgency. The Intergovernmental Panel on Climate Change (IPCC) has recently published the reports of the first three working groups of their Sixth Assessment Report (AR6)[31]. These comprehensive reports, which concern The Physical Science Basis (Working Group I); Impacts, Adaptation and Vulnerability (Working Group II); Mitigation of Climate Change (Working Group III), once again emphasize the urgency of the topic of climate change and the necessity of drastic measures to curb emissions of greenhouse gases in the coming years. If emissions stay at their current level or even increase, global temperature will continue to rise, which may have devastating consequences in all parts of the world. It is clear that mitigation as well as adaptation measures are necessary.

The most significant ways in which aviation contributes to anthropogenic climate change, are the emission of carbon dioxide (CO_2) and nitrogen oxides (NO_x), as well as the formation of (persistent) contrails, which increase cloudiness. Smaller contributions come from the emission of water vapor, soot and sulfate aerosols[38]. Finding ways to mitigate the climate effects of aviation is especially of interest, due to the fact that it is a sector which has grown substantially over the past decades and is expected to continue to grow in the coming years. This chapter describes the general process of climate change as well as some of its consequences in subsubsection 2.1.1. The climate effects due to aviation emissions are described in subsubsection 2.1.2.

2.1.1 Climate change

Climate change is the commonly used term that describes the ongoing global warming as a result of human influence, most notably the emission of greenhouse gases. The increased concentrations of greenhouse gases in the atmosphere result in a stronger greenhouse effect - a process through which the atmosphere warms up by trapping heat radiating from Earth's surface which would otherwise radiate back into space[55]. The greenhouse effect is a natural phenomenon which is instrumental to life on Earth, however increased greenhouse gas concentrations due to human emissions, resulting in a stronger greenhouse effect, are expected to cause a disturbance to the Earth's natural balance, which may have devastating adverse effects on the Earth's biosphere.

Greenhouse gases

Greenhouse gases are the gases which are the main contributors to the greenhouse effect, as they are capable of absorbing and re-emitting radiation in the thermal infrared range. The most notable greenhouse gases are water vapor (H_2O), carbon dioxide (CO_2), methane (CH_4), nitrous oxide (N_2O), and ozone (O_3). Greenhouse gases can generally be divided into two types: direct and indirect gases. Direct greenhouse gases, such as water vapor, carbon dioxide, methane and ozone, directly absorb solar energy, whereas indirect greenhouse gases such as carbon monoxide and nitrogen oxides produce other greenhouse gases through chemical reactions[29].

Although variations in Earth's temperature and atmospheric compositions over time are a natural occurrence, the rate of increase in greenhouse gas concentrations observed since the industrial revolution (+-1750) is unprecedented and can almost entirely be attributed to human activity[58]. Figure 1 shows the clear increase in the greenhouse gases carbon dioxide, methane and nitrous oxide, as a result of human activity since the Industrial Revolution. Carbon dioxide concentrations in particular can be estimated over long periods of time thanks to the studying

of ice cores which have preserved bubbles of air, and can therefore be used to indicate the atmospheric carbon dioxide concentration of the time period in which the air was preserved[50].

It is obvious from the figures that greenhouse gas concentrations are increasing, and they are likely to rise even further in the coming years: greenhouse gas emissions increase yearly, with 2021 having seen an estimated 54.6 billion tonnes of greenhouse gases emitted into the atmosphere[53]. Most greenhouse gas emissions are carbon dioxide (74.4%), followed by methane (17.3%) and nitrous oxide (6.2%). Emissions of trace gases such as hydrofluorocarbons (HFCs) and sulfur hexafluoride (SF_6) make up about 2% of greenhouse gas emissions.

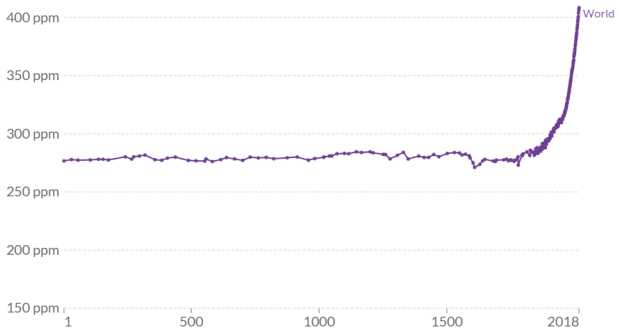

(a) Estimated atmospheric CO_2 in parts per million (ppm) over the past 2000 years

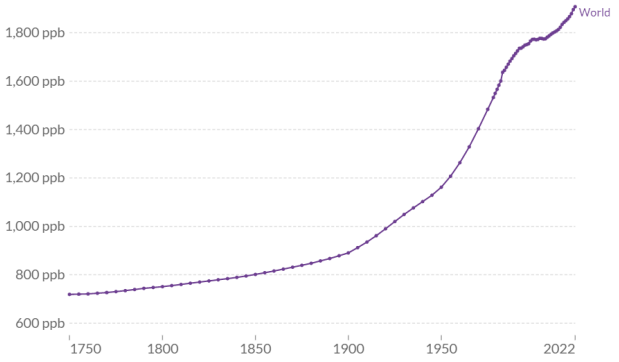

(b) Estimated atmospheric CH_4 in parts per billion (ppb) since 1750

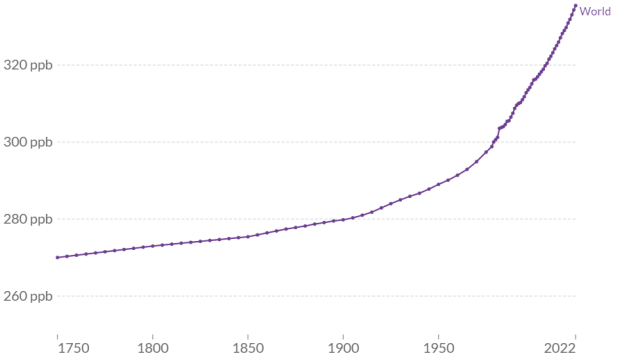

(c) Estimated atmospheric N_2O in parts per billion (ppb) since 1750

Figure 1: Atmospheric concentrations over time of CO_2, CH_4 and N_2O. Figures from [50]. Note that Figure 1a has a different time scale on the horizontal axis than Figure 1b and Figure 1c, as well as a different unit on the vertical axis

Clouds

In addition to greenhouse gases, the greenhouse effect is also influenced by clouds and aerosols. Cirrus clouds, which are high clouds consisting of ice crystals, have a net warming effect (positive radiative forcing), as they are capable of absorbing outgoing infrared radiation, while only reflecting a marginal amount of incoming solar radiation back into space[40]. The exact absorptive and reflective properties of cirrus clouds vary, depending on their thickness, ice water content and ice crystal size distribution. Cirrus clouds are generally more likely to have a net warming effect if they are thinner, as these thin cirrus clouds allow a lot of incoming solar radiation to pass through, while still absorbing and radiating back infrared radiation from the Earth's surface. Cirrus clouds can have large variation in ice particle sizes and shapes. Those clouds with larger ice crystals are generally more likely to have warming effects, compared to clouds with smaller crystals[40]. This is due to the fact that smaller crystals have a larger surface area per unit water, and thus can cause a stronger albedo effect than larger crystals. This makes them more likely to cause a cooling effect[66].

Cloud types of different compositions interact differently with radiation of different wavelengths, resulting in different radiative forcing. Other cloud types than cirrus clouds, such as liquid

clouds (low clouds which consist of water droplets) and mixed-phase clouds (which consist of a mix of water droplets and ice crystals) may have a net cooling effect (negative radiative forcing). These clouds have larger optical depth when it comes to incoming shortwave solar radiation, meaning they scatter a large amount of it back into space[36]. This albedo forcing may outweigh the amount of outgoing terrestrial radiation these clouds absorb, resulting in a net cooling effect (negative forcing). This is in contrast with high ice clouds which are optically thin to incoming solar radiation (i.e. they let a lot of it pass through to Earth's surface), and cause a net warming by absorbing more outgoing terrestrial radiation than the amount of incoming solar radiation they reflect back into space.

The exact radiative properties of a cloud are dependent on its microphysical characteristics as well as its water-to-ice content ratio, in the case of mixed-phase clouds. Artificial cirrus clouds may occur as a result of aviation contrails forming in the upper troposphere, depending on the surrounding weather conditions. These clouds have a warming effect (positive radiative forcing) and thereby contribute to anthropogenic climate change[38]. Contrails and their formation process are described in more detail in subsection 2.2.

Aerosols

Aerosols are fine particles suspended in the atmosphere, in a liquid, solid or mixed state, which may originate from either natural or anthropogenic sources. Natural sources include desert dust, forest fires and volcanic ash. Aerosols that result from human activities are also called anthropogenic aerosols, and may occur due to the burning of fossil fuels, deforestation fires and burning of agricultural waste, among other processes. The concentration of this type of aerosol has increased dramatically since the Industrial Revolution, contributing to the overall anthropogenic climate change, as well as man-made air pollution. Aerosols vary in physical and chemical properties, and therefore affect the atmosphere differently. They also vary in how long they reside in the atmosphere before falling to the ground or being washed out by precipitation, typically between the order of days to weeks[67].

Aerosols influence the atmosphere directly by their reflective and absorptive properties. Depending on the type of aerosol, incoming sunlight may either be reflected back into space (resulting in a cooling effect), or it may be absorbed and warm up the atmosphere. Black carbon in particular is a type of aerosol which is known to cause a significant warming effect. Together with mineral dust, it is known as a type of absorbing aerosol, capable of absorbing incoming solar radiation in the visible spectrum[15]. Aerosols such as black carbon may also absorb outgoing terrestrial radiation, but to a much lesser extent[67].

Aerosols also affect the atmosphere indirectly, through their interaction with clouds. By acting as cloud condensation nuclei or ice nuclei, aerosols can change the physical properties of clouds, which affects their lifetime, their albedo effects as well as their precipitation formation. More aerosols generally increase the albedo effect of clouds, by providing more nuclei around which cloud droplets can form, increasing cloud brightness. This dynamic is however complex and influenced by a number of factors, such as the types of aerosols which are present. The presence of absorbing aerosols counteracts the cloud brightening somewhat, however it still appears that cloud albedo increases with an increase in aerosol concentration. Sulphate aerosols are thought to cause a significant cloud albedo increase, moreso than non-sulphate aerosols[11]. One study found a monotonic increase of cloud albedo with aerosol index, up until a value of about 0.25. Beyond this, cloud albedo increases at a slower rate, due to the cloud becoming less susceptible to aerosol influence in a more polluted environment[7]. A secondary effect of aerosols on clouds is related to cloud lifetime. An increase in aerosol concentration suppresses rainfall, which in-

creases cloud lifetime and benefits its overall reflective properties[65].

Finally, aerosols are capable of impacting the climate through their deposition. In particular, the deposition of imported black carbon particles in the Arctic caused by forest fires at lower latitudes decreases the snow cover albedo and accelerates warming[15].

Radiative forcing

Changes in atmospheric composition, such as an increase in greenhouse gas concentrations, impact the radiative balance of the atmosphere, by changing its reflective and absorptive properties. This shift in energy balance may lead to either a cooling or a warming effect, depending on whether more radiation is absorbed in the atmosphere, or more is reflected back into space. Radiative forcing is a measure of the climate impact of a given climate driver. It is defined as the change in net radiative flux (unit W/m^2) at the top of the atmosphere, caused by a climate driver, usually compared to pre-industrial conditions (1750)[30]. Positive radiative forcing leads to atmospheric warming, whereas negative radiative forcing has a cooling effect. The change in surface temperature ΔT_s that is associated with a change in radiative forcing, can be estimated by:

$$\Delta T_s = \lambda \Delta F$$

where λ denotes the climate sensitivity parameter $[K/(W/m^2)]$ and ΔF the radiative forcing $[W/m^2]$[31].

Figure 2 shows a breakdown of all anthropogenic sources of radiative forcing, including the amount of radiative forcing they are estimated to have contributed. The total amount of anthropogenic radiative forcing relative to pre-industrial times (1750) is estimated at 2.29 W/m^2 as of 2011. The IPCC estimates that this has increased to 2.72 W/m^2 in 2019[31]. Notably, the most significant warming effects are due to an increase in the greenhouse gases carbon dioxide and methane. Aerosols contribute to net cooling effects, though they are associated with a larger amount of uncertainty.

Effective radiative forcing (ERF) is an alternative metric which is regarded as the more practical indicator of global mean temperature response to a climate forcer. Unlike radiative forcing, effective radiative forcing is a measure of energy imbalance resulting from a climate forcer, after allowing for rapid adjustments in atmospheric temperatures, water vapour and clouds[1]. Surface conditions remain fixed. By accounting for both the forcing agent itself as well as the rapid adjustments it brings about, ERF becomes a more accurate indicator of temperature response over a longer term to a given climate forcer. Particularly in the case of anthropogenic aerosols, which influence clouds and snow cover through rapid adjustments, the ERF value differs significantly from the RF value and provides a more accurate image of its effects[44].

Climate change impacts

Anthropogenic climate change is already having effects around the world, which are only expected to worsen if emissions are not drastically curbed in the coming years. The most well-known way in which climate change manifests is the increase in Earth's surface temperature, in addition to other measurable changes such as the decrease in ice sheets, oceanic warming and sea level rise, and increase in the atmospheric concentration of greenhouse gases such as carbon dioxide[57]. Figure 3 shows the average temperature anomaly relative to the average temperature between 1961 and 1990. A clear increase is visible, indicating an increase in average global temperature

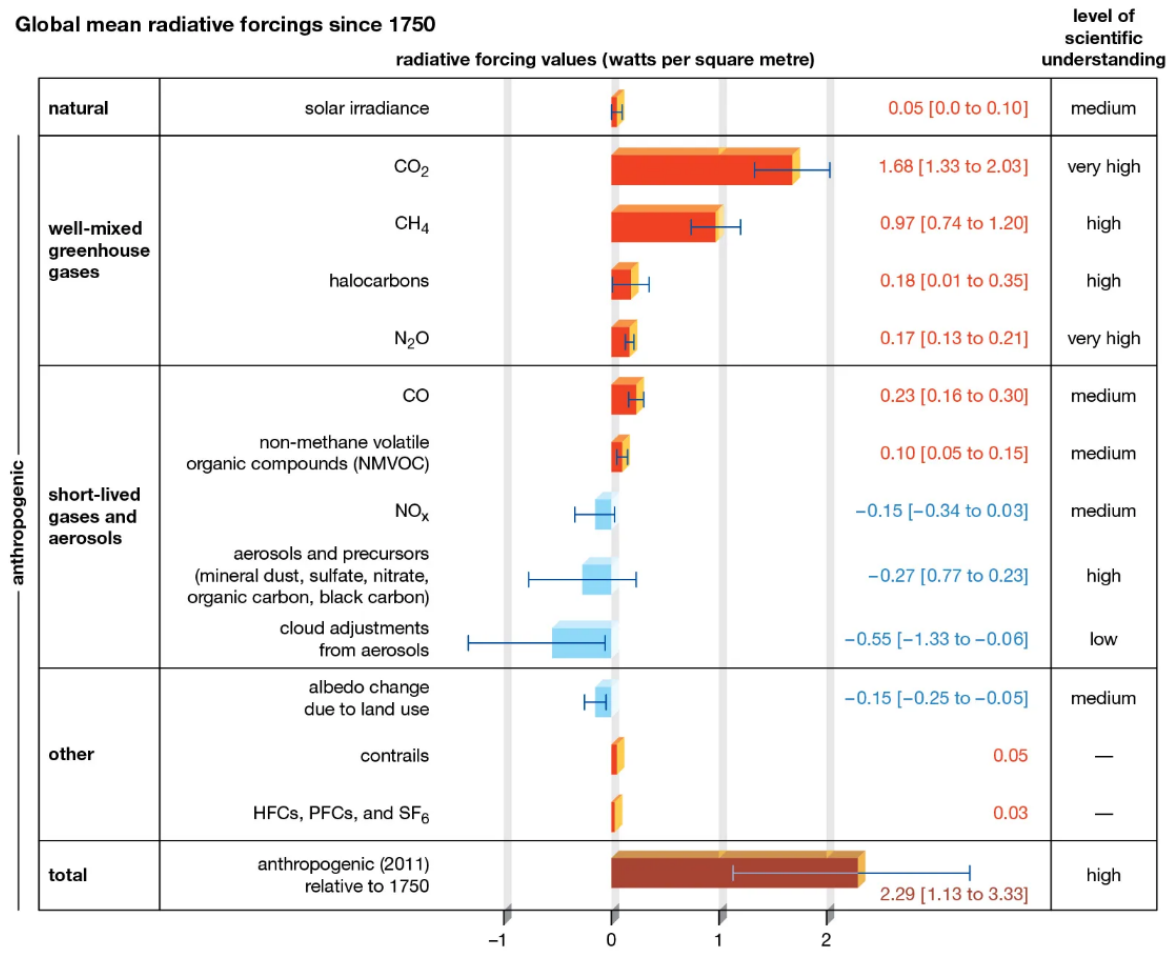

Figure 2: Estimated radiative forcings from anthropogenic sources since 1750, per emission species / climate effect, in Watts per square meter (W/m^2). Also shown is the level of scientific understanding of each emission / climate effect. Figure from [41]

of about 1.1 Celsius since pre-industrial times[52].

This temperature increase is already leading to changes in the Earth's natural system such as ocean warming, ocean acidification as a result of an increased absorption of atmospheric carbon dioxide, and the melting of permafrost, glaciers and sea ice. Due to the combination of thermal expansion and the aforementioned melting of glaciers and ice sheets, global sea levels have risen over 100 mm since the 1990s, and are expected to continue to rise, which may threaten people living in coastal areas and on islands in the coming decades[56]. Due to global warming, heat waves and wildfires are expected to become a more common occurrence, as well as other extreme weather events such as storms and droughts. Crop failures, as well as desertification of areas that were previously suitable for agriculture, may threaten food security and cause people to be forced to migrate. Human health may be further impacted due to lesser access to safe drinking water, and the easier spread of infectious diseases in warmer environments. Plant and animal species may have to relocate, or become extinct as a result of their changing living environment[31].

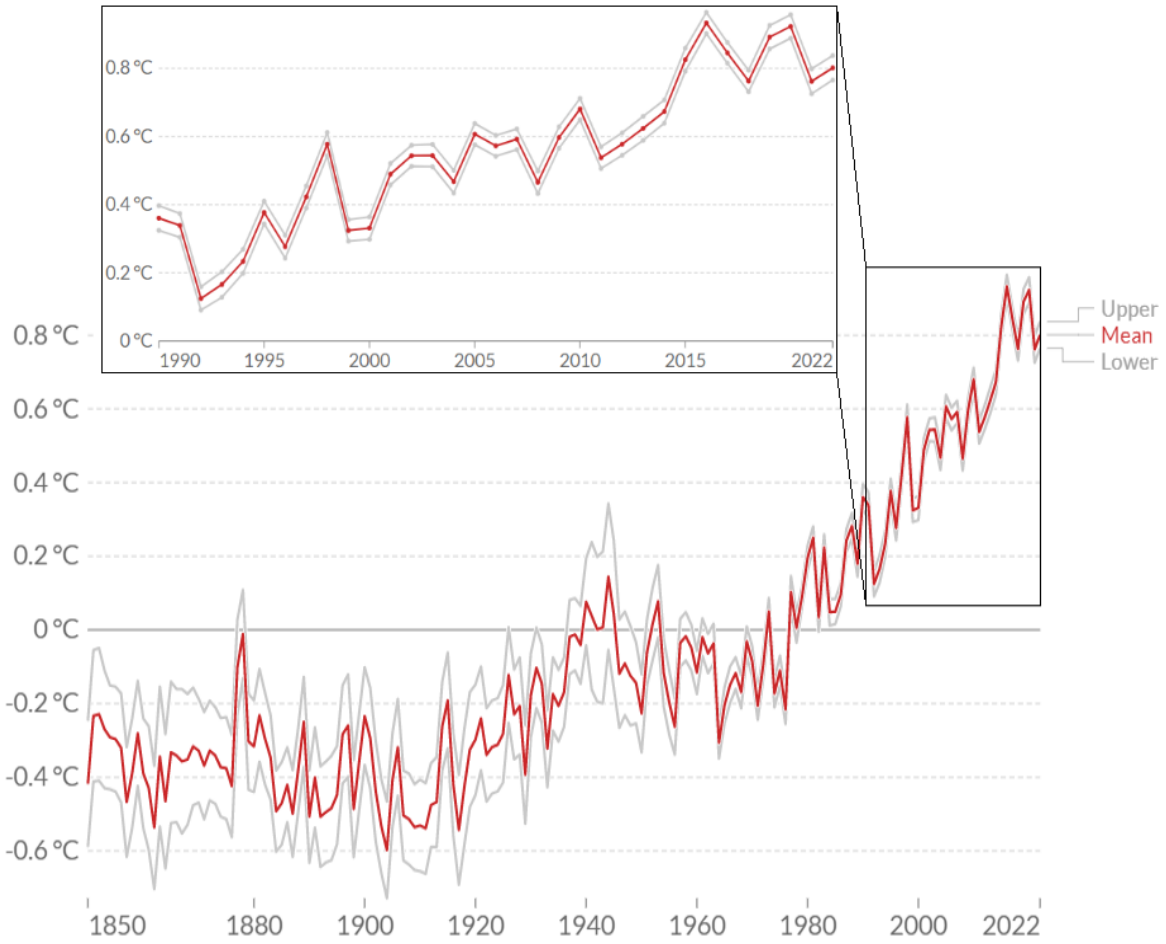

Figure 3: Average temperature anomaly relative to the 1961-1990 temperature average, with 95% confidence interval in grey. Figure from [52]. Also shown is a zoom-in on the development in more recent years, from 1990 to 2022.

Even if measures are taken to reduce the effects of human activity on the climate, there may still be processes which, once activated, cannot be reversed or even slowed down. Such a 'tipping point', once it is passed by reaching a certain threshold, leads to a self-reinforcing feedback loop which continues to feed into itself[18]. The effects of climate change are likely to be amplified through these tipping points, accelerating the harm done to the Earth's environment and biosphere. Some examples of (theorized) tipping points are the collapse of the Greenland and West Antarctic ice sheets, the die-off of Coral Reefs due to increased sea temperatures, and the dieback of the Amazon rainforest due to droughts, fires and deforestation. Extinction of plant and animal species may also be a tipping point, as it is an irreversible occurrence that may lead to negative impacts and possibly more extinctions within its ecosystem[18]. Large-scale freshwater runoff into the oceans as a result of the melting of glaciers and ice sheets, may bring about another tipping point in the form of the weakening or even the complete collapse of the Atlantic meridional overturning circulation (AMOC), which could have devastating effects on the climate of Europe[3]. Generally speaking, the more warming occurs, the bigger the chance for more tipping points to occur. A warming of 1°C relative to pre-industrial times is associated with a moderate risk of global tipping points, whereas a 2.5°C warming raises that risk to a high level. Tipping points may also be interlinked, meaning that they may trigger each other. It is therefore very important that measures to slow global warming are implemented worldwide.

2.1.2 Climate effects of aviation

Global aviation is estimated to contribute about 3.5% of all anthropogenic radiative forcing[38], through various emissions and atmospheric processes. Most notably, aviation contributes to anthropogenic climate change via the emission of carbon dioxide (CO_2), the emission of nitrogen oxides (NO_x), and the formation of (persistent) contrails which increases atmospheric cloudiness.

Figure 4 shows the quantified contributions of aviation radiative forcing. The net radiative forcing of aviation is estimated at $+100.9\ mW/m^2$ with a 5–95% likelihood range of (55, 145)[38]. Non-CO_2 ERF estimates are associated with a large amount of uncertainty: about 8 times as much as the CO_2 estimate. This section describes in more detail the climate effects of aviation, apart from contrails, which are covered in subsection 2.2.

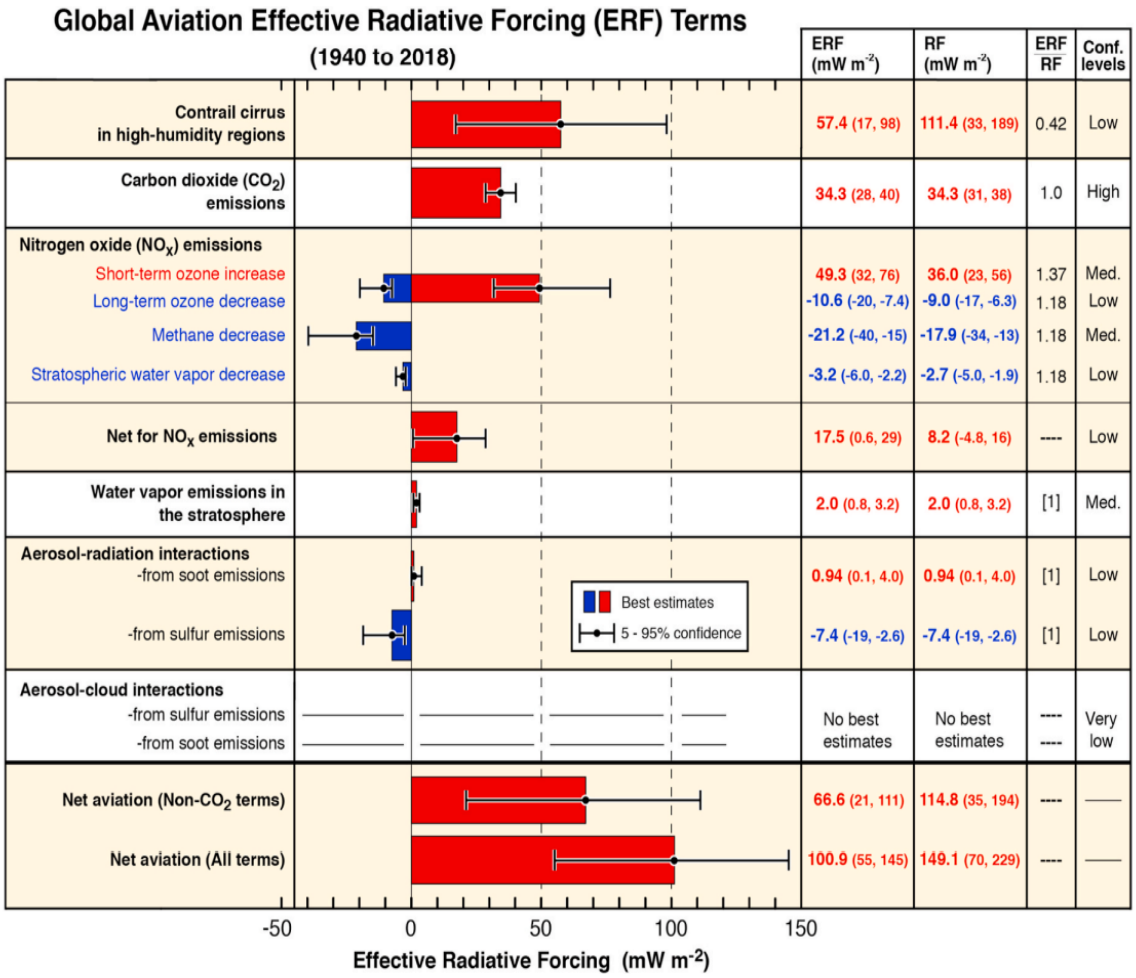

Figure 4: Estimated radiative forcing of aviation climate effects from 1940 to 2018, in mWm^{-2}. Figure from [38]

Carbon dioxide (CO_2)

Carbon dioxide (CO_2) is a direct greenhouse gas, which accounts for about three quarters of total greenhouse gas emissions[53]. Human activities have brought the concentration of carbon dioxide in the atmosphere up to well over 400 parts per million, whereas this concentration used to not exceed 300 ppm even at its peaks during Earth's natural climate cycle over the past 800,000 years[50]. CO_2 emissions cause a positive radiative forcing, resulting in a warming atmosphere. CO_2 is long-lived and can remain in the atmosphere for on average 100 years,

before being absorbed by the oceans and land biosphere. About 50% of CO_2 gets removed from the atmosphere within 30 years, while another 30% is removed within a few centuries. The remaining 20% may remain in the atmosphere for several thousands of years. This makes CO_2 a potent greenhouse gas, capable of influencing the climate long after its emission.

Aircraft emit carbon dioxide as a result of the combustion of kerosene. As of 2018, the CO_2 emissions of aviation are estimated to be at about 1.04 billion tonnes, which induce an effective radiative forcing (ERF) of 34.3 mW/m^2. This accounts for about one third of the total ERF of global aviation.[38]. It is estimated that aviation contributes about 2.5% of all global CO_2 emissions[51], however this number is expected to increase in the coming years. The International Civil Aviation Organization (ICAO) estimates that by 2050, aviation may account for 25% of the global carbon budget[16]. This increase is expected due to both the continued growth of the aviation industry, as well as decarbonization within other sectors, which would increase the relative CO_2 emission contribution of aviation. As opposed to other climate effects of aviation, the emission of CO_2 impacts the atmosphere in largely the same way, regardless of the altitude at which it takes place. CO_2 is the most well understood climate effect of aviation.

Nitrogen oxides (NO_x)

Nitrogen oxides (NO_x) are emitted by aircraft as a byproduct of the combustion of kerosene. Typically, aircraft emit both nitrogen oxide (NO) and nitrogen dioxide (NO_2). The emission of nitrogen oxides affects the atmosphere in various ways. Most notably, it causes an increase in ozone, and a depletion of methane.

Ozone (O_3) is a greenhouse gas, which exists in various concentrations at different altitudes. Its function also differs with altitude. In the stratosphere, ozone is formed through the photolysis of oxygen (O_2) molecules. Ozone is formed when the resulting O atom reacts with O_2:[39].

$$\mathrm{O + O_2 \longrightarrow O_3}$$

Conversely, ozone is also photolysed back into O_2 and O.

$$\mathrm{O_3 \xrightarrow{h\nu} O + O_2}$$

The stratosphere has a relatively high concentration of ozone, which serves as a shield from UV radiation. In the troposphere and tropopause, ozone exists at a lower concentration, and acts as an effective greenhouse gas. Some amount of ozone may enter from the stratosphere, however most tropospheric ozone is formed through chemical reactions. HO_2 reacts with NO into NO_2 and OH[39].

$$\mathrm{HO_2 + NO \longrightarrow NO_2 + OH}$$

Nitrogen dioxide (NO_2) photolyses to form NO and O[39].

$$\mathrm{NO_2 \xrightarrow{h\nu} NO + O}$$

The resulting O atom reacts with O_2 to form ozone. This results in a positive radiative forcing (a warming effect).

Another effect of the emission of NO_x is in the reduction of methane (CH_4). Methane is a potent greenhouse gas, estimated to be able to cause 28 times as much warming as an equivalent mass of carbon dioxide. It has a relatively short atmospheric lifetime, on average about 12 years. Methane emissions account for about 17% of all greenhouse gas emissions[53] and primarily come from agriculture; both livestock and cultivation of crops, most notably rice, cause most of the global methane emissions. Fossil fuel production, the decomposition of waste and the burning of biomass also produce methane[53]. Aviation affects atmospheric methane concentrations through the emission of nitrogen oxides. NO reacts with HO_2 to form NO_2 and OH[39].

$$\mathrm{NO} + \mathrm{HO_2} \longrightarrow \mathrm{NO_2} + \mathrm{OH}$$

The reaction of methane with the hydroxyl radical (OH) is a methane sink[39].

$$\mathrm{CH_4} + \mathrm{OH} \longrightarrow \mathrm{CH_3} + \mathrm{H_2O}$$

The resulting decrease in methane concentration has a negative radiative forcing (a cooling effect). Tropospheric ozone is itself a precursor for OH; through photolysis, O atoms are produced which then react with H_2O to form OH. This may further deplete methane concentrations.

Though the emission of nitrogen oxides results in both positive and negative radiative forcings, the positive forcing is estimated to outweigh the negative, which means NO_x emissions have a net positive (warming) effect. Its net radiative forcing is estimated to be about 17.5 mW/m^2, though it is associated with a low level of confidence[38].

Other aviation emissions

Aviation emissions with smaller radiative forcing effects include the emission of soot and sulphate aerosols. Aviation-emitted soot, mainly consisting of black carbon (BC) and organic carbon (OC), absorbs short-wave radiation and causes a positive radiative forcing. Sulphate aerosols (mainly SO_2) are emitted as a result of sulphur present in aircraft fuel. They scatter incoming short-wave radiation, resulting in a negative radiative forcing (cooling). The net radiative forcing associated with sulphate aerosols is estimated at $-7.4mW/m^2$[38].

Additionally, aircraft emit water vapor (H_2O) as a result of the combustion of fuel. H_2O is a greenhouse gas, and its emission results in a small positive radiative forcing[38]. Water vapor and soot particles play an additional role in aviation climate impact, due to the formation of (persistent) contrails. Emitted soot particles can serve as condensation nuclei around which water vapor can condense and subsequently freeze into ice crystals, which forms a contrail. Under the appropriate atmospheric conditions, contrails may persist for minutes to hours, and spread out into cirrus clouds. Persistent contrails and cirrus clouds both are capable of trapping outgoing radiation in the atmosphere, thus causing a warming effect[36]. The formation, radiative forcing and mitigation of aviation contrails are described in more detail in the following chapters.

2.2 Contrails

Condensation trails (contrails) are line-shaped clouds that form behind the aircraft engine exhaust when flying in the upper troposphere at 8-13 km altitude, and which mainly consist of water in the form of ice crystals. Whether or not a contrail forms, and whether or not it is able to persist (i.e. retain its linear shape for an extended amount of time, usually defined as 10 minutes or more), depends on the surrounding atmospheric conditions. Contrail formation depends on the surrounding atmospheric temperature, whereas contrail persistence depends on surrounding atmospheric humidity[36]. In case of low humidity, a contrail evaporates shortly after formation, whereas a contrail can persist for a duration for minutes to hours in case of sufficiently high humidity.

Persistent contrails cause an increase in cloudiness in the atmosphere which is referred to as aircraft-induced clouds (AIC), and which has an overall positive radiative forcing effect and thus contributes to global warming. Although the level of understanding of contrail formation and its exact impacts on the climate is lower than other climate effects such as CO_2 emissions, the radiative forcing of aviation induced cloudiness is known to be significant: recent studies estimate that more than half of aviation-induced radiative forcing may be attributed to AIC (also shown in Figure 5)[38]. A better understanding of contrail formation and climate effects, could thus be useful in mitigating the climate effects of aviation.

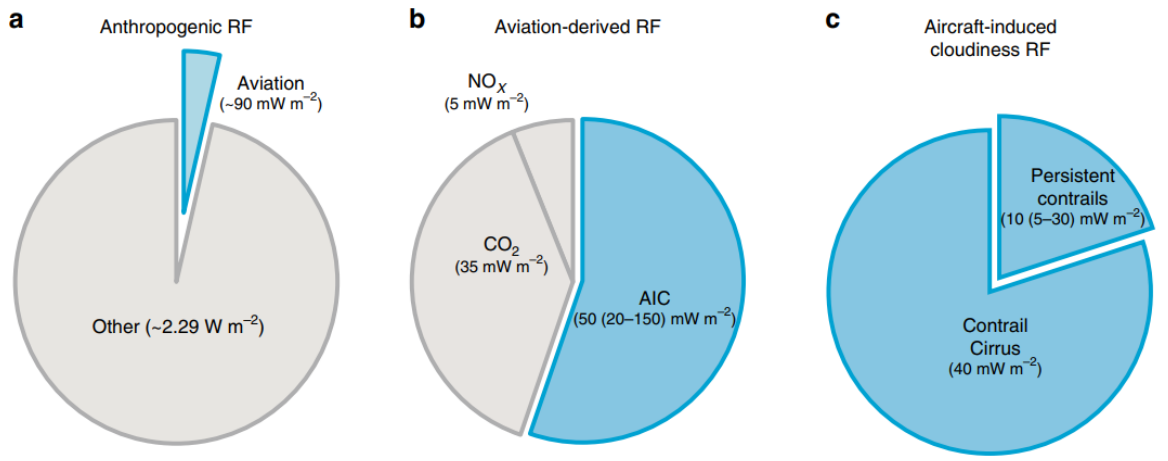

Figure 5: Estimated RF from aviation-induced cloudiness, relative to other RF sources. Figure from [36]

This chapter aims to describe in more detail the formation, lifetime and climate effects of aviation contrails.

2.2.1 Formation

The formation of (persistent) contrails is a process that takes place behind the engines of aircraft at cruise altitude (8-12 km), and consists of several stages, which range in duration from seconds to several minutes. Contrail formation involves multiple complex thermodynamic and microphysical processes, and requires a number of atmospheric boundary conditions to be fulfilled, specifically a low temperature and sufficient humidity.

Formation starts due to the expansion of jet engine exhaust plumes, and their subsequent mixing and interacting with the surrounding ambient air. The engine exhaust plumes contain a

number of aerosol particles, which may originate from emission of the engine (soot), they may be ultrafine aqueous particles which have formed within the plume, or they may have mixed into the exhaust plume from the ambient air[36]. As the exhaust plumes cool down and the aerosol particles interact with condensable vapours such as water vapour, emitted from the aircraft engine as a product of the combustion of fuel, they serve as nuclei around which water droplets form. This condensation process takes place due to the cooling of the plume, which causes the plume relative humidity to rise above liquid water saturation. This condition is necessary for contrail formation to occur, and is known as the Schmidt-Appelmann criterion[15]. Finally, due to the low ambient temperature, the water droplets freeze into ice crystals of varying sizes in the order of micrometers (μm).

The subsequent phase of contrail formation is characterized by the mixing of plumes from different aircraft engines with the aircraft wing vortices. Their circular motion captures most of the contrail. In the lower part of the wake, which undergoes a downward motion of about 100 m below the flight level, ice crystals are lost to sublimation. In the upper part of the wake, ice crystals are able to grow by uptake of water from the surrounding ambient air. Finally, the formation stage is ended due to turbulence which causes the flow pattern to collapse and mix with the surrounding ambient air. Figure 6 shows the process of contrail formation in a schematic way[36].

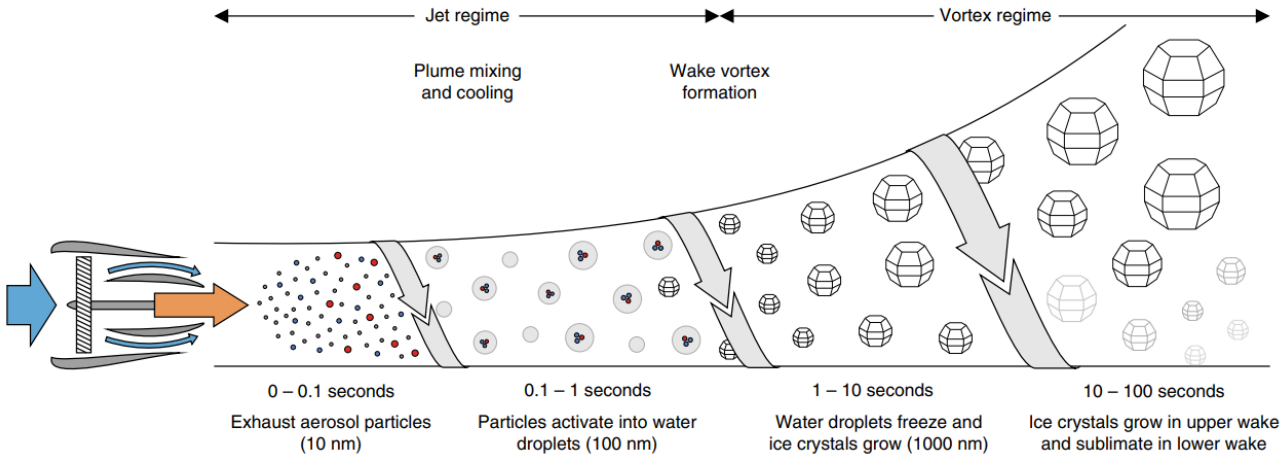

Figure 6: The various stages of the contrail formation process. Figure from [36]

Ice supersaturation

Ice supersaturation is an atmospheric condition which is required for a contrail to persist, and eventually evolve into contrail cirrus clouds. It denotes the situation in which the relative humidity with respect to ice exceeds 100%[15].

Humidity relative to water is the ratio of water molecule concentration currently present and the water molecule concentration at saturation. Alternatively, it is the ratio of partial pressure of water molecules and the partial pressure of water molecules at saturation. Saturation is a condition in which a dynamic equilibrium exists within the exchange of water molecules in liquid and gas phases: there may still be an exchange between the two phases, however the net flux is zero[15]. The water vapor is then said to be saturated, with a relative humidity of 100%.

A similar case can be described for the exchange between water vapor and water in solid form (ice). One difference however is that in ice, molecules have a stronger bond than in water. This

means that the flux of ice molecules into the vapor phase is smaller than in the case of liquid water. This means that saturation with respect to ice can be achieved with a smaller concentration of water in the vapor phase, compared to saturation with respect to water.

Supersaturation describes the case where there is a higher water vapor concentration present than what would be needed for saturation. Relative humidity then exceeds 100%. Supersaturation is an unbalanced state, and processes will occur (such as condensation in the case of supersaturation with respect to water) to drive the system back to equilibrium. Subsaturation is a state in which relative humidity is below 100%, and will bring about evaporation or sublimation processes to the condensed state, in order to achieve equilibrium[15].

Ice supersaturation is a condition which can occur at higher altitudes, due to lower air pressure and a lower saturation concentration for water vapor as a result of decreasing temperature (also shown in Figure 7). The water vapor concentration decreases only proportional to the lower air pressure, which results in increased relative humidity. Supersaturation can then occur as a result. In case of supersaturation with respect to liquid water, condensation occurs relatively easily around tiny particles that serve as nuclei, forming clouds consisting of water droplets. This makes supersaturation relative to liquid water in practice an instable state. Ice supersaturation, which is known to occur at lower partial pressures than supersaturation relative to liquid water, does not result in condensation and the formation of ice crystals as easily, due to the fact that ice crystal structure is highly organized and cannot form on any particle[15]. Only about one in one million aerosol particles is suited to serve as a nucleus around which ice crystals can form. This means that while ice supersaturation is a state that is achieved more commonly than supersaturation relative to liquid water, ice crystals do not readily form in the atmosphere once ice supersaturation occurs. This makes ice supersaturation a metastable state, which can last for some time (sometimes longer than 24 hours[32]), and can spread out over large air volumes.

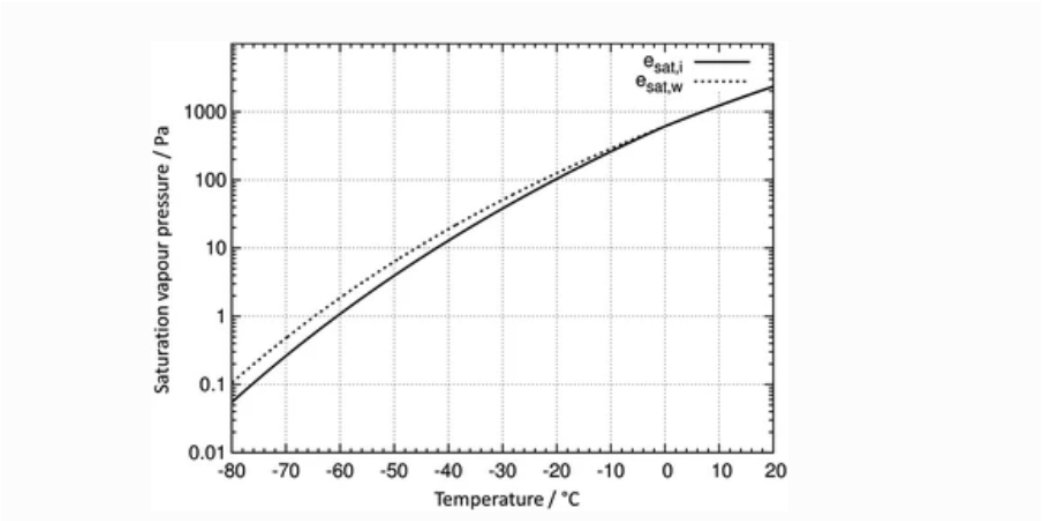

Figure 7: Saturation vapor pressures for different subzero temperatures, relative to liquid water (dotted line) and ice (solid line). Figure from [15]

Ice supersaturated region (ISSR) is a term which is typically used to refer to a cloud-free region in the upper troposphere where relative humidity exceeds ice saturation. These regions are especially interesting due to the fact that aviation contrails can form and persist here, impacting the Earth's climate through the radiative forcing of the contrails themselves and their resulting contrail cirrus. The Measurement of Ozone and Water Vapour by Airbus In-Service Aircraft (MOZAIC) project has previously shown that about 15% of its participating flights' cruising time was spent in ISSRs[37]. Large ISSRs and ISSRs with high degrees of saturation can also

be observed by satellite imagery. ISSRs are known to occur at different altitudes dependent on latitude: around the tropics, ISSRs occur at high altitudes above 150 hPa. Between 200 and 250 hPa, ISSRs occur mostly at mid-latitudes and rarely in the tropics. Below 250 hPa, ISSRs occur almost exclusively at mid-latitudes and even lower (300-500 hPa), they are mostly seen around the poles. ISSRs also vary in geometrical properties: about 80% of ice supersaturated layers are less than 1500 m thick; about 30% are less than 100 m thick. About 5% are estimated to be over 3000 m thick and can be detected by satellite observations.

Ice supersaturation is a condition which is required for contrails to persist and eventually spread out into cirrus clouds. It is therefore important to understand it well, when making an effort to mitigate the climate effects of aviation. The ability to avoid persistent contrails is dependent on a good ability to model and predict ice supersaturation. This is however still a challenge. The thesis project will focus on the discrepancies that currently exist between model and reality, when it comes to ice supersaturation conditions. This is explained in more detail in further sections.

2.2.2 Lifetime

A contrail persists in case humidity is sufficiently high for ice supersaturation to occur. In this case, the ice crystals present in the contrail are able to continue growing by drawing water vapor from the surrounding atmosphere. Persistent contrails lose their linear shape over time, spreading out into cirrus clouds which may span many kilometers in width, and multiple hundreds of meters in height. They may persist for hours and also be transported hundreds of kilometers away from where they originated. Over time, contrail cirrus can start to appear indistinguishable from natural cirrus to the human eye as well as satellite observations. A 'contrail outbreak' may occur over a congested airspace, which comprises multiple ice cloud layers and which can cover up to 100.000 km^2 and be visible in satellite imagery[43]. Finally, contrail cirrus dissipates when its ice water reduces due to sublimation and precipitation[4].

The ice supersaturated layers which support the persistent contrails and their resulting contrail cirrus vary in geometric as well as microphysical properties, which also affects the properties of aircraft-induced cirrus and its resulting climate impacts. Additionally, contrail cirrus may interact with and influence existing cirrus clouds. Cloud optical depth, a measure of the attenuation of radiation passing through a cloud, can be enhanced by the presence of contrail cirrus clouds. Contrail cirrus may also form where there is already natural cirrus present, which complicates the estimating of aviation-induced cirrus extent and climate impacts. Another challenge is posed by the fact that a lot of contrail cirrus is optically thin (optical depth of less than 0.02), which makes them difficult or impossible to spot either with satellite imagery or with the human eye[4]. Because they are believed to be abundant and have a large coverage, their radiative forcing impacts may not be negligible. It is estimated that 49% of contrail cirrus has an optical depth of less than 0.02[36].

2.2.3 Contrail radiative forcing

The total radiative forcing of aviation contrails consists of the sum of the radiative forcing of persistent contrails and the radiative forcing of the resulting contrail cirrus. The combined effects are referred to as aircraft-induced cloudiness (AIC)[36]. The total effective radiative forcing of AIC is currently estimated to be about 57.4 mW/m^2[38], however this number is associated with a large degree of uncertainty. An uncertainty of 70% is estimated for the overall radiative forcing of contrails and contrail cirrus, which can be attributed to several causes. Scenario uncertainty as well as model inadequacy play a role: radiative forcing estimates require knowledge

and modelling of complex atmospheric processes, spanning the entire contrail cirrus life cycle, which is associated with a low level of scientific understanding. Another source of uncertainty is natural variability: varying weather can play a big role in contrail radiative forcing properties. There is also some uncertainty associated with the interaction of contrail cirrus with naturally occurring cirrus clouds[38].

It is estimated that contrail cirrus causes much more radiative forcing than the persistent contrails which they originate from: only 10-20% of AIC radiative forcing is believed to be caused by persistent contrails. Radiative forcing from non-persistent contrails (i.e. contrails which form under ice-subsaturated conditions and which disappear in a matter of seconds to minutes) are considered negligible when compared to these other two contributors[36]. Contrail radiative forcing has both a negative (cooling) and a positive (warming) component. Cooling is achieved through the reflection of incoming shortwave solar radiation, whereas warming is caused by the trapping of outgoing longwave radiation. Contrail cirrus also may cause changes in natural cloudiness, through the deposition of atmospheric water vapor into contrail cirrus ice particles, which would otherwise be deposited into natural cirrus. This affects the optical properties of natural cirrus, and is thought to bring about a negative radiative forcing (cooling), however not much is known about these interactions[4]. Overall, the net effect of contrails is a positive (warming) one, as the trapping of radiation outweighs the reflected radiation. The quantified radiative forcing of a contrail is approximated by the integral product of its spatial coverage and its effective optical depth τ[4].

Contrail radiative forcing is known to vary a lot depending on the time of day as well as the time of year. At nighttime, contrails only have a warming effect due to the absence of incoming solar radiation to be reflected back into space. The trapping of outgoing longwave radiation results in an increase in warming of about 33%. During the day, contrails are estimated to have a net warming effect of about 10%, less than at night due to the fact that incoming solar radiation is reflected back into space[2]. Flights during winter time are found to cause larger contrail radiative forcing than those during other seasons. One case study showed that winter flights account for half of the overall contrail radiative forcing over the year, despite making up only 22% of all flights. The same study found a 60 to 80% radiative forcing contribution of night flights, despite making up just 25% of daily flights[61]. Contrail properties are also known to vary with the type of aircraft that has caused it: for instance, larger aircraft cause contrail with larger optical thickness than smaller aircraft[33]. This may be an additional consideration in the mitigation of contrail climate effects.

2.3 Mitigation of aviation climate effects

The aviation sector has undergone rapid changes in the past decades. Thanks to improvements such as technological innovations in aircraft, larger aircraft which can carry more passengers, and a higher passenger load factor, aircraft emissions per revenue passenger kilometer (RPK) have decreased dramatically. The red graph in Figure 8 shows this effect for the emission of CO_2. On the other hand, air travel volume has grown so rapidly that despite the increased efficiency, aircraft emissions have still increased by a factor 7 since 1960, and factor 3 since 1970. The black solid and dashed lines in Figure 8 show the rapid and continued increase in revenue passenger kilometers (RPK) and available seat kilometers (ASK), respectively[51].

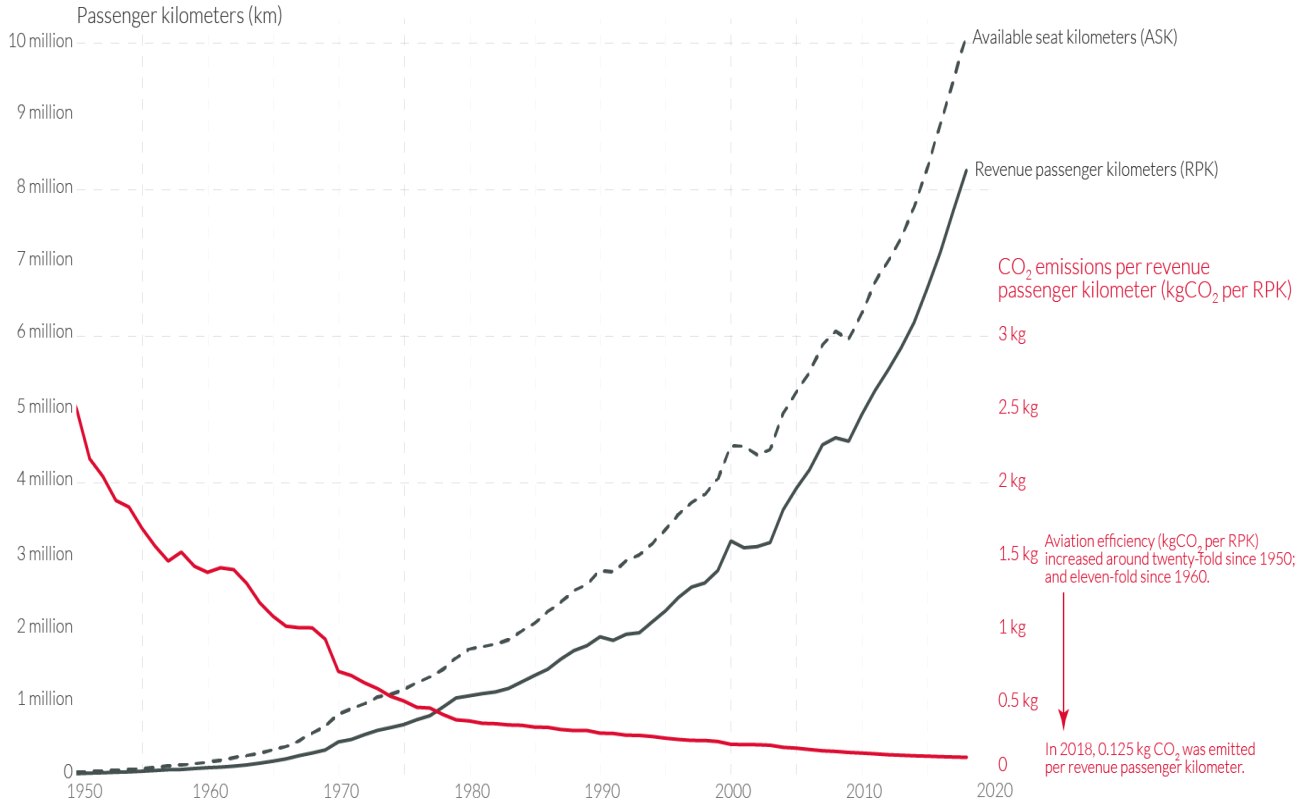

Figure 8: Available seat kilometers (ASK), revenue passenger kilometers (RPK) and CO_2 emissions in kg per RPK, from 1950 until 2020. Figure from [51]

The expected further growth of global aviation presents a substantial challenge to climate goals, set out by governments as well as international organizations such as the United Nations. Where sectors like energy and other transportation sectors are making progress in applying novel technologies such as electric and hydrogen-powered plants and vehicles, the aviation sector has so far not been able to do the same. There is substantial research into the topic of hydrogen-powered, electric-powered and hybrid aircraft; for instance, Airbus aims to develop the world's first zero-emission aircraft by 2035, powered by hydrogen[51]. However, there are no technologies yet that can be applied and scaled up to suit the demands of the sector. Electric powered planes may be viable in the future, however the limited power storage ability of batteries is likely to be a challenge and a limiting factor for aircraft size and range. Hybrid aircraft may be a possibility sooner[36].

Shifting to more sustainable fuels, as well as working to increase aircraft fuel efficiency are additional technological measures to mitigate aviation climate effects. Alternative fuels such as sustainable aviation fuels (SAFs) have, as an added benefit, a lower emission of soot particles.

Exhaust soot particles are regarded as the main nucleation site of contrail ice crystals. Therefore, a lower soot emission results in lower contrail optical depth, thereby decreasing contrail occurrence, lifetime and radiative impacts[35]. It is estimated that a 50% decrease in soot emissions can bring about a 15% decrease in contrail radiative forcing[5]. Additionally, lean combustion technologies, which features a high air-to-fuel ratio, can also reduce soot emissions[36].

Other ways of mitigating aviation climate effects are operational, rather than technical, in nature. This chapter lays out some of the research done to mitigate aviation climate effects, specifically contrail formation, as well as the difficulties currently encountered in this research area.

2.3.1 Operational mitigation measures

Operational mitigation methods of aviation climate impacts are especially relevant, given that they can typically be achieved with existing technology. Therefore, these methods can be implemented in a relatively short term, when compared to the technological innovations that are still in their development stages. This is especially interesting in light of the necessity to curb climate change in the coming years and decades. Despite the projected growth of the aviation sector, operational mitigation methods may be able to limit some of the associated climate effects. One operational mitigation measure is the general reduction of air travel through means like the banning of short-haul flights and instead encouraging less environmentally harmful transportation methods like trains. Capping airline emissions provides an incentive to seek more efficient operations and technologies. Financial measures like charging carbon taxes and subsidizing the development of more sustainable air travel can further reduce aviation climate effects. Limiting the number of night time flights has the potential to reduce radiative forcing by (persistent) contrails, given that contrails formed at night only have a warming effect, due to the lack of incoming radiation to reflect back into space. It is estimated that night flights cause 60-80% of contrail radiative forcing, despite making up only 25% of total flights[61].

Another operational measure to mitigate the climate effects of aviation is by optimizing flight routes with regards to climate impacts. For instance, flying more direct routes, rather than using air corridors, has the potential to reduce aviation emissions. This is especially relevant for reducing carbon dioxide emissions, for which the climate effects are similar regardless of where the emissions take place. However, there is more to consider than only CO_2: most of the non-CO_2 climate effects of aviation, which are estimated to account for two-thirds of its total radiative forcing, depend strongly on location. Flight altitude, latitude and the type of weather encountered all play a role in determining how much radiative forcing a given flight will cause. Avoiding regions that are especially sensitive to non-CO_2 emissions may make a flight less environmentally harmful, even though the flight may not necessarily be the shortest flight possible. One comprehensive study of trans-Atlantic flights in winter, which used climate cost functions to weigh the climate effects of different aviation emissions, found that a 25% decrease in climate impact can be achieved at an increased economic cost of only 0.5%[17]. The achieved climate benefit is mostly driven by the avoidance of contrail formation, which is highly location-dependent.

Contrail avoidance is an interesting measure of mitigation, due to the fact that it can be achieved at a relatively low cost in terms of flight maneuvers[42]. Persistent contrails and contrail cirrus also have a lifetime that is much shorter than other aviation-induced climate drivers such as CO_2 (a lifetime in the order of hours versus decades to centuries). This means that contrail avoidance is a suitable measure for the rapid mitigation of some of the climate impacts of aviation[36]. However, a solid understanding and an accurate prediction of the formation of persistent contrails is necessary to make this happen. This is due to the fact that flight rerouting

to avoid contrails is likely to come at an added cost of additional non-contrail climate effects, as well as the possible added flight time and operational costs incurred by the airline. Thus it is important to be able to accurately predict persistent contrails, such that a trade-off can be made to find the least environmentally harmful flight, at an acceptable cost for the airline.

2.3.2 Contrail avoidance

Flight route optimization, especially with regards to avoiding the formation of persistent contrails, is an increasingly relevant topic of research. It is estimated that at the current rate of growth, global aviation will cause three times the contrail radiative forcing in 2050 that it does today[5]. Avoiding the regions that are prone to contrail formation has the potential to reduce a substantial amount of contrail radiative forcing at relatively low operational cost.

One case study of contrails over the United States has shown that elevating cruise altitude of flights which are expected to fly through ice supersaturated regions by 2000 or 4000 ft, is capable of reducing the number of flights which generate contrails by 14.8%, and contrail radiative forcing by 92%. This is also associated with a slight decrease in fuel burn, thanks to lower drag at higher altitudes[2]. This lower drag also helps to compensate for the additional fuel burnt during the longer climb and descent phases. The study shows a significant overlap in altitudes with ice supersaturated regions, and cruise altitudes of the studied flights. Specifically, it appears that the occurrence of ice supersaturated regions drops dramatically at FL360 and above, whereas most flights cruise below this altitude, typically at FL340 or FL350. A relatively small increase in cruise altitude can thus achieve significant climate benefits, simply by avoiding cruising at those altitudes at which ice supersaturated regions are most prevalent.

In general, it appears that at mid-latitudes the best way to avoid contrail formation is flying higher, whereas above the tropics it is more effective to fly lower[13]. Flying higher at mid-latitudes would reduce contrails due to lower humidity in the dry stratosphere, whereas flying lower at tropical latitudes would result in fewer contrails, due to too high temperatures. In theory, flying lower at mid latitudes would also result in fewer contrails for this same reason, however the adverse effects of cruising at (much) lower altitude such as increased fuel burn due to more drag, more turbulence and limitations of available air space would likely outweigh the benefits of the achieved contrail mitigation. Multiple other case studies have shown the possibility of significantly reducing contrail radiative forcing, with only a small increase in fuel burnt[59],[42],[60].

Thanks to the relative shallowness of ice supersaturated regions, small vertical maneuvers can bring about a substantial reduction in persistent contrail formation and its resulting radiative forcing[42]. A slightly more involved, but possibly more effective strategy that makes use of this fact, was investigated by another study[62]. This strategy involves adjusting flight altitudes based on weather forecast and likelihoods of (persistent) contrail formation, rather than preventively flying at a different altitude regardless of weather and atmospheric conditions. It also involves prioritising the avoidance of those contrails that are predicted to have the worst radiative impacts, while allowing for contrails which are predicted to have an overall negative radiative forcing (cooling) effect. Aiming to avoid 100% of contrails is not efficient in terms of overall climate impact: the additional fuel burnt would result in more (adverse) effects such as CO_2, NO_x and other emissions which would likely outweigh the contrail radiative forcing avoided by the maneuvers[60]. Additional operational costs such as increased flight time also make it infeasible to avoid all contrails. The study estimated that by rerouting 15.3% of flights to avoid the contrails with the worst climate impacts and allow contrails with cooling effects, a reduction in contrail energy forcing of 105% can be achieved. This comes at the cost of a 0.70% increase in fuel burn[62]. When taking into account both contrails and CO_2 effects, an

optimum solution by not only reducing contrail forcing by the same amount as before, but also achieving a decrease in fuel burnt of 0.40%. However, this strategy involves diverting 20.1% of the flights investigated in the study, and was associated with a loss of separation in 9 to 14% of cases, which affects air traffic management and safety standards.

Another study suggested a similar method of avoiding contrail formation, through the use of existing weather instrumentation such as the Rapid Update Cycle (RUC), which predicts wind, temperature and humidity, and the Corridor Integrated Weather System (CIWS), which gives a weather forecast. These instruments can be used in a complementary way to avoid those regions which are prone to persistent contrail formation, and which do not contain clouds yet. Avoiding severe weather is also taken into account. The study showed a potential of 63.7% reduction in contrails with a 2000 ft change in altitude, and a 92.6% decrease in case of a 4000 ft altitude change[6].

Ideally, a trade-off should be able to produce the most efficient solution in terms of climate impacts as well as operating costs. To make this possible, it is necessary to be able to accurately and reliably predict the occurrence on (persistent) contrails.

2.3.3 Contrail prediction

The thermodynamic requirements for (persistent and non-persistent) contrail formation, also known as the Schmidt-Appleman criterion, can be predicted with relative ease. Accurate prediction of persistent contrails is however more challenging, as it requires the ability to predict the requirement for contrail persistence: ice supersaturation. This is a problem, given that it is exactly the persistent contrails and the contrail cirrus that results from them that cause significant radiative forcing.

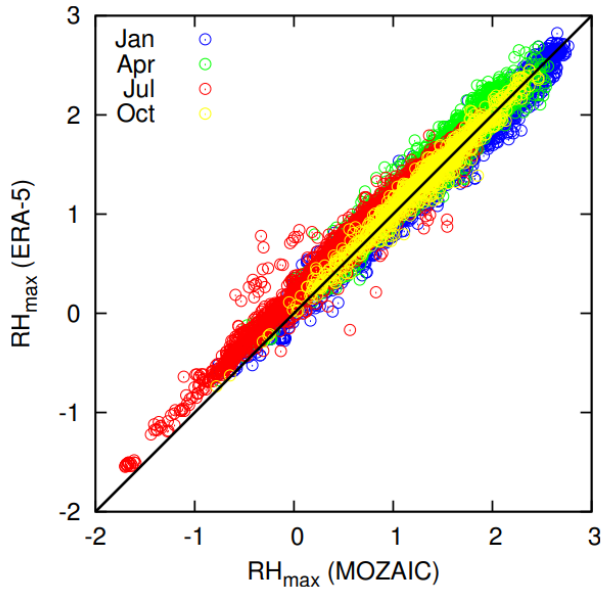

(a) Modelled (vertical axis) versus observed (horizontal axis) values of RH_{max}

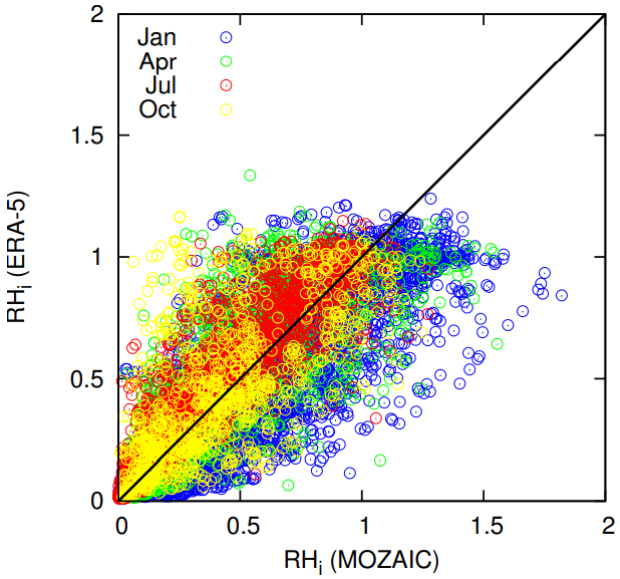

(b) Modelled (vertical axis) versus observed (horizontal axis) values of RH_i

Figure 9: Figures from [14]

One study investigated the current ability to predict persistent contrails, for the purpose of avoiding those contrails which are estimated to have the worst climate impacts ('big hits'). It showed that while temperature and relative humidity can be predicted with some accuracy, predicting relative humidity with respect to ice proves a lot more difficult[14]. Figure 9a shows

the relative humidity as modeled by ERA-5, which is part of the European Centre for Medium-Range Weather Forecast (ECMWF), versus measured humidity data from the MOZAIC-IAGOS project. Throughout the year, but especially during fall and winter, relative humidity can be predicted with quite impressive accuracy. Figure 9b shows the same comparison for relative humidity with respect to ice. It is obvious that there is not nearly the same degree of correlation between the modelled and measured data, thus it appears that the current ability to predict relative humidity with respect to ice is poor. Specifically, it appears that the model underpredicts ice supersaturation, which would lead to too low estimates of contrail persistence, optical depth and radiative forcing.

Several efforts have been made to better understand and predict atmospheric ice supersaturation. One study combined in-flight atmospheric measurements of the MOZAIC project with the Atmospheric InfraRed Sounder (AIRS), which is an instrument onboard the NASA Aqua satellite. AIRS is capable of providing temperature and relative humidity estimates, however it struggles to detect ice supersaturated layers which are shallow (500 m on average) due to its coarse vertical resolution[37]. The MOZAIC data were used to develop a calibration method for the AIRS instrument, in order to better estimate the frequency of ice supersaturation occurrence. A way to calculate the probability of ice supersaturation in a given vertical layer, based on the relative humidity measured by AIRS, was developed using MOZAIC data. The resulting climatology was compared to MOZAIC measurements alone, as well as ECMWF forecasts and ECHAM4 simulations. It showed relatively similar results, but suffered from deficiencies around the tropopause due to AIRS' higher uncertainties in this region.

In addition to satellite observations like those provided by AIRS, radiosondes are also used to measure atmospheric properties which can be used to detect ice supersaturation. A study of radiosonde temperature and humidity data from the UK, which used visual observations of persistent contrails for validation, showed that radiosondes can predict the occurrence of ice supersaturation with good accuracy[54]. Radiosondes (as well as in-situ measurements) provide observations at high vertical resolutions compared to satellites, however they are not capable of providing global and continuous observations, like satellites can[37]. Despite this, radiosondes may still be a valuable tool in predicting ice supersaturation in those regions with a lot of air traffic such as Europe and North America[54]. One known problem however is that radiosondes are known to often underestimate relative humidity in the upper troposphere, leading to a 'dry bias' which should be accounted for[8].

There have also been efforts made to simulate ice supersaturation within atmospheric models and forecasts. The European Centre for Medium-Range Weather Forecasts (ECMWF) has integrated ice supersaturation into its Integrated Forecast System[63]. Validation with in-situ data from the MOZAIC project, remotely sensed data as well as ground-based contrail observations shows a reasonable prediction ability of ice supersaturation location, magnitude and frequency. In particular, it seems that the model suffers less from 'dry bias' and returns higher relative humidity values. This is positive for the prediction of persistent contrails, given that relative humidity is the deciding factor in their occurrence.

Overall, it appears that contrail avoidance by diverting flights away from those regions which are prone to the formation of persistent contrails, is a promising option for mitigating the climate effects of aviation in the short term. However, the ability to predict the condition which makes contrails persist, atmospheric ice supersaturation, is still difficult and forms an obstacle in implementing such a mitigation method. More research is needed in order to better understand and model ice supersaturation.

3 Project description

From literature, it is clear that there is a gap in the understanding of contrail formation regions, especially when it comes to the phenomenon of ice supersaturation and the occurrence of ISSRs. In-situ measurements such as those from the IAGOS project provide a valuable opportunity to gain a better understanding of these regions, by providing quasi-continuous, high-quality observations at those altitudes where ISSRs are common and likely to result in persistent contrails and eventually contrail cirrus, when aircraft fly through them. A better understanding of ice supersaturation and ISSRs could aid in developing a better strategy to avoid contrail formation, which would benefit efforts to mitigate the climate effects of the aviation sector.

3.1 Research objective

The data from IAGOS-CORE (and to a lesser extent, its predecessor MOZAIC), form the starting point of the project. The main objective of this project is to gain a better understanding of the nature of ISSRs, using in-situ observations, by addressing three types of knowledge gaps currently associated with ISSRs. These three knowledge gaps also form the basis of the three main parts of this project:

1. IAGOS data is used to evaluate the current ability of atmospheric models to simulate ISSRs, by using data generated by the ECHAM5 atmospheric model, and analysing its agreement with IAGOS

2. Similarly, IAGOS data is used to evaluate the current ability of weather models to predict ISSRs, by using data from the ERA5 reanalysis model, and analysing its agreement with IAGOS

3. Finally, IAGOS data over a period of 10 years to investigate the temporal evolution of ISSRs. In particular, changes due to natural causes such as seasonality, but also anthropogenic causes like climate change are interesting to look at during this part of the project

The rest of this report broadly follows the structure and order of the aforementioned research objectives.

3.2 Relevance of the research

The results of the research may benefit the mitigation of aviation climate effects, by contributing to a better understanding of not only the nature of ISSRs, but also to understand the current ability to model and simulate ISSRs. Understanding the current strengths, weaknesses and biases associated with the modelling of ISSRs might help in improving the ability to simulate and predict (persistent) contrail formation. In the longer term, such predictions could be used in aircraft maneuvering strategies in order to avoid ISSRs and thereby avoid causing persistent contrail and contrail cirrus formation.

It should be noted that some trade-off exists between the climate benefits of avoiding persistent contrail and contrail cirrus formation by avoiding ISSRs, and the costs associated with the maneuvers that would achieve that. That is, there may be cases where the costs of a maneuver outweigh the benefits of avoiding the ISSR in question. It is therefore not always the most beneficial option to avoid ISSRs entirely. In a later stage, the radiative forcing associated with an aircraft flying through an ISSR could be accurately predicted and set off against the radiative forcing induced by the avoidance maneuver, based on which an optimal decision could be made. Additional economic costs due to increased fuel burnt and flight time from a maneuver may also

play a role in this trade-off.

The fact that there are costs associated with maneuvers to avoid ISSRs also underlines the usefulness of addressing those cases in which a given simulation may indicate contrail formation, when in reality these conditions are not present (a 'false alarm'). Such a case is undesirable, just like its inverse (a 'miss'), due to the fact that a maneuver may be performed unnecessarily in response, which would lead to unnecessary increased costs, both economic and climate-related. For this reason, it is decided to include in the analysis of ECHAM5 and ERA5 a more general evaluation of their ability to model humidity relative to ice and temperature. Initially, the research plan was to focus on sampling from IAGOS measurements conditioned for contrail formation and finding out whether the model under investigation would also indicate contrail formation conditions. This is still part of the analysis of ECHAM5 and ERA5, however a more general analysis with data which is not conditioned specifically for contrails is also included, which would investigate also these 'false alarm' discrepancies between model and reality.

The final part of the research, the temporal evolution analysis of ISSRs, can contribute to a better understanding of the temporal trends that may occur within the properties of ISSRs. A good understanding of how the properties of ISSRs vary over time, can feed into the modelling of ISSRs and possibly serve to verify modelling and simulation efforts of ISSRs. Not only seasonality is investigated, but also evolution over the course of several years. The latter is especially interesting in light of climate change and its possible effects on ISSRs.

4 IAGOS observational data

4.1 About IAGOS

The observational data used for the project will be retrieved from IAGOS, which stands for In-service Aircraft for a Global Observing System. IAGOS is a project which collects atmospheric measurements on a global scale, by equipping commercial aircraft with scientific instrumentation. The resulting data can be used to study and monitor the Earth's atmosphere, its composition and chemistry. In particular, the data are valuable for studying air quality and climate change. Insight into the Earth's changing atmosphere helps policy makers to make informed decisions in addressing and mitigating climate change. The data gathered by IAGOS also helps improve the understanding of meteorological conditions in the troposphere and lower stratosphere, which in turn can result in improved weather forecasts to avoid flying through severe weather, validation of existing weather, climate and air quality models, as well as for the purpose of avoiding regions with suitable conditions for contrail formation[46]. The IAGOS project has operated since 2011 and combines the benefits of the infrastructure of commercial aviation on a global scale with the expertise of scientific institutions[19]. IAGOS data sets are available for download online.

IAGOS-CORE builds upon the former Measurement of Ozone and Water Vapour on Airbus In-service Aircraft (MOZAIC) project, which was active from 1994 until 2009 and consisted of one package. IAGOS-CORE consists of two packages, the first of which is installed on all IAGOS aircraft and conducts ozone, carbon monoxide, humidity and cloud particle measurements. Package 2 is an additional instrument for which there are currently five options: package 2a measures total odd nitrogen (NO_y), package 2b nitrogen oxides (NO_x), package 2c aerosol, package 2d greenhouse gases (CO_2 and CH_4) and package 2e aerosols and nitrogen dioxide (NO_2) to assess air quality[24]. Only one instrument of package 2 can be installed on a given aircraft at a time. To facilitate the measurements, a plate with inlet probes is mounted on the aircraft fuselage. Cloud particle measurements are taken by a Backscatter Cloud Probe (BCP), also present on the plate. The IAGOS Humidity Sensor accommodates the measuring of ambient relative humidity and temperature[25]. IAGOS-CORE measurements are quasi-continuous and provide large geographical coverage, due to its presence on commercial aircraft of several airlines.

IAGOS-CARIBIC (Civil Aircraft for the Regular Investigation of the Atmosphere Based on an Instrument Container) provides measurements of about 100 different species, using a special air freight container filled with scientific instrumentation. This container flies aboard the cargo bay of an Airbus A340-600 operated by Lufthansa about once per month. Measurements like ozone, water vapour, carbon monoxide and dust particles are performed in-fight. Air samples are also collected, for later laboratory research into species like greenhouse gases, hydrocarbons and fluorocarbons. A complex inlet probe is mounted on the aircraft, connecting to the scientific equipment inside the container. IAGOS-CARIBIC provides a more detailed look into atmospheric composition, however at a lower geographical and temporal coverage due to its limited operating window. The container operates about 10 to 12 times per year, each time for four consecutive long-haul flights [23].

4.2 IAGOS data

The data used for this project come from the IAGOS-CORE project, as well as its predecessor, MOZAIC (for the ISSR time evolution analysis).

4.2.1 Data format

The IAGOS datasets are delivered as a timeseries, with each file containing data for one flight. The data are stored in the NetCDF4 format. The NetCDF (Network Common Data Form) format is a common choice for storing multidimensional data such as climate and meteorology data. It is especially suitable for this purpose due to the fact that it is array-oriented and capable of storing large amounts of data, by storing data in the HDF5 (Hierarchical Data Format) format[34]. NetCDF files can be easily accessed and read in Python by importing the NetCDF package. It also enables the user to access the file metadata such as dimensions, measurement units and variable names ('keys'). Given that the IAGOS files are time series, each variable depends only on the time dimension ('UTC-time'). Measurements are taken every 4 seconds in the case of both IAGOS-CORE and MOZAIC datasets.

4.2.2 Data selection

The year 2018 was selected for the comparison of IAGOS data with the ECHAM5 atmospheric and the ERA5 reanalysis models. This is because it is a relatively recent year, however still before the COVID-19 pandemic which disrupted global aviation. It is also a year for which data are available in IAGOS-CORE, ECHAM5 and ERA5, which are all necessary for the analysis.

Within the IAGOS online data base, the user can select several filters. When selecting for all measured variables and all longitudes and latitudes (i.e. all flights recorded, regardless of location), a total of 4006 flights were found for the year 2018. All flights were downloaded for the analysis. Each file may store different variables, depending on what instrumentation (package) the IAGOS aircraft was carrying during the flight corresponding flight. When assessing the acquired flight files, the relevant variables for the project are specified, selected and stored for analysis:

- The **file name** contains the day of take-off of the flight, which is selected and stored for the later analysis. This will later be necessary to be able to access the correct simulated values within ECHAM5 and ERA5.
- Time (**'UTC-time'**) in seconds since midnight of the day of take-off.
- Longitude (**'lon'**) in degrees east [-180,180]. ECHAM5 and ERA5 measure longitude in degrees east, from 0 to 360. It is decided to correct the IAGOS longitude values into the ECHAM5 and ERA5 system for the comparison, as this will have less impact on the subsequent processing and analysis than adjusting the ECHAM5 and ERA longitude system.
- Latitude (**'lat'**) in degrees north [-90,90].
- Temperature (**'air-temp-AC'** or **'air-temp-P1'**) in K. The 'air-temp-P1' variable also has an associated **air-temp-P1-error**, **air-temp-P1-process-flag**, **air-temp-P1-validity-flag** and is therefore chosen over 'air-temp-AC'.
- Air pressure in Pa (**'air-press-AC')**, and its validity (**'air-press-AC-validity-flag'**).
- Relative humidity relative to liquid water (**'RHL-P1'**) and relative to ice (**'RHI-P1'**). Both variables also have an associated error (**'RHL-P1-error'** and **'RHI-P1-error'**), processing level (**'RHL-P1-process-flag'** and **'RHI-P1-process-flag'**) and validity (**'RHL-P1-validity-flag'** and **'RHI-P1-validity-flag'**).
- Barometric altitude (**baro-alt-AC**) in meters

4.2.3 Data quality

Within IAGOS, the measured properties contain several indicators of their quality and validity. First, there is the data processing flag, which indicates the extent to which the provided data has undergone transformations, quality checks, or been derived from other data by users or partners of IAGOS, or the wider scientific community. The processing levels range from level 1 (raw data) to level 4 (elaborated products)[20]. All data used in this project is of level 2, final quality controlled observational data, and the main IAGOS product.

Then, there is the validity flag associated with the data gathered by IAGOS instrumentation (in this project, the air temperature, air pressure, humidity relative to liquid water and humidity relative to ice. These flags have five possible values: 0 ('good'), 2 ('limited'), 3 ('erroneous'), 4 ('not validated'), 7 ('missing values'). In the latter case, the associated (missing) measurement is masked in the time series. Most of the data used for this project are selected to be of label 0 ('good'), however due to data size limitations in the ISSR time evolution analysis, also data of 'limited' quality is selected. Given that these data are known to have failed non-critical documented metrics or subjective tests[21], it still seems reasonable to include them when other data does not result in enough samples for analysis. Data of worse quality is not selected for analysis at any point in the project.

Finally, the uncertainty associated with a measurement is given in terms of its standard error. The uncertainty is associated with the error of the sensor used for the measurement. For this project, the relative humidity is most impactful for analysis. IAGOS-CORE measures relative humidity using a capacitive relative humidity sensor, part of package 1. Temperature is measured at the humidity sensing surface using a platinum resistance sensor[46]. The humidity sensor can be deployed autonomously for up to 2 months and its data transmission takes place post-flight[25]. MOZAIC, the predecessor of IAGOS-CORE of which some data is also used in the temporal evolution analysis of contrails, featured a similar sensor for its relative humidity measurements.

A preliminary analysis is performed to decide on how to approach some issues arising from the RHI error. From a preliminary gathering of sample data, it appears that for some relative humidity measurements which pass the quality requirement (i.e. they are non-masked and have a 'good' validity label), the associated RH error is masked (missing). About 2.73% of the errors associated with the investigated RHI values are masked. Upon further examining specifically these RH values with masked errors versus those which have a specified associated error value, it appears that those RH values with masked errors are much more likely to be (extreme) outliers than RH values with specified errors. Figure 10 shows RHI values with masked errors, versus RHIs with non-masked errors, where the RHIs with masked errors reach values of over 1100%, as well as negative values that go towards -300%. The RHI values associated with non-masked values stay within a much more reasonable range, with outliers of up to about 190%, and no values in the negative. The values associated with masked errors do not seem likely to be accurate and may indicate that RHI values with masked errors are not reliable or suitable for analysis. Moreover, there is no way to meaningfully use a missing RH error value in further analysis. This is why it is decided to only consider measurement points with non-masked RH error values for further analysis. This is ensured by requiring the RHIerror associated with the current index to be larger than 0.

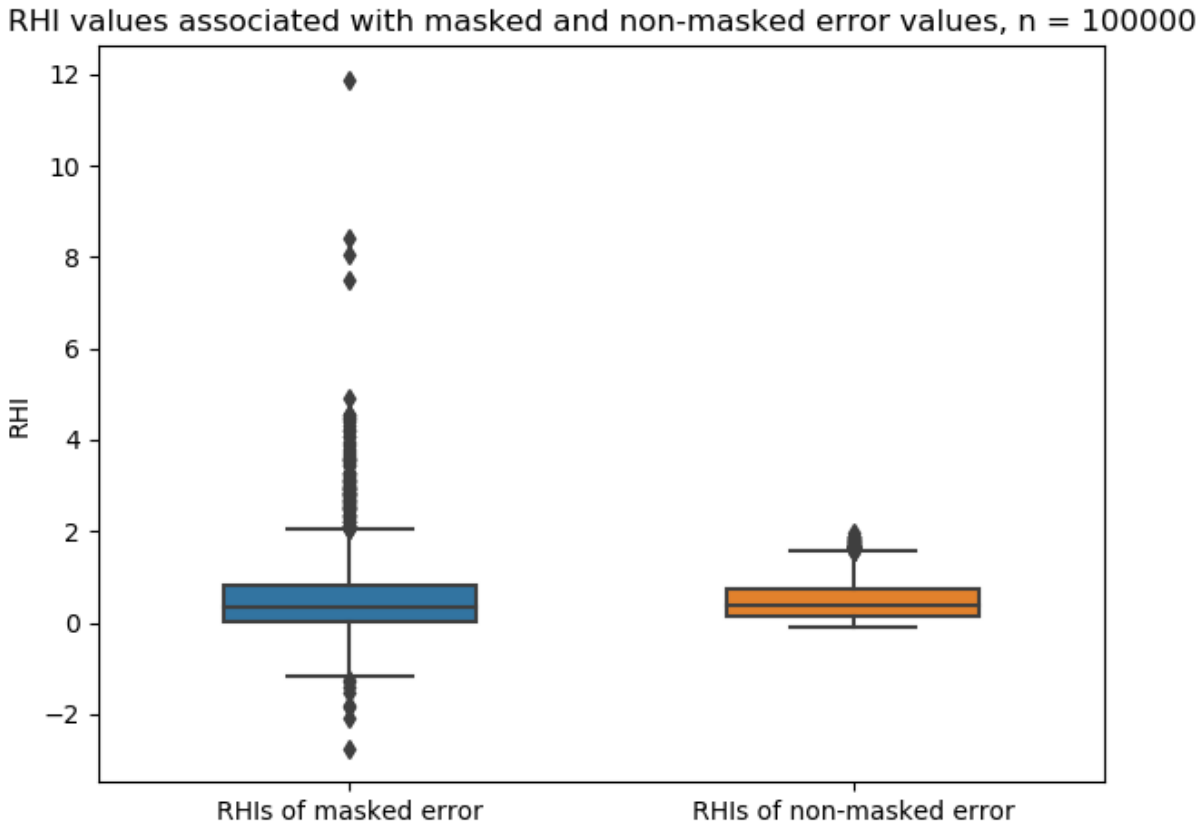

Figure 10: IAGOS RHI values associated with masked versus non-masked values, n = 100.000

To summarize, the data quality requirements for the gathering of IAGOS data for analysis are as follows:

- Selected data points must feature a processing label 2, indicating final quality controlled observational data
- Only temperature, pressure and RHI values with validity flag 0 ('good') were selected. This also immediately filters out the missing (masked) values.
- A non-masked RHI error value is selected for by requiring that the RHI error > 0 (value is always positive), in order to exclude extreme and unlikely outliers and also to be able to further use the RHI error in further analysis.

4.3 Preliminary analysis and data gathering

The downloaded IAGOS flights were used to gather data for further analysis and for the evaluation of ECHAM5 and ERA5. The first assessments were performed on single flights or flights over one month, before expanding to all 2018 flights. Extensive documentation on the data is available in both the metadata as well as online on the IAGOS website.

From a first preliminary analysis, it appears that not all IAGOS flights record relative humidity: of all 2018 flights, three did not contain relative humidity observations. Without relative humidity, there is no way to assess whether conditions suitable for contrail formation were present. These three flights were therefore skipped during the data gathering. 4003 recorded flights over

2018 remained.

Three sets of data were gathered in total from the 4003 IAGOS data files for the analysis. Two sets of data are gathered for the purpose of assessing the ability of ECHAM5 and ERA5 to simulate temperature and humidity relative to ice. Both of these data sets are not selected for contrails, however they are selected for a low enough temperature, at which the relative humidity value in ECHAM5 and ERA5 denotes the humidity relative to ice. 65.0% of data points are found to be suitable for the evaluation of ECHAM5, whereas 69.0% is found to be suitable for ERA5. These data will be used later to evaluate the general ability of ECHAM5 and ERA5 to simulate humidity relative to ice and temperature, the two most impactful conditions for persistent contrail formation. Not yet selecting for contrails is useful to gain a general idea of the ability of ECHAM5 and ERA5 to simulate the variables which play a role in contrail formation, some biases which may exist, and the strengths and weaknesses of each model.

The third dataset collected is conditioned for contrail formation conditions. This dataset is used to evaluate both ECHAM5 and ERA5 on their ability to simulate persistent contrail formation, specifically. The following conditions are imposed for the formation of a new persistent contrail, in addition to the previously described data quality requirements:

- The surrounding air is in a state of ice supersaturation, that is, the variable 'RHI' exceeds 1.
- The surrounding air has a temperature below -38 degrees Celsius, or 235.15 Kelvin.
- The surrounding air is subsaturated with respect to liquid water, i.e. the variable 'RHL' is below 1.

Based on some preliminary findings of the IAGOS data, a few steps were taken to aid in a more efficient processing of data going forward. First, it was found that out of the three conditions necessary for new persistent contrail formation, ice supersaturation is the condition that occurs most rarely, at about 5.62% of all 2018 data points. It is therefore most beneficial in terms of processing time to first select for this condition. The temperature threshold is met in about 67.5% of data points, and water subsaturation is present in 98.4% of data points. This is therefore the order in which each criterion is considered to check for new persistent contrails.

From analysing the 2018 flights, it is found that all conditions for persistent contrail formation of the recorded flights in this year occur between 178.0 and 479.8 hPa. This knowledge can be used to manage and slim down the large datasets of the models, specifically ERA5, to the relevant pressure levels, which benefits processing time and effort, as well as the size of the data files to be obtained and downloaded.

Further analysis of the 2018 contrails shows that about 5.89% of all measurements indicate conditions suitable for contrail formation, which is similar to the figure of ice supersaturation, the most stringent requirement for contrail formation.

Verification and validation

The contrail measurements recorded are plotted geographically in order to verify the samples as well as to check for the level of representation of IAGOS flight coverage over 2018. Throughout the project, the Basemap package is used to visualize results geographically. Figure 11 shows the gathered measurements, whereas Figure 12 shows the global IAGOS flight coverage since 2011.

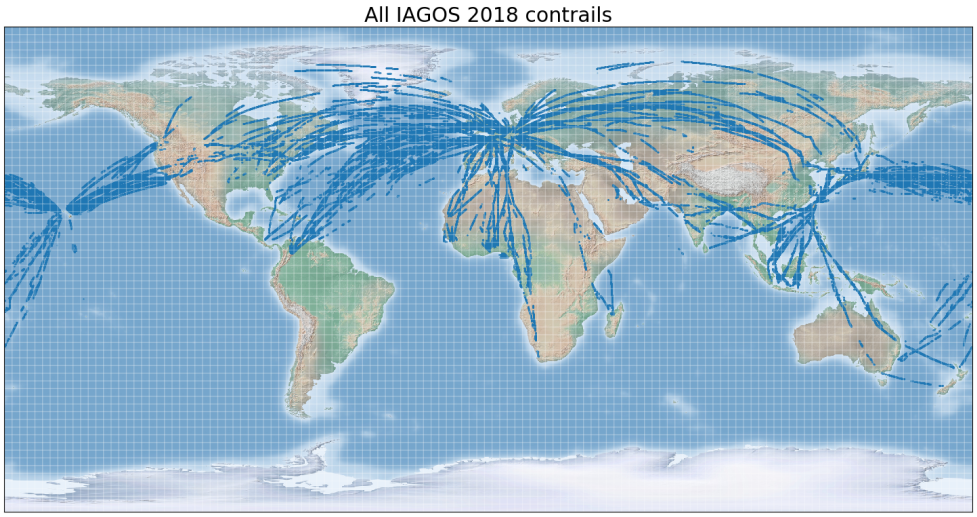

Figure 11: All 2018 contrails observed by IAGOS-CORE

In 2018, the IAGOS-CORE fleet consisted of 9 aircraft, of which 2 were operated by AirFrance, 3 by Lufthansa, 2 by China Airlines, 1 by Hawaiian Airlines, and 1 by Cathay Pacific[22]. The Iberia aircraft mentioned in Figure 12 operated until 2016, which explains the lack of contrail coverage along its shown flights. The Air Canada aircraft only started operating with IAGOS-CORE in 2023, which also explains why its flights do not show up on the 2018 contrail coverage figure. Taking this into account, both figures show good agreement and it is therefore assumed that the samples gathered are representative of the 2018 IAGOS flights and the areas that these flights were able to cover.

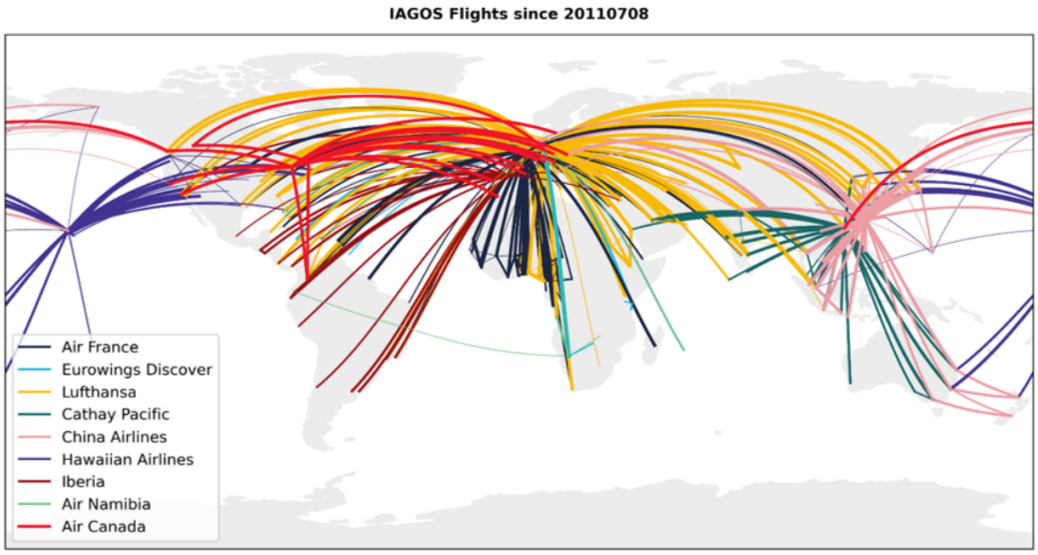

Figure 12: IAGOS flight coverage since 2011, from [26]

The IAGOS in-flight measurements form the basis of this project and a starting point for the analysis in the following sections. It should be acknowledged that these measurements are limited by the flight coverage of the IAGOS fleet in 2018, as visualized broadly in Figure 11. The limitations in geographical coverage may therefore impact the extent of how representative the findings of this project are, when applied generally and on a global level.

5 IAGOS-ECHAM5 comparison

5.1 About ECHAM5

The ECHAM/MESSy Atmospheric Chemistry (EMAC) model is a global chemistry and climate simulation model which combines the Modular Earth Submodel System (MESSy) as a framework and the 5th generation of the European Centre HAMburg general circulation model (ECHAM5) as its base model. MESSy was developed by a consortium of German research centers and universities and includes interface components as well as submodels which are capable of simulating various physical and chemical processes within the Earth's climate system, as well as interactions with land and ocean surfaces and anthropogenic influences[28]. ECHAM5 was developed by the Max Planck Institute for Meteorology and builds upon forecast models created by the European Centre for Medium-Range Weather Forecasts (ECMWF)[45]. ECHAM is capable of calculating weather system development such as temperature, wind, and clouds, as well as atmospheric chemical composition. Within EMAC, it serves as the core atmospheric model and can be used at different horizontal and vertical resolutions. By default, EMAC can resolve the atmosphere at a resolution of 10 hPa, however for studying the stratosphere and lower mesosphere, this can be reconfigured to 0.01 hPa.

5.2 ECHAM5 data

The project uses data from ECHAM5, the base model of EMAC. The data were provided internally by the Aircraft Noise and Climate Effects (ANCE) department at the faculty of Aerospace Engineering.

5.2.1 Data format

ECHAM5 can feature several resolutions. For this project, the truncation level T42 is used, resulting in 128 longitude and 64 latitude points, corresponding to a spatial resolution of about 2.8° x 2.8°. The model features 31 vertical hybrid pressure levels, which at flight level feature a vertical resolution of about 1 km[64]. The level indexes (1-31) are in order from low to high pressure (or high to low altitudes). The time interval is 12 hours, resulting in an instantaneous simulation at midnight and noon of each day of 2018. The ECHAM5 data, like the observational data from IAGOS, are delivered in the NetCDF format.

5.2.2 Data selection

The year 2018 was selected and simulated, resulting in 12 data files, one for each month. The files are merged in Python along the time dimension, to allow for a smoother analysis when taking random samples throughout the year.

5.2.3 Preliminary analysis

The ECHAM5 files feature four dimensions: time in a 'YYYYMMDD' format, longitude ('lon'), latitude ('lat'), and 31 hybrid vertical levels ('lev'). The relevant variables for this project are pressure, temperature, geopotential, and relative humidity. It is not immediately apparent from the documentation in the ECHAM files what exactly this latter variable contains (i.e. humidity relative to liquid water, ice, or some combination of the two). It appears that in ECHAM5, the relative humidity variable refers to humidity relative to liquid water when the grid-box mean temperature is 0° C or higher. Below -35° C, it refers to humidity relative to ice. In between these temperatures, a parameterization is used, in which the relative humidity used is dependent on whether or not ice is present in the grid box[48].

Verification of the model

A general vertical profile of temperature and relative humidity within ECHAM5 is constructed and compared with profiles from literature, in order to verify broadly the simulated values of ECHAM5.

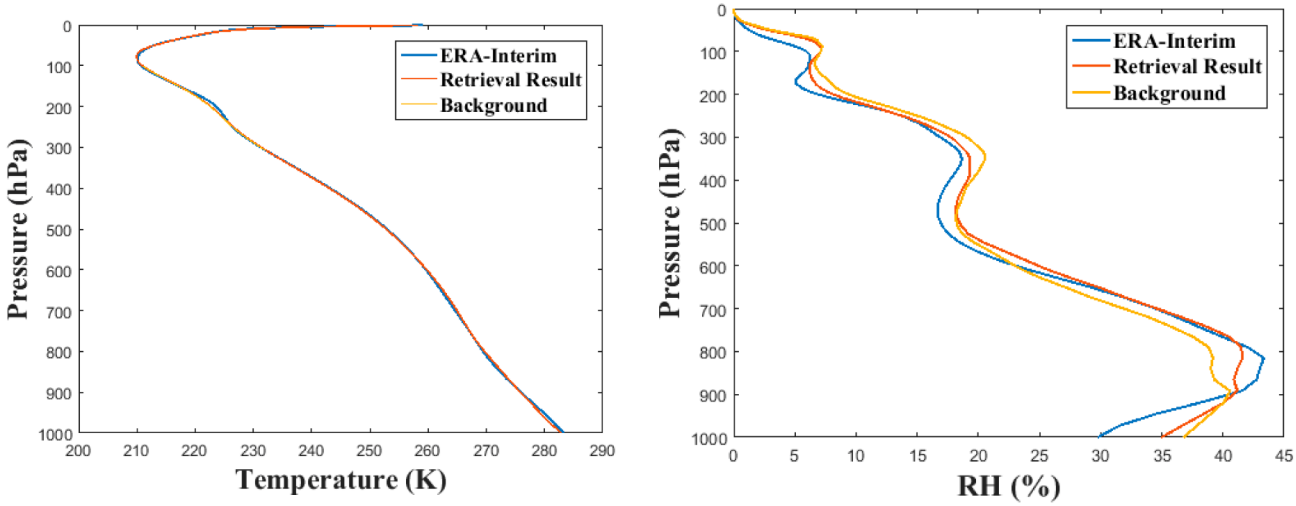

(a) RH and temperature profile as a function of air pressure. From [68]

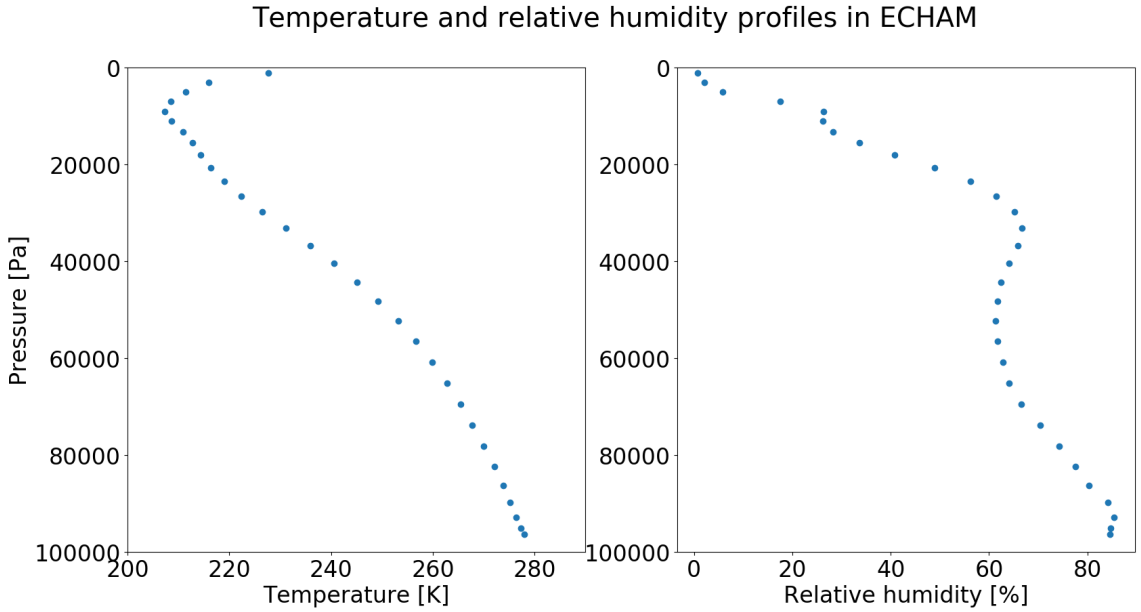

(b) RH and temperature profile in ECHAM as a function of air pressure

Figure 13: A comparison of RH and temperature vertical profiles between literature and data from the ECHAM5 atmospheric model

Figure 13b shows the constructed ECHAM profiles, whereas Figure 23a shows profiles from literature. The ECHAM5 profiles seem to agree well with literature, however they do show higher relative humidity at low altitudes. At the altitudes relevant for the project, this difference is less pronounced, but still somewhat present. Additionally, ECHAM5 appears to return lower temperatures than the reference values seen in literature. Both factors may have an impact on the results of the analysis.

5.3 Methodology

The approach for assessing the ability of ECHAM5 to accurately simulate temperature and humidity relative to ice, the most important indicators of whether or not (persistent) contrail formation is possible, is described in this section. The previously gathered IAGOS data are used for this purpose, using both the data gathered which was not conditioned for contrails (part 1 of the analysis) and later the data which was conditioned for contrail formation (part 2). The general approach taken in both parts of the analysis is to take a number of random samples from the gathered IAGOS measurements, and find the corresponding conditions simulated by ECHAM5 for each measurement, specifically the simulated values for those conditions which influence contrail formation: temperature and relative humidity. Comparing and observing discrepancies between the observed and simulated values can give insight into how well the ECHAM5 model is currently able to simulate contrail formation.

This section describes the approach taken to finding the corresponding ECHAM5 temperature and RHI values to a given IAGOS sample. Given that these variables are stored in four-dimensional arrays in ECHAM5, four indices are to be found for each sample: time, longitude, latitude and the vertical level.

5.3.1 Time dimension

The first step taken is to find the corresponding time index within ECHAM5 for the recorded contrail measurement. IAGOS records time in its variable $'UTC\_time'$, in terms of seconds after midnight since the day of takeoff. The day of takeoff is contained within the file title, which can be read by Python and recorded. ECHAM5 files contain time periods in a dimension called $'YYYYMMDD'$, which lists the 12-hour periods in terms of the day in a year, month, day format. Each day contains a simulation at midnight, denoted by a .0 after the YYYYMMDD value (e.g. 20180101.0 for the simulation of January 1st, 2018 at midnight) and a simulation at noon denoted with a .5 after its YYYYMMDD (e.g. 20180101.5 for noon of January 1st, 2018).

The ECHAM5 model delivers instantaneous simulations with a 12-hour time interval. A preliminary investigation of the temporal evolution of the relative humidity and temperature at a given latitude, longitude and pressure level, found a large variability over time between instantaneous values. The question arises whether each ECHAM5 value can be considered representative for the full 12-hour interval it is associated with, or whether an adjustment should be made to account for the relatively coarse temporal resolution of the ECHAM5 data.

In order to deal with this issue, a new variable called ΔT is introduced. This variable serves to limit the number of IAGOS contrail samples that fall very far outside of the instantaneous time stamps for which ECHAM5 simulates a temperature and relative humidity. When the variable is set (to a value of up to 6 hours), those IAGOS samples that fall outside of the ECHAM5 simulation timestamp - ΔT and the timestamp + ΔT are discarded from the analysis. For instance, if the variable is set to 3, the IAGOS samples that fall between noon plus and minus 3 hours, and midnight plus and minus 3 hours, are taken into account for analysis. The rest are considered too far off the ECHAM5 simulations in terms of time to be suitable for comparison, and therefore discarded. The ΔT variable can be adjusted and therefore a trade-off exists between number of IAGOS samples available for analysis, versus temporal proximity of the used IAGOS samples to the ECHAM5 simulations. That is, a low ΔT results in fewer IAGOS samples for analysis, however they lie closer to the ECHAM5 simulation timestamp and may therefore be more representative, and vice versa. The number of IAGOS samples before and after introducing ΔT are compared in order to record how many samples are lost.

Each IAGOS measurement that falls within the ΔT interval is binned according to its corresponding timestamp (i.e. the closest simulation in ECHAM5). From this, the time index is found that indicates the temporal location of the IAGOS measurement within ECHAM5. The code also accounts for longer flights which may feature data points that would fall into different bins, i.e. points that would correspond to different sequential simulation timestamps within ECHAM5. Flights that extend overnight are also accounted for. Corrections are made in the code for flights that extend over different months (e.g. correcting a time index from 20180132.0 to 20180201.0). None of the analysed flights extend into 2019.

5.3.2 Longitude and latitude dimensions

The longitude and latitude of a selected sample is taken by a Python function and the corresponding indices within ECHAM5 are found and recorded. It is chosen not to use interpolation, due to the fact that the geographical resolution in terms of longitude and latitude in ECHAM5 is not very coarse. In addition, a preliminary analysis did not show a large variation between longitude and latitude points in terms of their simulated temperature and humidity relative to ice.

5.3.3 Vertical dimension

Several methods were considered for finding the approximate RHI and temperature values in the vertical dimension. The ECHAM5 data sets have 31 vertical levels in total, which may be too coarse for finding an accurate representation at the desired pressure level. The interpolation function interplevel is therefore introduced. This function is part of the wrf-python package, which is part of the Weather Research and Forecasting (WRF) model. The function takes a specified vertical level and interpolates within a three-dimensional field to a horizontal plane at this level, using linear interpolation[9].

The pressure and relative humidity and pressure and temperature field, at the previously found timeindex (therefore making each of them a 3D array) are used as input for the interplevel function. The recorded air pressure by IAGOS is entered to indicate the altitude for which the relative humidity and temperature are to be interpolated. The result is a plane at this pressure level, for which the latitude and longitude indexes within ECHAM5 of the given contrail measurement, which have previously been found, are entered. This finally results in an approximation of the relative humidity and temperature that ECHAM5 simulates at the location of the IAGOS data sample. These values are used for the analysis.

5.4 Results

The analysis is first performed for those measurements which were not conditioned for contrail formation conditions. Throughout the project, the humidity relative to ice (RHI) is the more impactful variable, however temperature is also investigated as this condition too plays an important role in contrail formation.

For the present analysis, a ΔT value of 1 hour is used, resulting in the retaining of about 16% of measurements, which is about what is expected when using 1/6 of the time interval. This leaves about 1.870.000 unconditioned measurements and 170.000 contrail measurements to sample from.

5.4.1 General evaluation of temperature and RHI simulation

A sampling was performed on the (non-conditioned for contrails) data gathered from IAGOS, for comparison with ECHAM5. Figure 14 shows the sampled points geographically, which feature a decent level of representation of the 2018 IAGOS flight coverage.

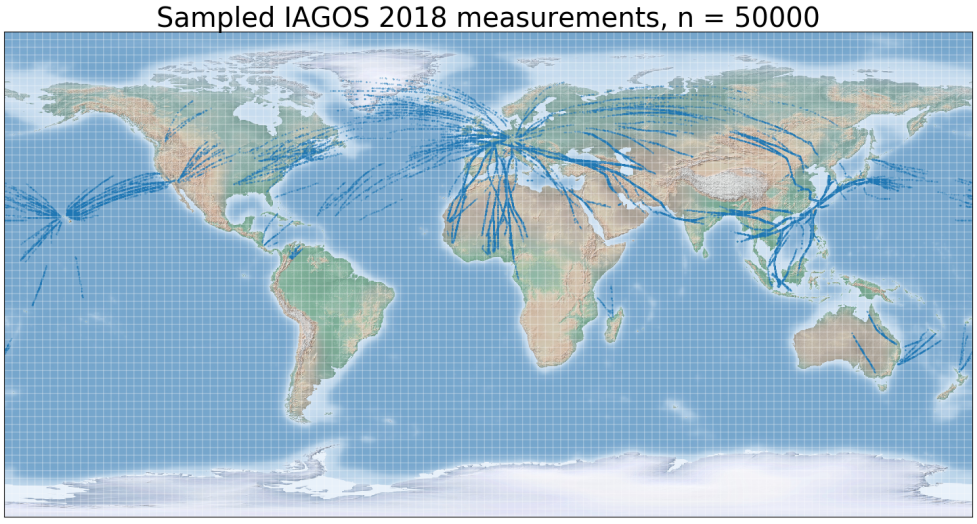

Figure 14: Sampled points from IAGOS for comparison with ECHAM

The RHI and temperature values of ECHAM5 corresponding to the IAGOS samples were approximated using the strategy described in the methodology section. Figure 15 shows the visual distribution of the simulated versus the observed values. The sampled and simulated temperatures seem to agree to some extent, however one interesting thing to note is the apparent underestimation of ECHAM when it comes to temperature. It is possible that this discrepancy stems from IAGOS sensor error, however the same phenomenon was not found with ERA5. The previous model verification also showed an underestimation of temperature in ECHAM5 compared to values from literature.

When it comes to humidity relative to ice, the results are much more scattered. A higher density of points is observed in the bottom left of the figure, suggesting that ECHAM has a decent capability of simulating lower RHI values. In the slightly higher RHI values, more points are located to the left of the x=y diagonal line than to the right, which would indicate that the ECHAM model overestimates RHI between about 40% to just below saturation level. Another higher density region is seen at the horizontal level at simulated RHI = 100%. The density

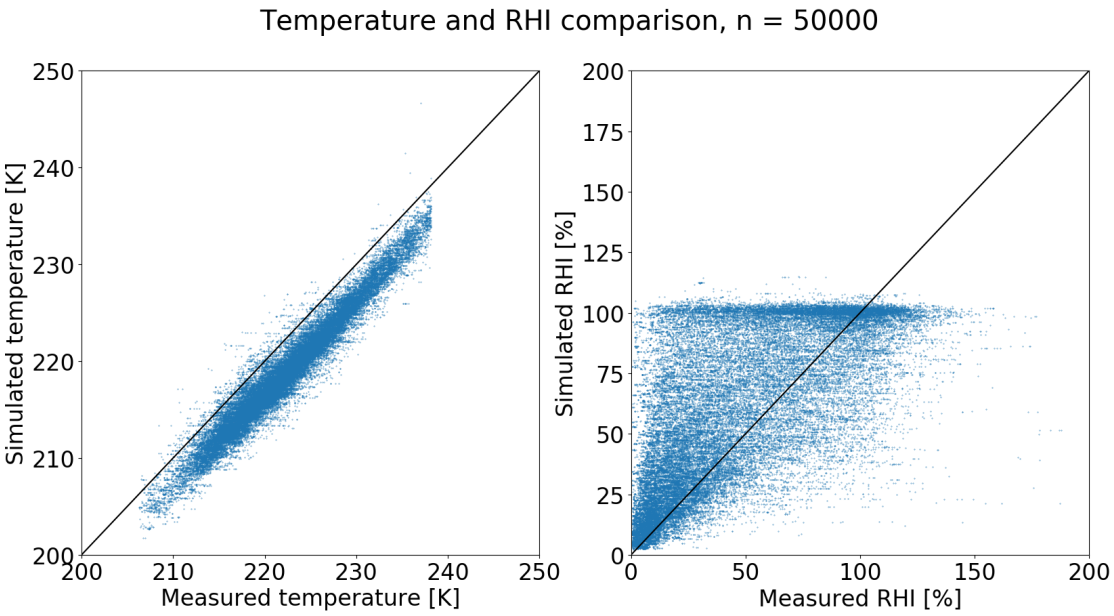

Figure 15: Sampled points for ECHAM; RHI and temperature distributions

region is at its thickest at around (100,100) and extends to the right of the x=y line. This would indicate that ECHAM has difficulty simulating (high values of) ice supersaturation. This is further supported by the presence of points to the right of the x=100% vertical line, far below the x=y diagonal, which indicate a vast RHI underestimation of ECHAM in case of observed (high levels of) ice supersaturation.

The results can also be visualized in the form of boxplots. The same underestimation of temperature by ECHAM is observed in the simulated temperature plot in Figure 16a. The bias results in a difference of about 3.4 K between the means. Boxplots for the measured versus simulated RHI values are shown in Figure 16b. The figures seem to confirm the overestimation of ECHAM for saturation levels below saturation, given the higher mean and higher box of the simulated versus measured RHI values. The difficulty of ECHAM to simulate (high) ice supersaturation levels is also confirmed. Some values above 100% are present (with a maximum of over 175%) however the high supersaturation values observed by IAGOS are not recreated.

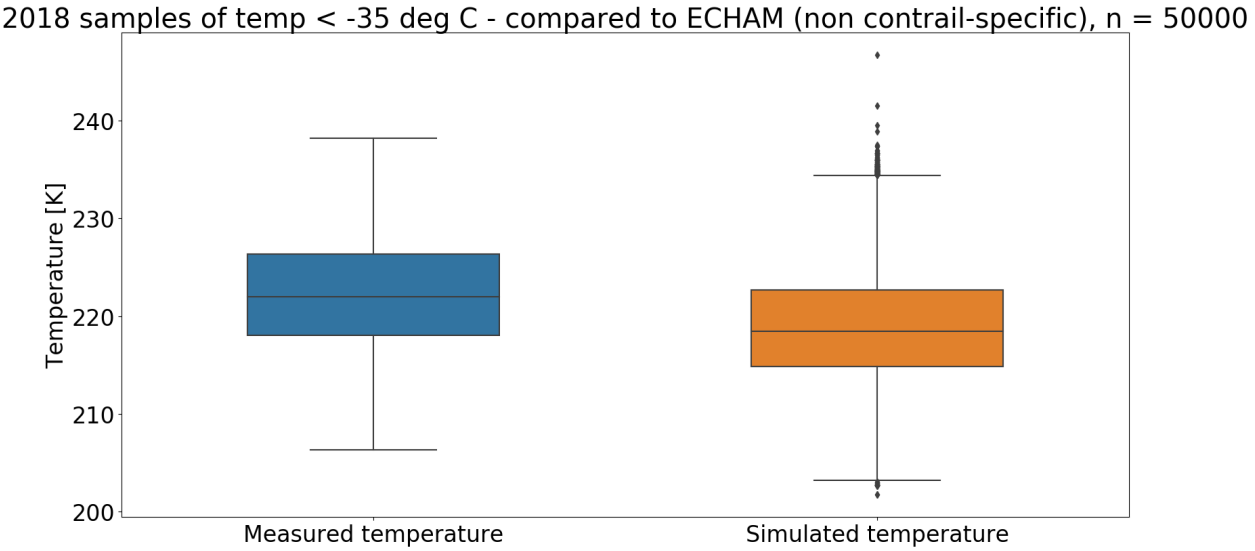

(a) Sampled points for ECHAM; temperature

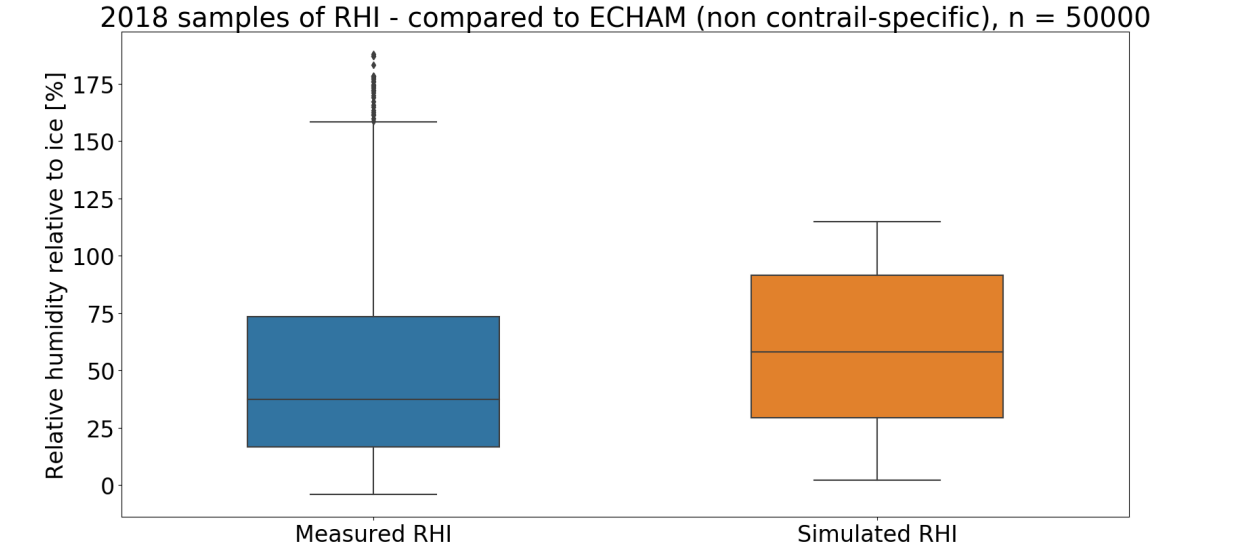

(b) Sampled points for ECHAM; RHI

Figure 16: Temperature and RHI of sampled points; measured versus simulated by ECHAM5

Verification of results

Several papers mention a 'cold bias' within ECHAM5, particularly in the lower stratosphere, which may be the cause of some of the temperature discrepancies found[37]. It seems as if in this research the temperature bias is somewhat constant, though, rather than increasing along temperatures corresponding to that of the stratosphere. It is possible that the tendency of ECHAM5 to overestimate relative humidity below saturation level, could be explained to some extent by its cold bias. Given that lower temperatures correspond with higher relative humidity, these biases in ECHAM5 may be interrelated with each other.

5.4.2 Simulation of contrail formation conditions

One can also investigate the selected samples on whether or not they would indicate persistent contrail formation (using the same requirements as described in the IAGOS section). It can then be determined whether the corresponding ECHAM5 values would indicate persistent contrail formation conditions, and whether there is agreement between IAGOS and ECHAM5. Four possibilities exist: YY denotes a case in which contrail formation conditions were measured by IAGOS, which were also correctly simulated by ECHAM5. YN is a case in which IAGOS indicates contrail formation conditions, but ECHAM5 does not (a 'miss'). NY is a 'false alarm', where IAGOS does not measure contrail formation, but ECHAM5 does simulate it. NN means that neither IAGOS nor ECHAM5 indicated conditions suitable for contrail formation.

Table 1 shows the results for the selected set of samples. A threshold of 90% RHI is currently used to indicate ice supersaturation in ECHAM5. The threshold is used to account for the relatively coarse spatial resolution in ECHAM5, which results in large grid boxes. This means that a grid box with a mean RHI just below 100% is likely to contain some ice supersaturated air parcels, which would be discarded when using a threshold for supersaturation of 100%. Furthermore, recalculation of data and interpolation onto different grids within the model can introduce bias in the relative humidity values[32]. Several other thresholds are implemented later in the sensitivity analysis. The majority of cases feature no contrail formation conditions in either IAGOS or ECHAM. 6.49% of samples feature contrail formation conditions which are correctly simulated by ECHAM5. Interestingly, 19.5% of cases feature an NY discrepancy (no in IAGOS, yes in ECHAM - a false alarm), a significant proportion of the samples. 2.97% feature a YN discrepancy, where IAGOS indicates contrail formation but ECHAM does not (a miss). The following section goes further into the discrepancies found between IAGOS and ECHAM.

n	YY	YN	NY	NN
50000	3245	1486	9767	35502
100%	6.49%	2.97%	19.5%	71.0%

Table 1: Assessment of contrail formation prediction capabilities of ECHAM5

YN discrepancies

1486 YN cases (where IAGOS indicates contrail formation conditions but ECHAM does not) were found in the analysis. 100% of these cases were found to be attributable to the relative humidity; i.e. the simulated relative humidity in ECHAM5 was not high enough to indicate ice supersaturation, even when using the 90% threshold. This makes sense, given the previously mentioned cold bias of ECHAM5. Indeed the plots in Figure 17a show the cold bias of ECHAM relative to IAGOS measured temperature values, resulting in a 2.5K difference between the means.

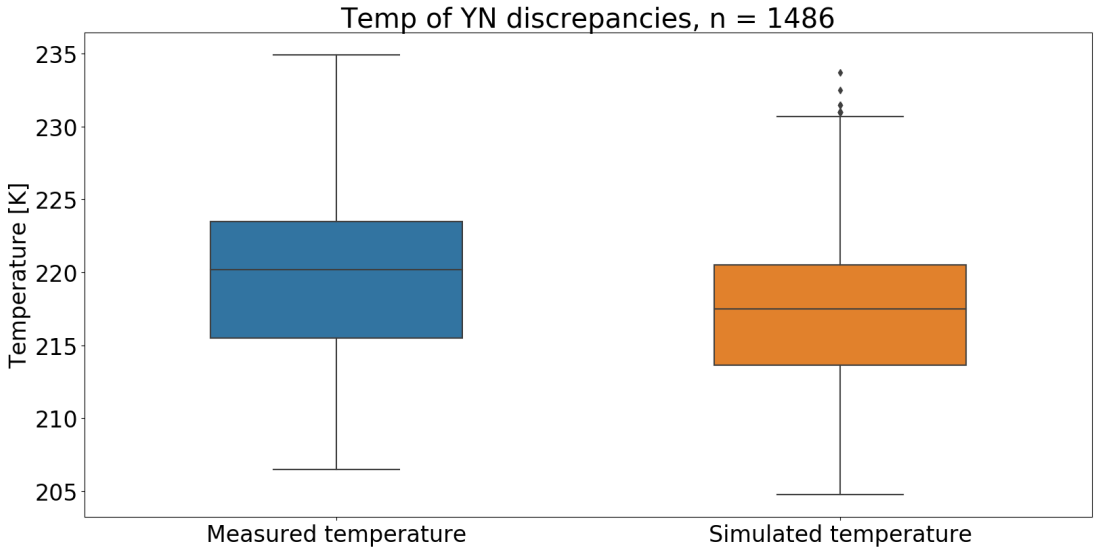

(a) Temperature distribution associated with YN discrepancies

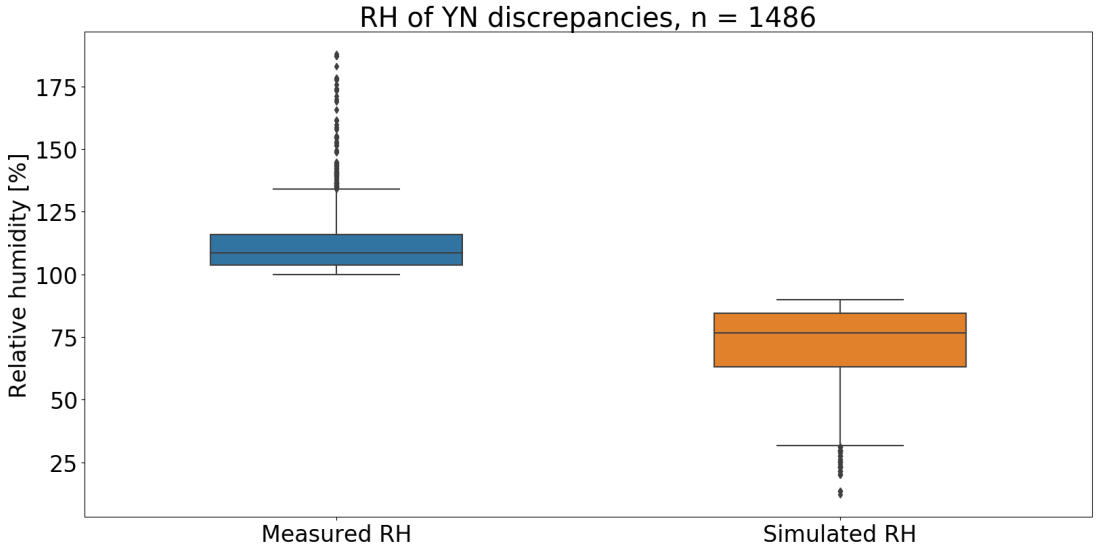

(b) RHI distribution associated with YN discrepancies

Figure 17: Temperature and RHI of YN discrepancies; measured versus simulated by ECHAM5

The RHI values of IAGOS versus ECHAM5 of the YN discrepancies are shown in Figure 17b. It is interesting to note from this figure that the mean RHI simulated by ECHAM5 lies quite significantly below the supersaturation threshold of 90%, at a mean value of 71.9%, versus a mean of 111.6% for the measured values. Again, it appears that ECHAM5 has difficulty simulating (high values of) ice supersaturation and tends to underestimate these values significantly.

NY discrepancies

9767 NY discrepancies (where IAGOS did not indicate contrails, but ECHAM5 did) were found. This is a significant proportion of all samples. It is expected that some of these discrepancies are caused by the RHI threshold of 90%, however it seems from Figure 18b that a significant number of the RHI values simulated by ECHAM5 lie above 100%. It is found that the mean simulated RHI lies at 98.7%, with 43.5% of values above 100% RHI. The measured values are much lower, with the mean at 63.2% and minima reaching down to near-zero values. This indicates that ECHAM5 also has a tendency to overestimate RHI values which in reality lie (significantly) below saturation level. This was previously observed in Figure 15 and Figure 16b, as well.

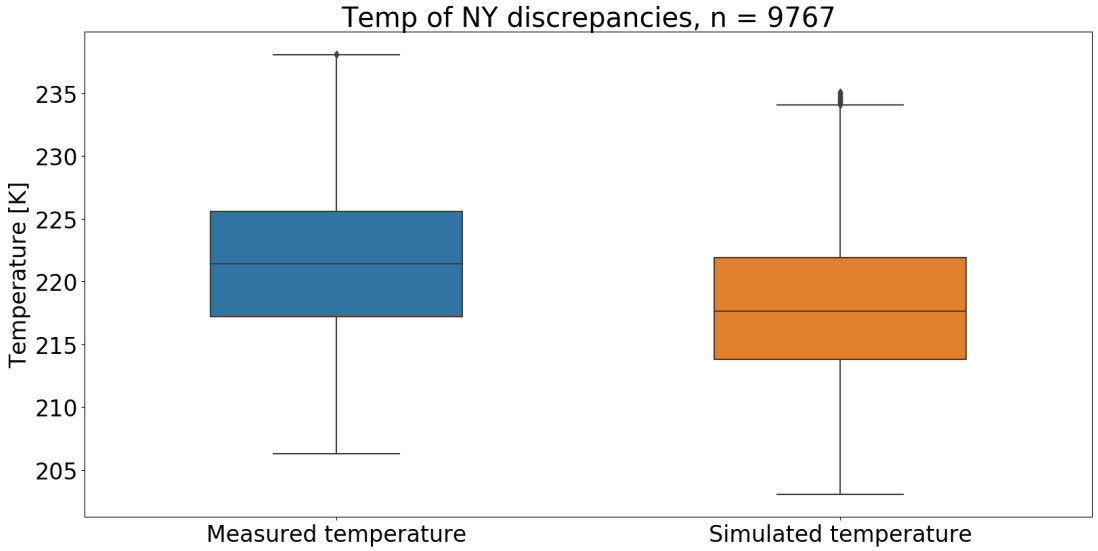

(a) Temperature distribution associated with NY discrepancies

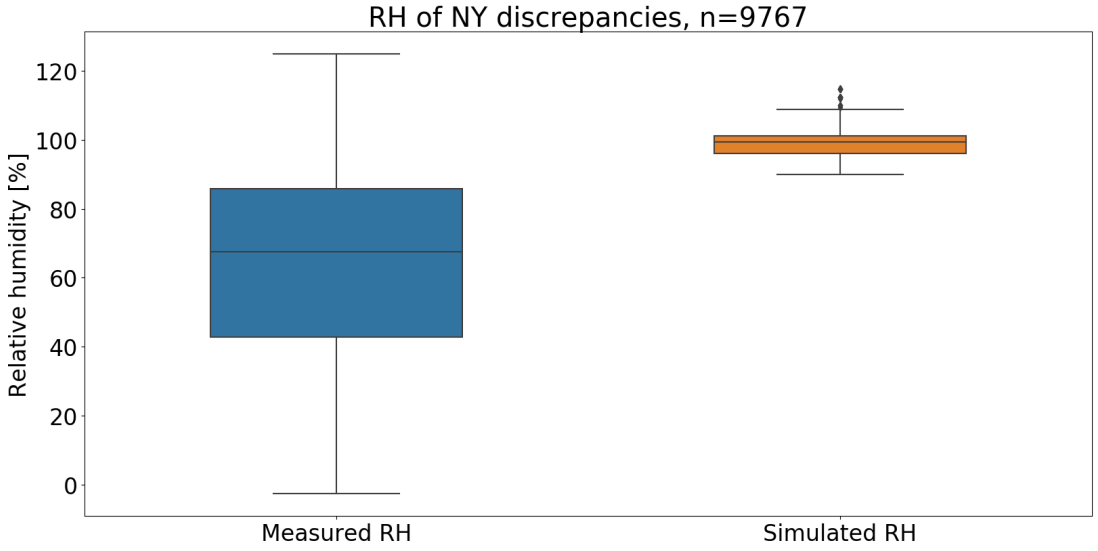

(b) RHI distribution associated with NY discrepancies

Figure 18: Temperature and RHI of NY discrepancies; measured versus simulated by ECHAM5

5.4.3 Sampling for contrails

The ability of ECHAM5 to correctly simulate contrail formation conditions is further evaluated by sampling specifically from the previously gathered 2018 IAGOS measurements conditioned for contrail formation conditions. The same method for finding the approximate values in ECHAM5 as described in the methodology section is used, and a threshold of 90% is set to indicate ice supersaturation within ECHAM5.

It is found that in 68.9% of cases (n=50.000), ECHAM5 correctly predicts the conditions for contrails. In those cases where ECHAM5 is unable to simulate contrail formation conditions, it is always due to an underestimation of RHI. The mean measured RHI value at 112.1% while the mean simulated RHI is 90.5%. Figure 19a shows the distribution of measured RHI from the samples versus the simulated RHI by ECHAM5.

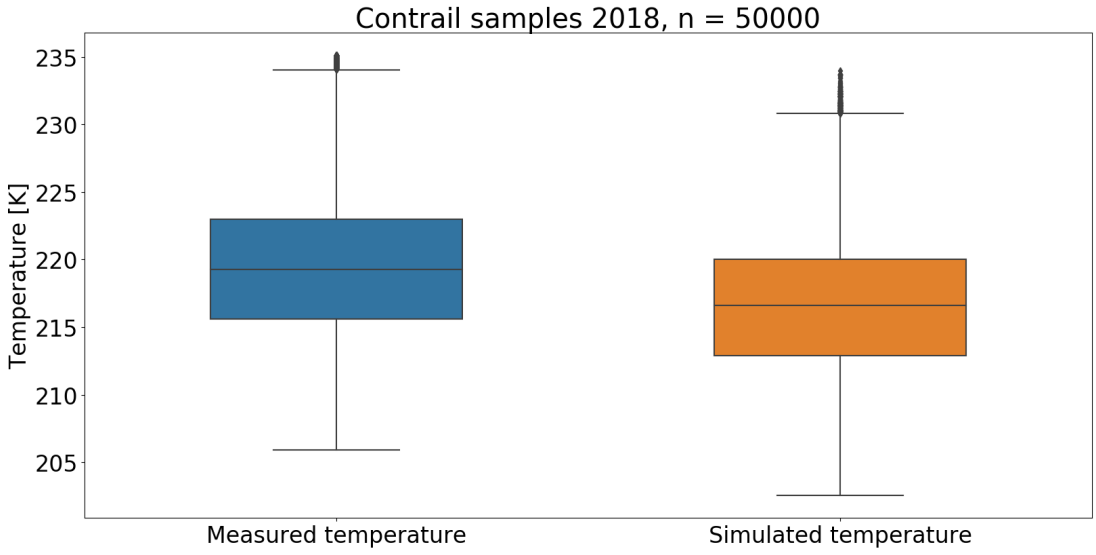

(a) Contrails ECHAM5 RH

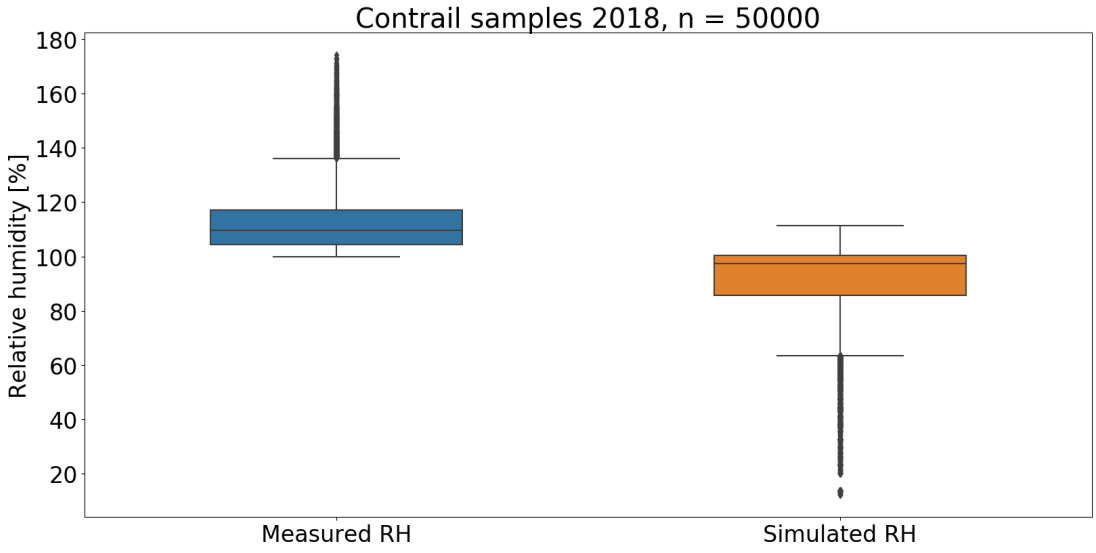

(b) Contrails ECHAM5 temperature

Figure 19: Temperature and RHI of NY discrepancies; measured versus simulated by ECHAM5

Figure 19b shows the temperature distributions for the sampled data. The cold bias of ECHAM5 is visible again, which may be part of the reason why there are no cases where ECHAM5 was unable to indicate contrail formation due to a too high temperature.

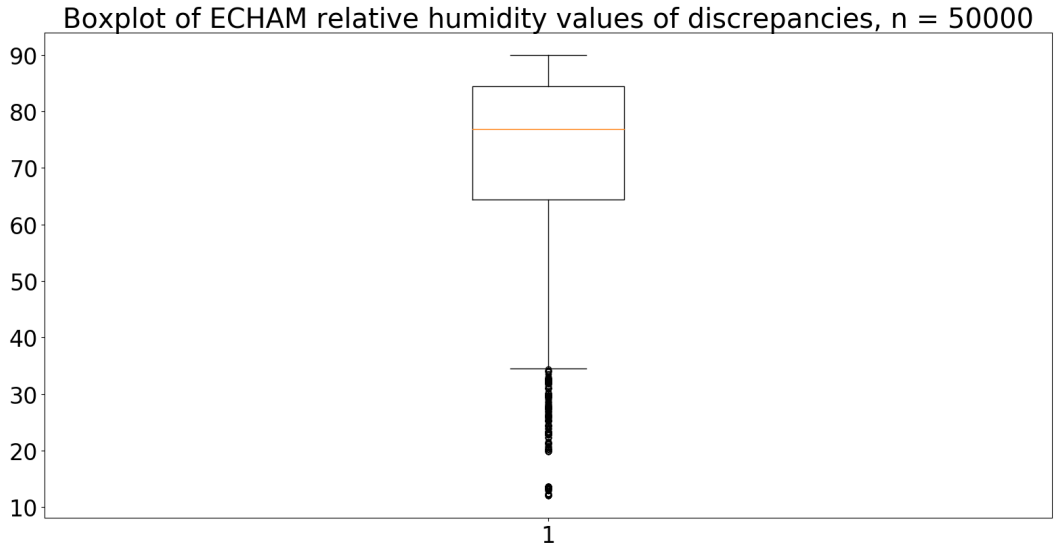

Figure 20: Incorrect simulated RH values associated with contrail samples

Figure 20 shows the distribution of RHI values simulated by ECHAM5 for those cases where a discrepancy was found. Interestingly, the RHI values lie quite significantly below the 90% threshold, at a mean of 72.0% and a median of 76.7%.

5.4.4 Sensitivity analysis

A sensitivity analysis is performed, by varying several impactful values, while keeping all others constant, and investigating how this influences results.

Supersaturation threshold

The sensitivity of the contrail prediction to the imposed supersaturation threshold is investigated, by ranging the threshold between values of 100 and 80%. It is expected that the percentage of correct simulations increases with decreasing threshold, however due to the previously shown large RHI underestimations of ECHAM5, with values reaching lows of 20% or even lower, the proportion of correct predictions is not expected to approach 100% in the current analysis.

Table 2 below shows the results of the sensitivity analysis. One thing to note is the fact that with a threshold of 100%, ECHAM5 is able to simulate only 30.9 % of contrail conditions. However, lowering the threshold to 95% nearly doubles the correct predictions to 57.3%. This stark increase indicates that many ECHAM5 values which correspond to ice supersaturation in real life, lie just below 100% in the simulation. This also further explains the usefulness of setting the threshold for ice supersaturation slightly lower than 100%.

Supersaturation threshold [%]	100	95	90	85	80
Correct contrail predictions [%]	30.9	57.3	68.3	73.8	80.7

Table 2: Supersaturation threshold sensitivity analysis

Figure 21 shows a visual representation of the impact of the supersaturation threshold on the number of correct predictions, featuring steps of 1%. A sharp increase in correct predictions is seen between a threshold of 100 and 97%, after which the curve flattens out more, but continues to increase to about 80% correct predictions at a threshold of 80%.

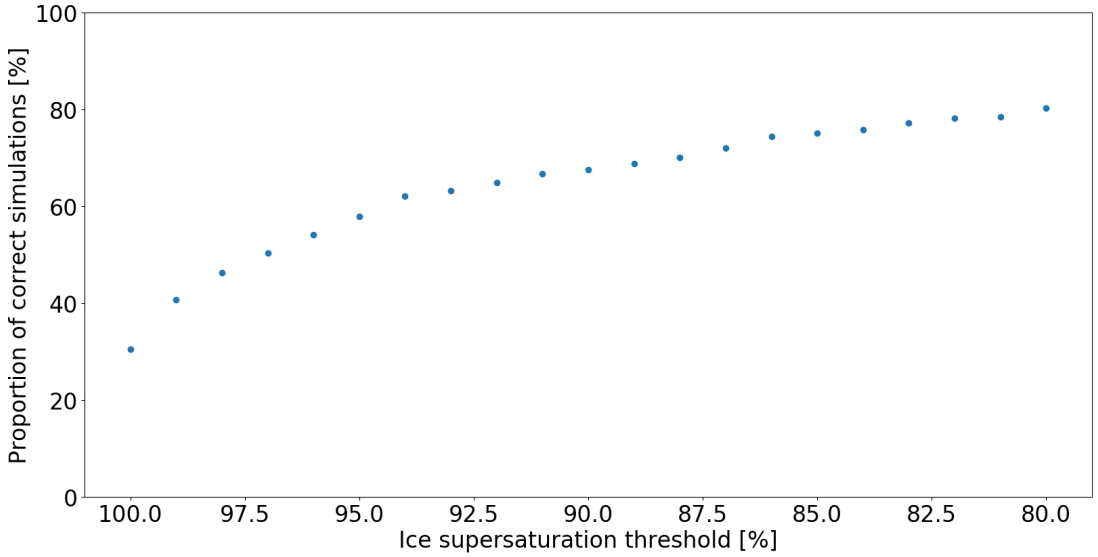

Figure 21: Supersaturation threshold sensitivity

RHI sensor error

The maximum allowed sensor error associated with the RHI value of a given IAGOS sample is also varied. From the findings, it appears that lower allowed RHI errors results in fewer contrail finding within the measured data. This would suggest that within IAGOS, higher RHI values are associated with higher sensor errors.

It appears that selecting for lower RHI error, filters out the RHI extremes, which ECHAM5 has difficulty with simulating. This results in better agreement between IAGOS and ECHAM5. Table 3 shows the variation in YY, NY, YN and NN findings with different allowed RHI errors, as well as the percentage of samples that remain when selecting for a given maximum RHI error value.

Max allowed RHI error	0.25	0.20	0.15	0.10	0.05
% of measurements kept	99.7	98.5	93.8	49.1	23.9
YY	316	310	267	116	0
YN	175	138	136	54	0
NY	934	980	992	719	605
NN	3575	3572	3605	4111	4395

Table 3: RHI sensor error sensitivity analysis

When sampling within contrail condition measurements, while selecting for maximum RHI error in steps of 0.01, not much variation is found in the results. The number of samples becomes fewer as RHI error decreases, due to the aforementioned correlation between higher RHI and higher RHI error. This also means that below RHI error 0.08 , the required 5000 samples could not be gathered. The number of correct predictions do not show much variation, besides a small decrease from an RHI error value of 0.125 and below.

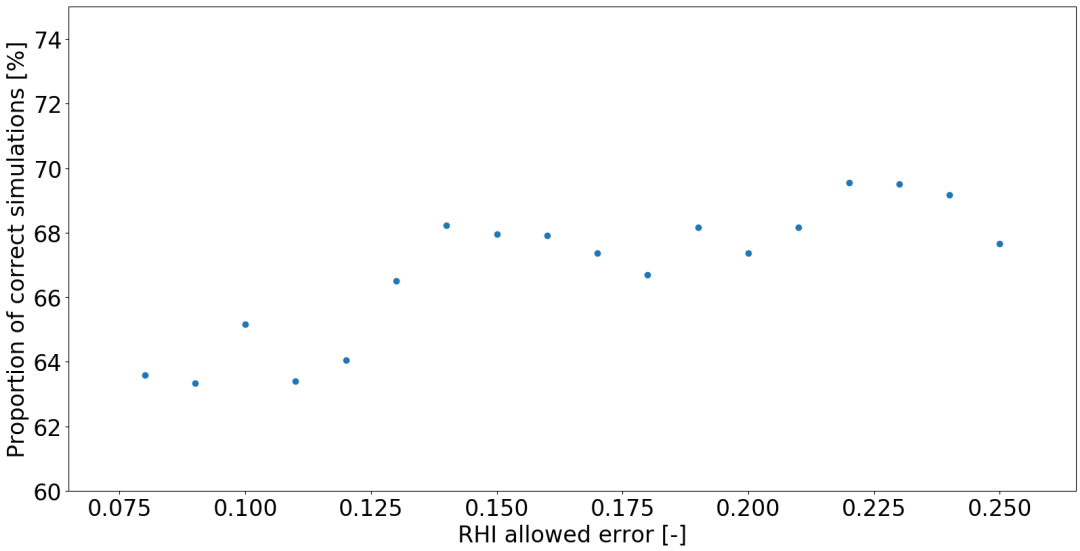

Figure 22: RHI error sensitivity; impact on contrail prediction capabilities

6 IAGOS-ERA5 comparison

6.1 About ECMWF

The European Centre for Medium-Range Weather Forecasts (ECMWF) is a weather service as well as a research institute, and has its headquarters in Reading, UK. It is an intergovernmental organisation, supported by 35 states. ECMWF provides numerical weather predictions to its member states, using a supercomputer facility that is among the largest in Europe[10]. A meteorological data archive is also kept. In addition, research is carried out for the purpose of modeling the Earth climate system, which can improve weather forecasts. The integrated forecasting system (IFS) is an atmospheric model and data assimilation system, which is the basis of ECMWF forecasts.

ECMWF also uses reanalysis methods to create global datasets which describe the state of the atmosphere, land surface and oceans in the recent past, based on archived observations. Reanalysis combines modelled data with observations to produce a complete and consistent dataset that is as accurate as possible (a best estimate), using the laws of physics. The ECMWF Reanalysis v5 (ERA5) is currently used for this purpose. ERA5 is capable of providing hourly estimates of atmospheric, land and oceanic climate variables, which can be used to monitor climate change. ERA5 is able to produce a snapshot of the global atmosphere, land and ocean from 1959 onwards. ERA5 is the successor of the ERA-interim reanalysis model[10].

6.2 ERA5 data

The data used for this part of the project come from the ERA5 (reanalysis) project. The data are available for download on the Copernicus Climate Data Store website.

6.2.1 Data format

ERA5 data can be downloaded online using several filters. The user can choose the desired variables, pressure levels, years, months, days, hours, and geographical region. The data can be downloaded in either a GRIB or NetCDF format. For this project, the data was retrieved in the NetCDF format, for the sake of consistency and familiarity.

The spatial resolution of the data is 0.25 deg, resulting in 721 latitude and 1440 longitude points. The time resolution is 1 hour.

6.2.2 Data selection

The simulated variables relative humidity and temperature are selected for the data downloads. The previously found minimum and maximum pressures at which contrails recorded by IAGOS in 2018 have formed (178.0-479.8 hPa), are used to determine the pressure levels selected for download. The pressure levels 175, 200, 225, 250, 300, 350, 400, 450 and 500 hPa are selected. The maximum available geographical region is selected. All data for every day of 2018, with a temporal resolution of 1 hour, is selected.

Even when only selecting the aforementioned pressure levels and relative humidity and temperature as the only desired variables, the files are of such large size that only a few days at a time can be processed and downloaded. The year is therefore split up into periods of 5-6 days, resulting in a total of 72 netCDF files, 6 per month of the year.

6.2.3 Preliminary analysis

ERA5 features four dimensions: longitude from [0,360], latitude from [-90,90], 'level' (the 9 selected pressure levels), and time, measured in hours since midnight of January 1st, 1900. The relevant variables for the current analysis are: temperature ('t') in Kelvin, and relative humidity ('r') in %.

Similar to ECHAM5, it is found that the ERA5 data files contain only one relative humidity variable. From documentation, it appears that whether this variable indicates humidity relative to liquid water or ice, is temperature-dependent: above 0°C, the humidity is calculated over water. Below -23°C, it is calculated for relative humidity over ice. Between these two temperatures, it is a value derived by quadratic interpolation between the ice and water values.

Verification of the model

A vertical profile of relative humidity and temperature in ERA5 was constructed and compared to a reference from literature, in order to verify the ERA5 values. Similar to ECHAM5, the RH values simulated are higher than the reference values at low altitudes, but the difference is less pronounced at flight levels. The temperature profiles agree well. Figure 23b shows the constructed profiles from ERA5, and Figure 23a shows the profiles from literature.

6.3 Methodology

Similar to the ECHAM5 analysis, random samples are again taken from the gathered IAGOS data sets. The corresponding RHI and temperature values in ERA5 are found in a similar manner to ECHAM5, only differing in the fact that the time dimension works slightly different within ERA5: its time dimension is measured in hours since midnight of 1-1-1900. The IAGOS samples are therefore first assessed on the day of take-off of the flight it was measured on (retrieved from the name of the file) and its UTC-time. This is rounded to the nearest hour and matched to the corresponding ERA5 time point (accounting for the offset of hours between 1-1-1900 and 1-1-2018). Given that the time resolution in ERA5 is 1 hour, no measures are taken to account for coarse time resolution, like was done with ECHAM5.

It was purposely decided to keep the analysis approach for ERA5 as similar to that of ECHAM5 as possible. This was done in order to be able to not only assess the individual models, but to also have some ability to compare the models to each other. Finding out some strengths and weaknesses of each of the models may assist in developing methods to model contrail formation along a flight path in the future, possibly combining several models together to produce an optimal estimate. Therefore, the current research part follows largely the same structure as the ECHAM5 analysis.

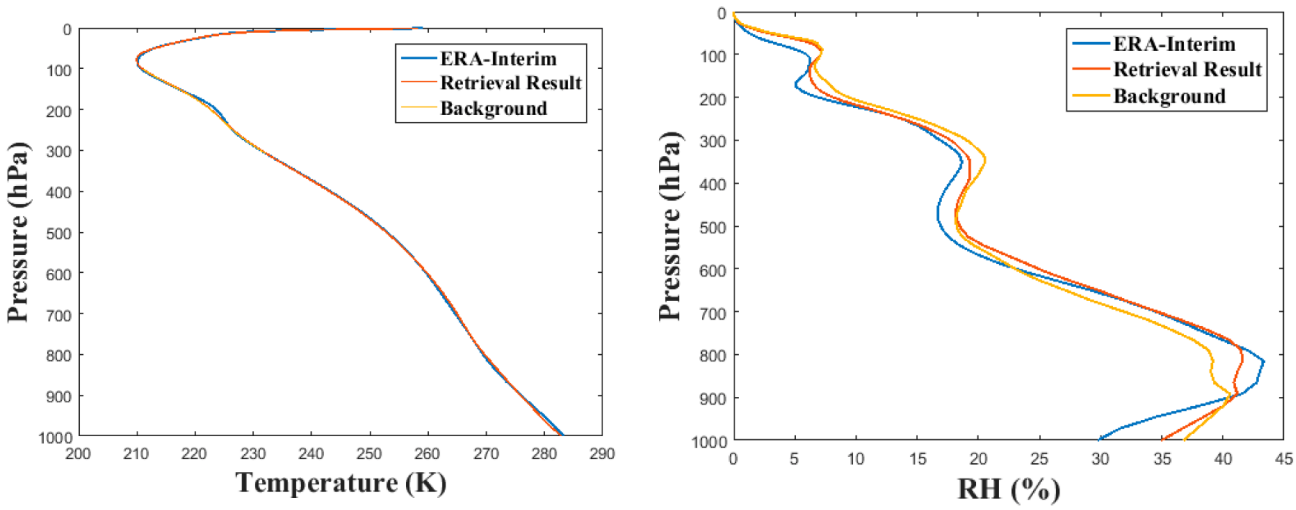

(a) RH and temperature profile as a function of air pressure. From [68]

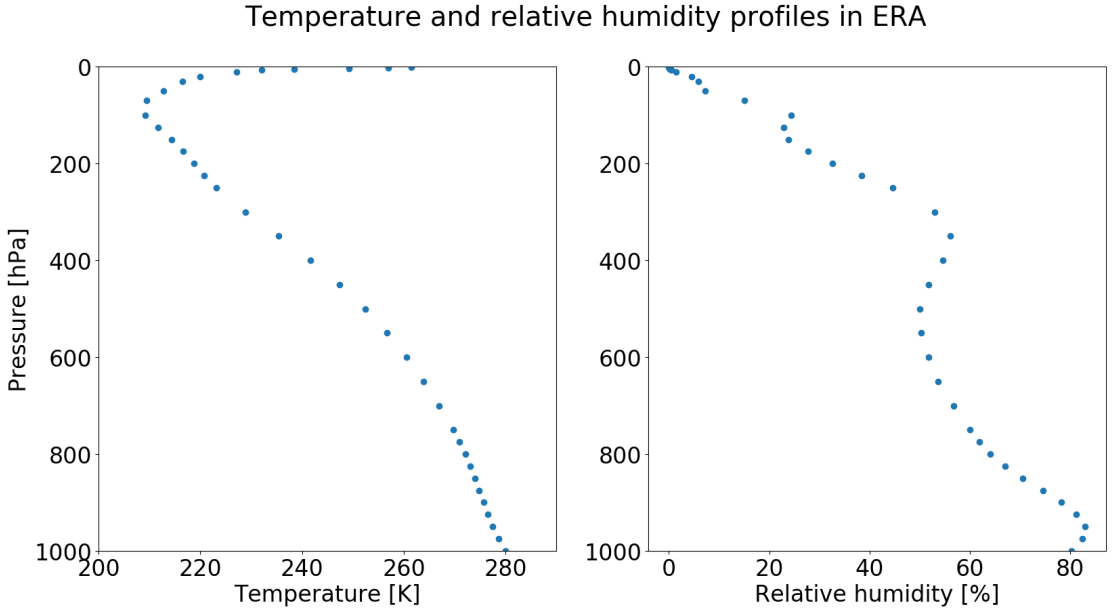

(b) RH and temperature profile in ERA5 as a function of air pressure

Figure 23: A comparison of RH and temperature vertical profiles between literature and data from the ERA5 reanalysis model

6.4 Results

6.4.1 General evaluation of temperature and RHI simulation

Figure 24 shows the geographical spread of the samples from the (non-conditioned for contrails) IAGOS data gathered for the evaluation of ERA5.

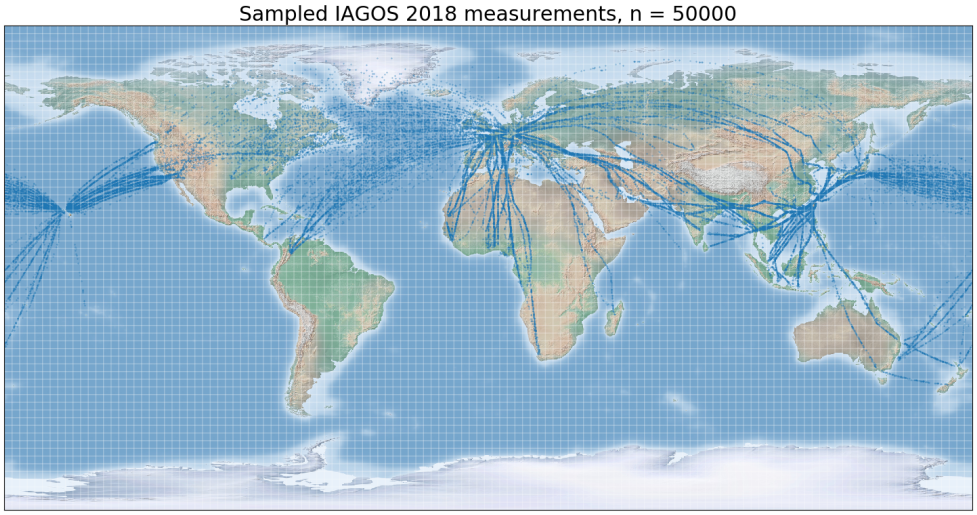

Figure 24: Sampled points from IAGOS for comparison with ERA5

Figure 25 shows the distributions of the sampled points in terms of their temperature and humidity relative to ice. The temperature data appear to agree well, and do not suffer from a consistent bias, the way ECHAM5 does.

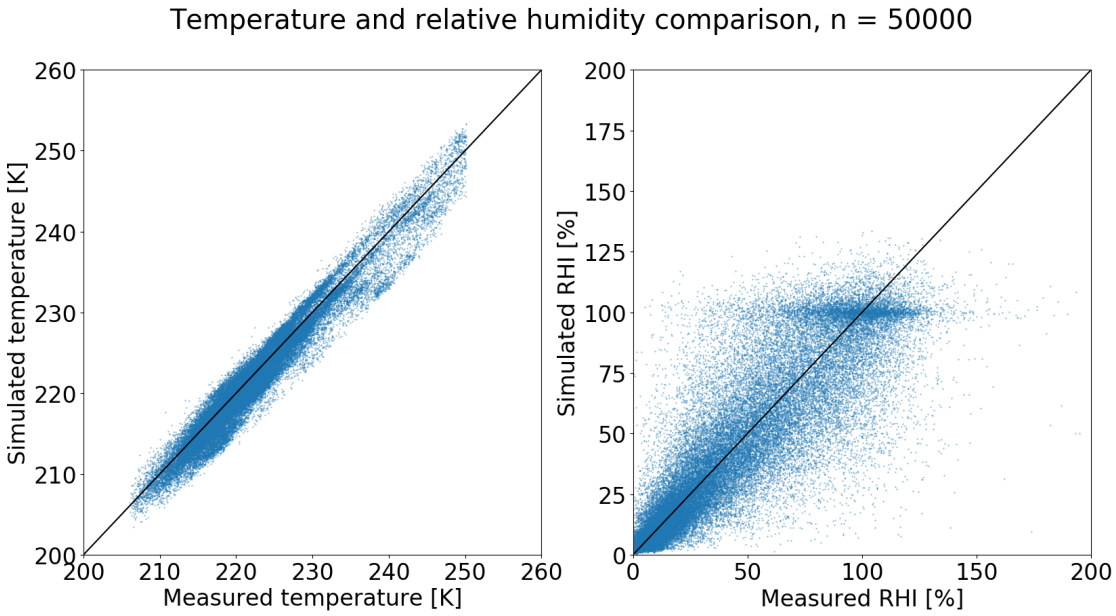

Figure 25: Sampled points for ERA5; RHI and temperature distributions

Like ECHAM5, the RHI values are somewhat more scattered. At low values of RHI, the agreement between IAGOS and ERA5 seems to be decent, with a higher density region of values

concentrated at and around the x=y line. The spread becomes larger above 40% RHI or so, ending in a horizontal region of higher density at y=100%. Interestingly, the horizontal region extends both to the left and right of the x=y line to about an equal extent. It seems that ERA5 has a tendency to return values of approximately 100% for measured values between about 80 and 120%.

The sampling results are shown in boxplots. The agreement in temperature seen in the scatterplot is also seen in the boxplots in Figure 26a. Good agreement is also seen in the RHI boxplots in Figure 26b. The distributions appear nearly identical, with mean values of 45.8% (measured RHI) and 45.0% (simulated RHI) and very similar spread. The only noticeable difference is the difficulty of ERA5 to recreate the outliers measured: values reaching down to zero or slightly below, as well as those above 135% or so.

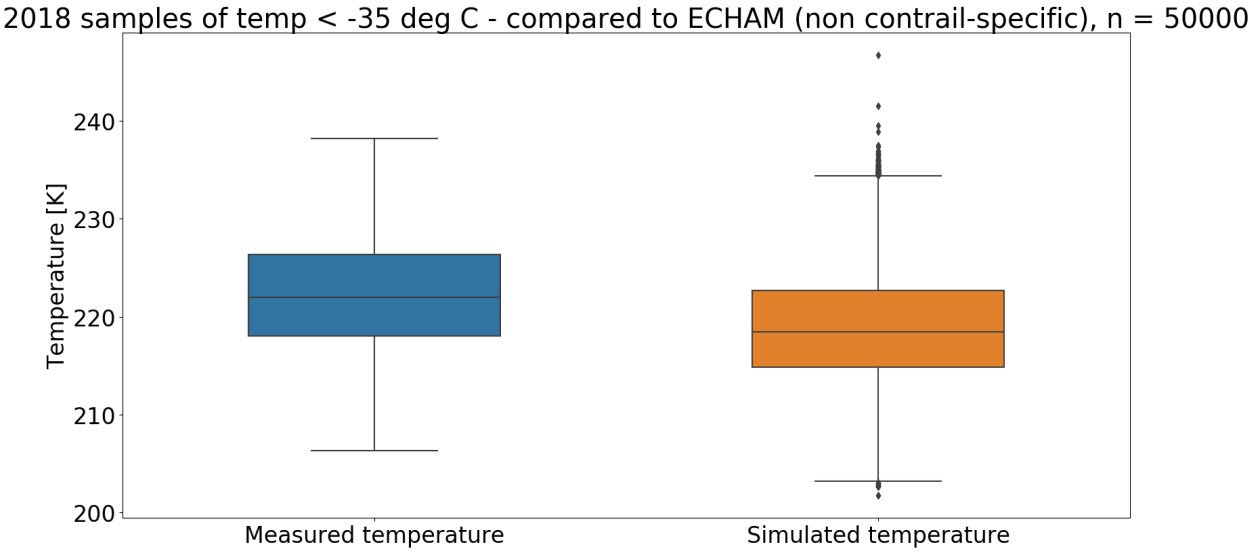

(a) Sampled points for ERA5; temperature

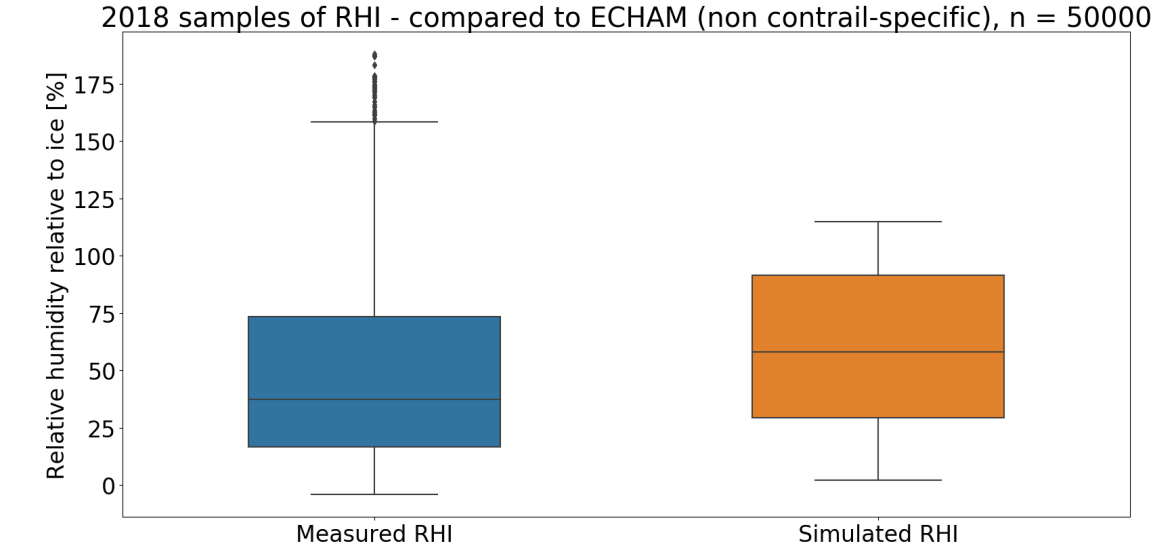

(b) Sampled points for ERA5; RHI

Figure 26: Temperature and RHI of sampled points; measured versus reanalysis by ERA5

6.4.2 Simulation of contrail formation conditions

Table 4 shows the results for the ability of ERA5 to simulate contrail formation conditions. Similar to ECHAM5, a threshold of 90% is used to indicate supersaturation. Interestingly, ERA5 shows a lower rate of NY discrepancies than ECHAM5, at 9.26%. A higher rate of NN cases is found, at 82.0%. The YY and YN cases show similar rates to ECHAM5, at 6.16 and 2.54%, respectively.

n	YY	YN	NY	NN
50000	3082	1268	4628	41022
100%	6.16	2.54	9.26	82.0

Table 4: Assessment of contrail formation prediction capabilities of ERA5

YN discrepancies The distributions for YN discrepancies (where IAGOS indicates contrail formation but ERA5 does not) are shown in Figure 27a and Figure 27b. 10 cases in which ERA5 failed to indicate contrail formation conditions, due to an overestimation of temperature, were recorded. These cases are seen in the outliers above 235K in the simulated temperatures boxplot in Figure 27a. All other discrepancies were due to an underestimation of RHI by ERA5, as visible in Figure 27b. The distribution show a large underestimation of RHI, with a mean simulated value of 69.0% versus a mean measured RHI of 111.4%.

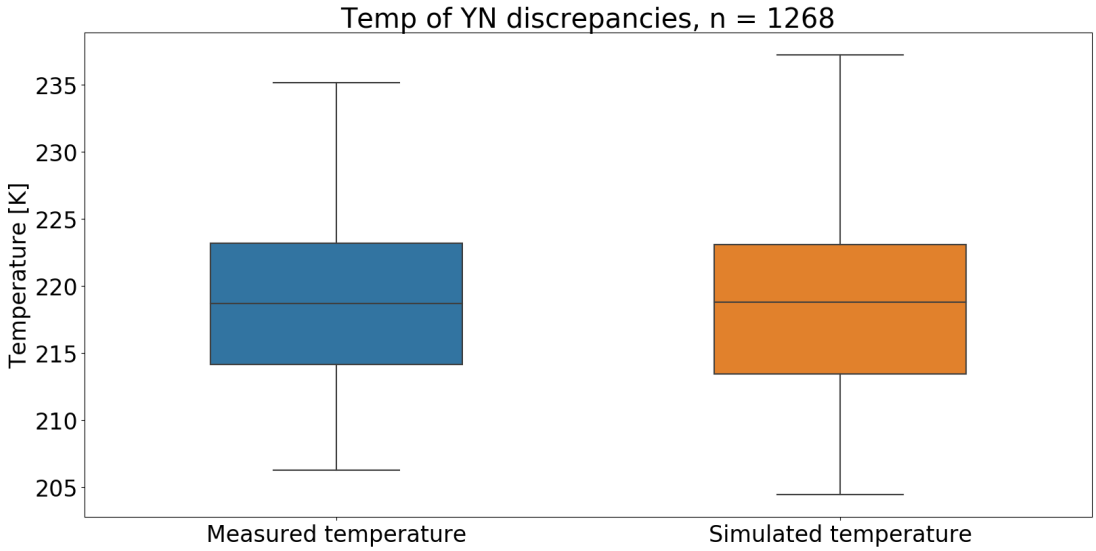

(a) Temperature distribution associated with YN discrepancies

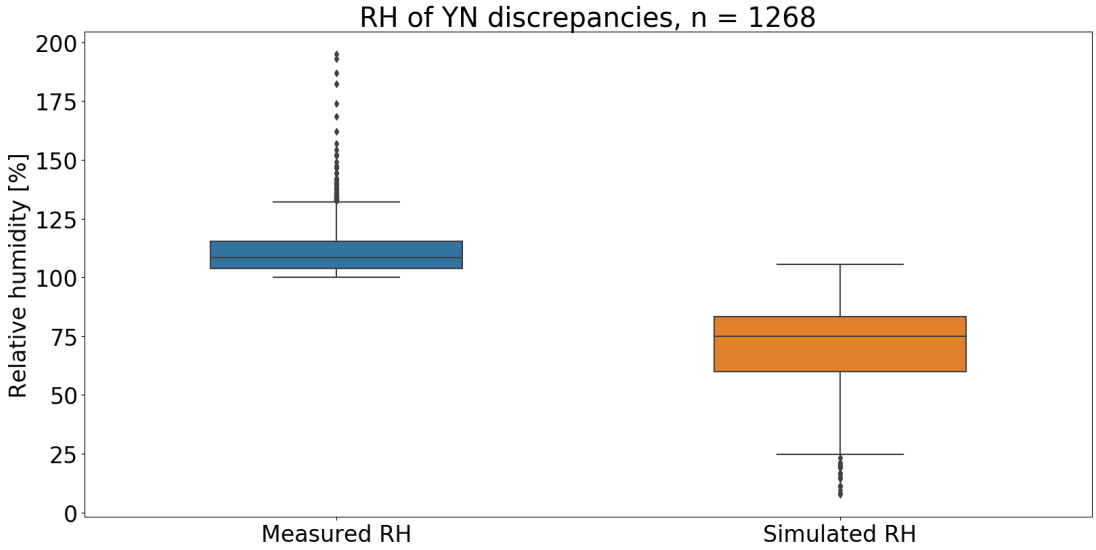

(b) RHI distribution associated with YN discrepancies

Figure 27: Temperature and RHI of YN discrepancies; measured versus reanalysis by ERA5

NY discrepancies The temperature and RHI distributions associated with NY discrepancies are shown in Figure 28a and Figure 28b, respectively. A mean measured RHI of 78.3% is found, versus a mean simulated RHI of 99.8%.

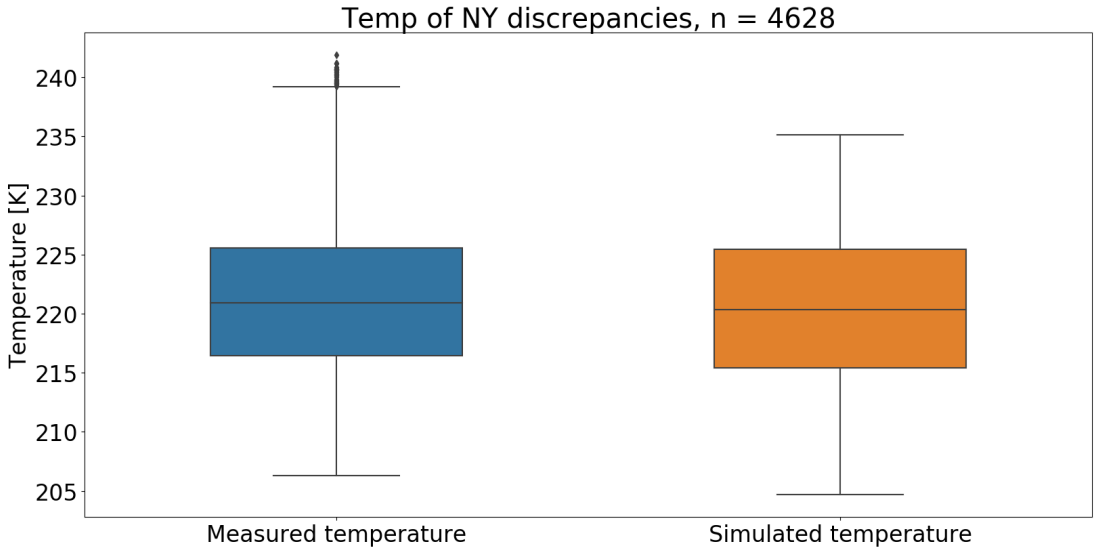

(a) Temperature distribution associated with NY discrepancies

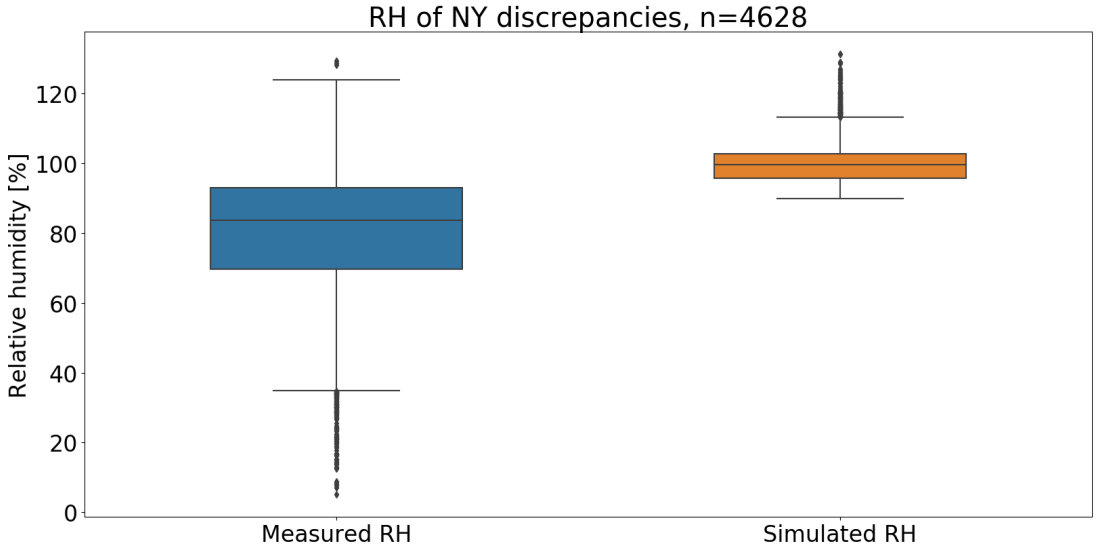

(b) RHI distribution associated with NY discrepancies

Figure 28: Temperature and RHI of NY discrepancies; measured versus reanalysis by ERA5

6.4.3 Sampling for contrails

The ability of ERA5 to predict contrail conditions is evaluated by taking random samples from the contrail conditions data from IAGOS over 2018. A threshold for ice supersaturation in ERA5 of 90% is used. Several other thresholds are implemented later in the sensitivity analysis. ERA5 correctly simulates 70.1% of sampled contrail conditions. This is higher than ECHAM5. The mean real RHI value associated with contrail conditions is 112.3%, versus a mean simulated value of 92.2%.

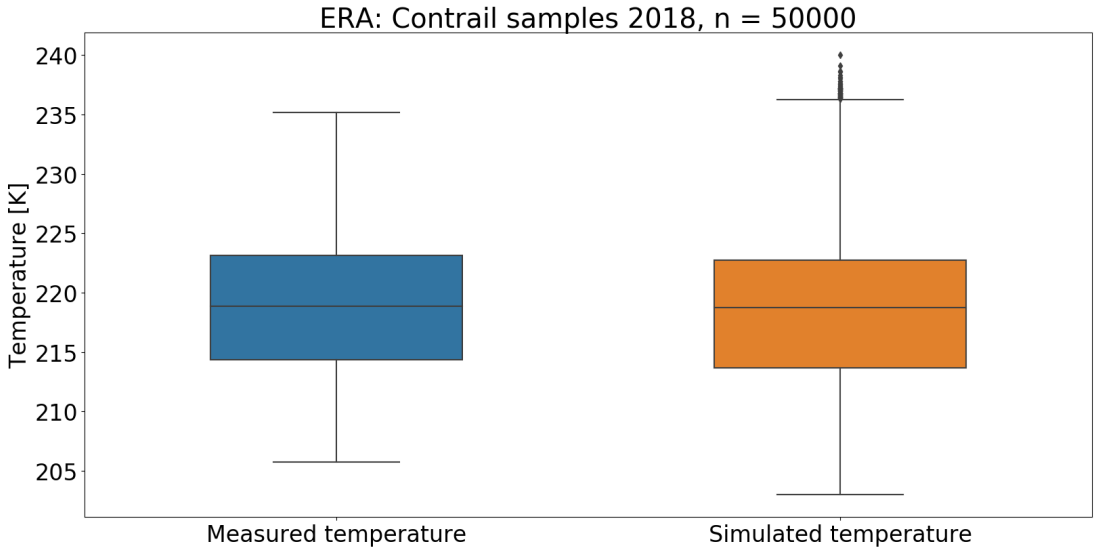

(a) Temperature of contrail samples

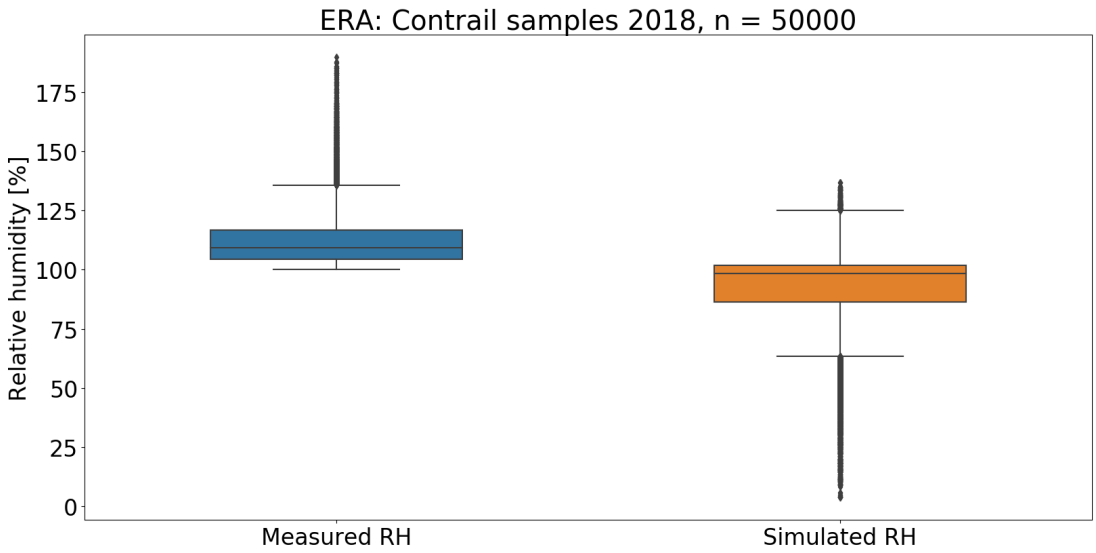

(b) RHI of contrail samples

Figure 29: Temperature and RHI of contrail samples; measured versus reanalysis by ERA5

Figure 30 shows the RHI values of ERA5 associated with the cases in which ERA5 failed to indicate contrail formation conditions. The mean RHI value lies at 74.8%. An interesting observation is the RHI values which lie (significantly) above 90%, which were not seen in the analysis of ECHAM5. These values correspond to cases where ERA5 failed to predict persistent contrail formation, due to a too low temperature. This same phenomenon was not observed in ECHAM5, likely due to its cold bias. ERA5 does not exhibit a consistent temperature bias, resulting in these discrepancies where not the RHI value, but a too low predicted temperature was the cause of a 'miss' in predicting persistent contrail formation.

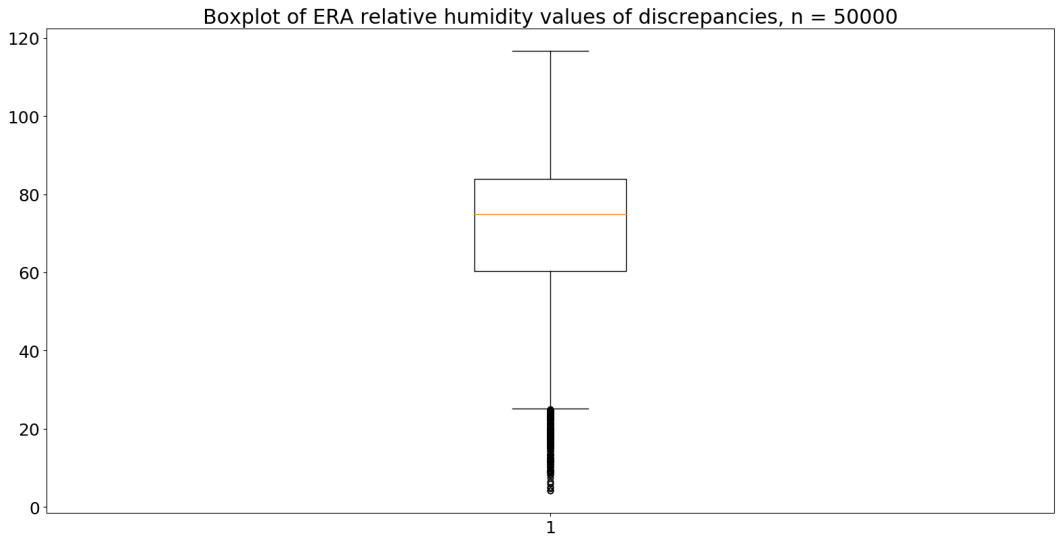

Figure 30: Incorrect simulated RH values associated with contrail samples

Verification of the results

The difficulty of ECMWF to predict (high levels of) ice supersaturation, is a known phenomenon. Good agreement is generally found for RHI values below 100%, but much less so at supersaturation or above[49]. Figure 31 shows this discrepancy visually.

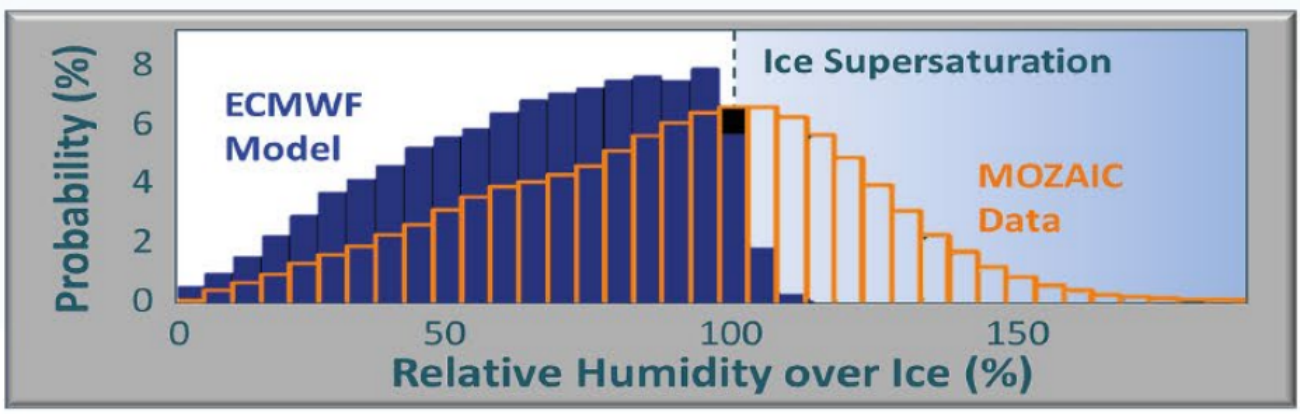

Figure 31: ECMWF RHI discrepancies, from [19]

It is known that ERA5 adjusts supersaturated RHI values to 100%, in case ice clouds are detected in the grid cell[49]. It is possible that this could partly explain the mean of the ERA5-simulated RH values being closer to 100% than the mean of the measurements (not so much the lower outliers). Even though the IAGOS contrail measurements do not select points with liquid supersaturation, it is possible that some of the points which are selected are within the ERA5 grid cell which contains clouds, which would bring the RHI of the entire grid cell down to 100%.

6.4.4 Sensitivity analysis

A sensitivity analysis is performed by varying the ERA5 supersaturation threshold, as well as the allowed RHI error of IAGOS data to sample from.

Supersaturation threshold

Several thresholds for ice supersaturation in ERA5 are tried and evaluated on how many correct contrail predictions are made. When setting a threshold of 100%, only about 37% of contrail conditions sampled are correctly recreated. Lowering the threshold to 95% increases the proportion of correct predictions to 63%, suggesting that many RHI values in ERA5 which correspond to supersaturated values in IAGOS, are quite close to saturation level.

Supersaturation threshold [%]	100	95	90	85	80
Correct contrail predictions [%]	37.12	62.7	69.24	76.1	80.7

Table 5: Supersaturation threshold sensitivity analysis

A visual representation of the sensitivity analysis using steps of 1% for the saturation threshold, also shows the steep increase in correct predictions when varying the threshold from 100 to about 95%. Similar to ECHAM5, the curve then flattens out slightly but continues to increase to a value of about 80% correct simulations corresponding to a threshold of 80%.

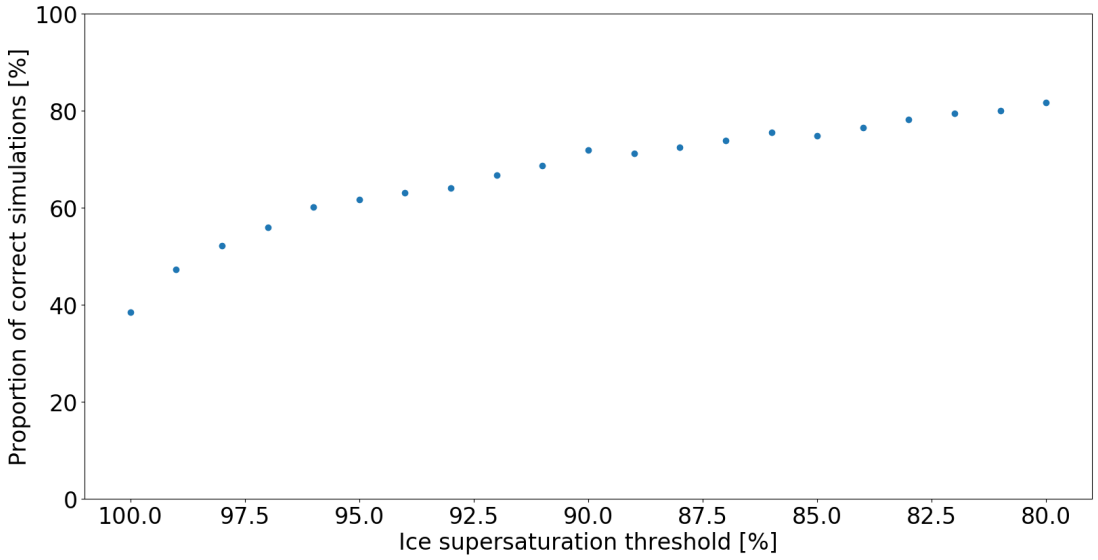

Figure 32: Supersaturation threshold sensitivity

RHI sensor error

The allowed RHI sensor error is varied from 0.25, 0.2, 0.15, 0.1, 0.05. A similar trend is observed as in ECHAM5, where a lower allowed RHI error results in fewer contrail conditions indicated in IAGOS.

Max allowed RHI error	0.25	0.20	0.15	0.10	0.05
% of measurements kept	99.8	98.5	93.1	55.2	17.0
YY	298	274	282	141	0
YN	131	113	130	60	0
NY	453	445	404	301	71
NN	4118	4168	4184	4498	4929

Table 6: RHI sensor error sensitivity analysis

When it comes to the effect of RHI error on the ability of ERA5 to simulate contrails, no clear trend is observed, similar to ECHAM5. Below an RHI error value of 0.07, the required 5000 contrail samples cannot be retrieved due to the aforementioned correlation between RHI and RHI error.

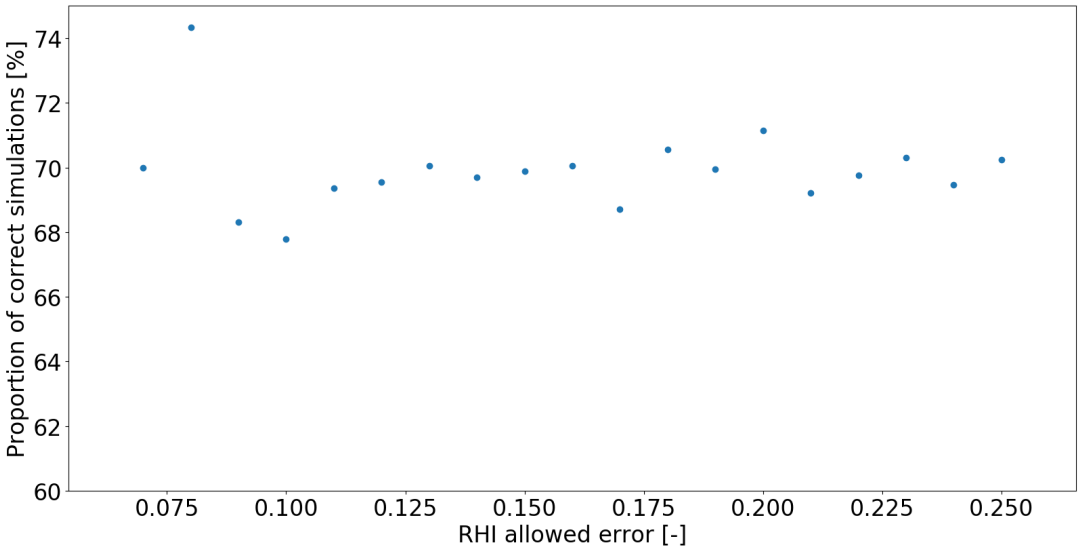

Figure 33: RHI error sensitivity

7 Temporal evolution of ISSRs over the North Atlantic

In addition to the previous analysis, IAGOS data can also be used to gain insight into another aspect of ISSRs: their temporal evolution throughout the year as well as over several years. A 10-year analysis of ISSRs in the North Atlantic region is presented, using data from IAGOS-MOZAIC (from January 2010 until July 2011) and IAGOS-CORE (from July 2011 until December 2019). This time frame is chosen because it is relatively recent, however before the COVID-19 pandemic which disrupted air travel. The IAGOS data base has decent flight coverage and available data for these years. The geographic region of the North Atlantic was chosen due to its importance as a flight corridor, as well as the fact that it is located at mid-latitudes and therefore shows variation throughout the seasons, which is more interesting to investigate than regions with relatively stable weather throughout the year. The same background information about the IAGOS project and its data as described in section 4 apply here.

7.1 Methodology

The North Atlantic is chosen as the region to be investigated, because it contains highly travelled routes. The previous analysis has shown frequent contrail formation in this region, which makes it an interesting topic of investigating and trying to better understand ISSRs. The MOZAIC and IAGOS-CORE data base contains recorded flights for this route for all months of all 10 selected years.

7.1.1 Data selection

The MOZAIC project was succeeded by IAGOS-CORE in 2011, which is why both projects are selected for this analysis. From the data, it appears that MOZAIC eveolved into IAGOS-CORE on the 16th of July, 2011. This requires a few changes in the processing of the data, due to a slightly different format and naming convention within the datasets, however these changes are small and once they are implemented, the necessary data properties can be extracted for analysis with relative ease regardless of whether they originate from IAGOS-CORE or MOZAIC flight data. Measurement methods and instrumentation between MOZAIC and IAGOS-CORE remained the same[27]. A total of 6674 flights were recorded in the selected time frame and geographical region.

In this section, the North Atlantic is defined as the region between 40 to 60 degree latitude and -65 to 5 degree longitude. These geographical bounds are used for filtering the IAGOS data to be used in the analysis. The region is shown visually in Figure 34.

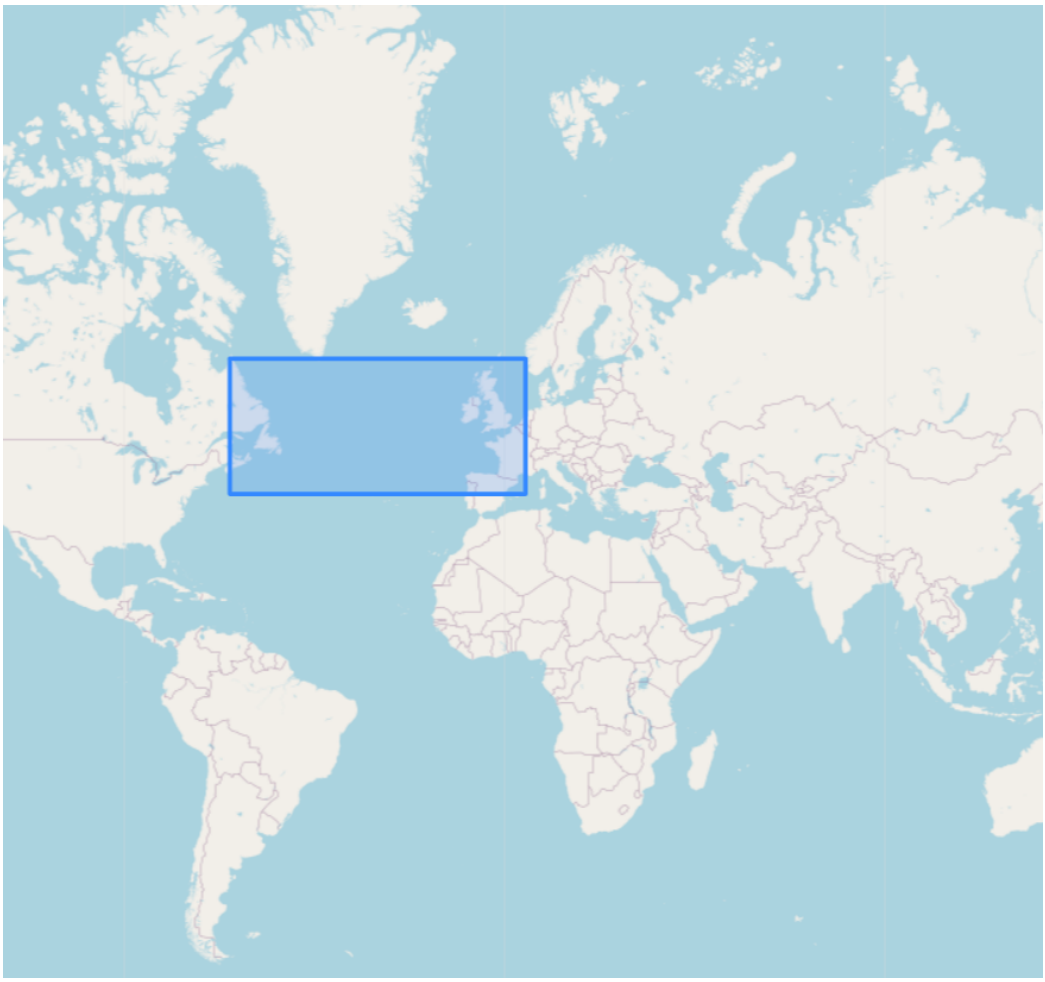

Figure 34: Boundaries of the North Atlantic region as defined in this section

Measurements of ISSRs are gathered according to several criteria. There is the obvious requirement of a humidity relative to ice which exceeds 100%. Additionally, an ambient temperature below 233 K and ambient pressure below 350 hPa (corresponding to altitudes above approximately 8 km) are required. These conditions correspond to the threshold for homogeneous freezing and ensure that the humidity sensor data is not contaminated by supercooled liquid water droplets [49]. Another requirement is subsaturation with respect to liquid water (i.e. RHL $<$100%), as water supersaturation would suggest the presence of liquid water clouds[12].

Finally, there are the requirements regarding data quality. The data validity flag for the collected data points is to be either 1 ('good') or 2 ('limited'). These requirements are more lenient than in the previous analysis. The reason for this is explained in the following section.

The requirements for the gathering of ISSR data can be summed up as follows:

- a latitude between 40 and 60 degrees
- a longitude between -65 and 5 degrees
- a temperature validity label of 0 or 2
- a pressure validity label of 0 or 2
- an RHI validity label of 0 and an RHI error > 0
- an RHL validity label of 0 or 2

- humidity relative to ice $> 100\%$
- temperature < 233 K
- pressure < 35000 Pa
- humidity relative to water $< 100\%$

7.1.2 Data quality and limitations

When performing a preliminary analysis from data gathered from the MOZAIC/IAGOS data using the quality requirements used in section 4, some problems arise. It appears that for several months, no data is gathered. Only 1702 flights (out of 6674) return measurements. Looking further into this, it appears that part of the problem lies in the requirements regarding the data validity flags. A validity flag label of 0 ('good') is required, however it appears that no data which otherwise meets the geographical and ISSR requirements, has this label. It is decided to also allow data which has validity label 2 ('limited') into the data selection, which results in more months being represented. However, there are still 1876 flights (4798 do) which do not generate any measurements.

An example of a month with no samples is May of 2013, when IAGOS-CORE has recorded only 5 flights in the North-Atlantic region. 4 for these flights only spent a very short amount of time in the specified geographic region (right before landing or right after departure), which makes their data not usable for the present analysis. Only one flight spent its cruise phase in the North-Atlantic region, however its temperature data was given a validity label 3 ('erroneous'). Due to the poor quality of the available data as well as the fact that all data would have come from only one flight, this month was disregarded for further analysis.

A threshold of 30.000 samples per month is imposed, in order to ensure some measure of representability. This threshold results in the loss of 14 months. These months do not contain enough usable samples due to not having enough flights, not having enough data which meets the data quality requirements, or which are relevant for analysis because they only spend a short time (non-cruise phase of the flight) in the North Atlantic region, making the data not usable.

7.2 Results

The gathering of ISSR data from the MOZAIC and IAGOS-CORE datasets results in large datasets which can be evaluated on several aspects and through several approaches. The current analysis investigates four main characteristics related to ISSR occurrence: occurrence rates of ISSRs, their associated temperature, humidity relative to ice, and pressure/altitude. The data are visualized in such a way that makes it possible to evaluate evolution not only throughout a given year (so as to observe seasonal variation), but also the evolution over the course of several years, which may be interesting in light of climate change.

7.2.1 Occurrence rates of ISSRs

A first analysis of the data shows that of all data points which meet the requirements surrounding data quality, about 11.5% also meet the requirements for an ISSR. Figure 35 shows the ISSR occurrence rates for all months, excluding those where there were not enough measurements which met the data quality requirements. The rates are shown to vary quite significantly, with highs in the 30-35%-range, and lows between 0 and 5%.

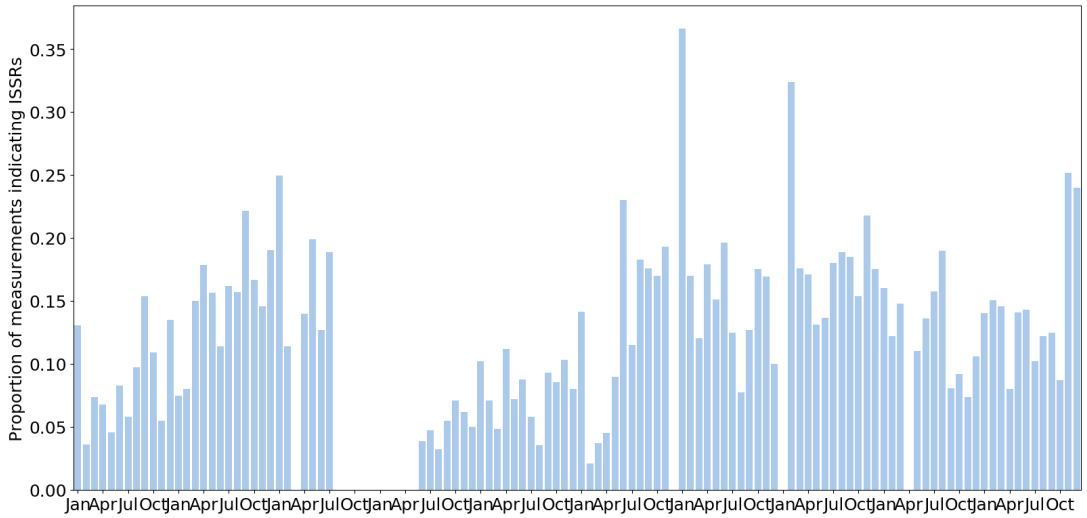

Figure 35: Rates of ISSR occurrence in the North Atlantic region from 2010-2019

To get a clearer picture of the temporal variation of ISSR occurrence rates, Figure 36 is plotted. It shows the same data as the previous plot, however grouped by months and connected by their averages. The years 2012 and 2013 are not plotted, due to the many months of data missing from those years, resulting from the sample threshold and data quality requirements. The figure shows that ISSR occurrence rates show some variation throughout the year. It seems that ISSRs are somewhat more common in winter than in summer months, however the differences are not very large and do not show a very clear seasonal trend.

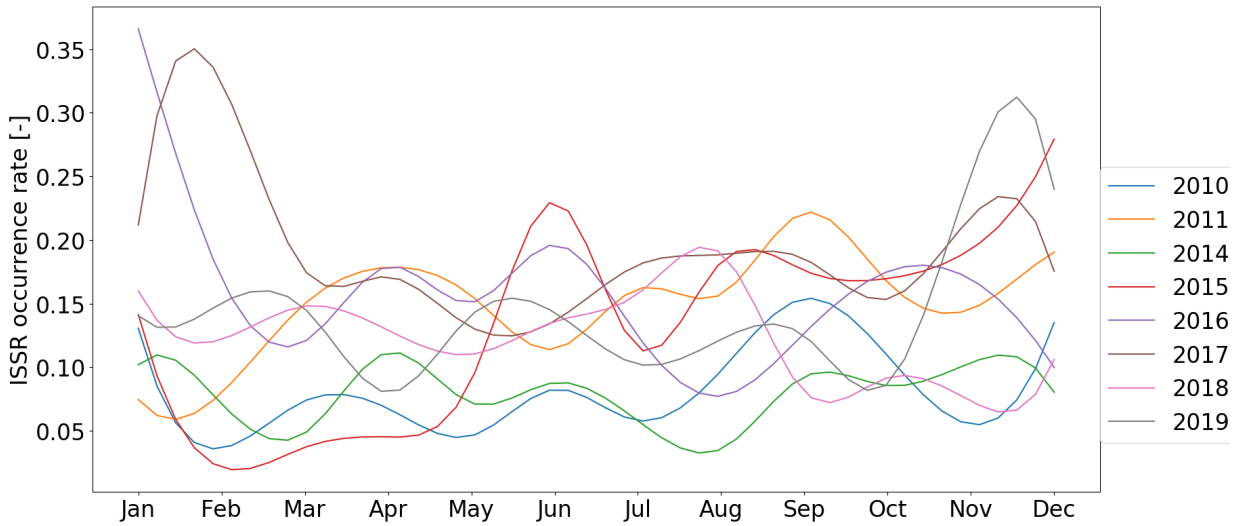

Figure 36: Rates of ISSR occurrence in the North Atlantic region from 2010-2019

7.2.2 Temperature of ISSRs

Figure 37 shows the temperatures observed in ISSR observation, again plotted to show variation throughout the year as well as over several years. Some amount of seasonality can be seen in the highs which are reached from June to September, and lows from about December until February. The seasonal variation is quite pronounced in some years: in 2010, mean ISSR temperatures ranged from about 210K in late winter, to 225K in summer. 2015 and 2019 show ISSR temperature highs at the beginning of the year, which fall outside the general trend.

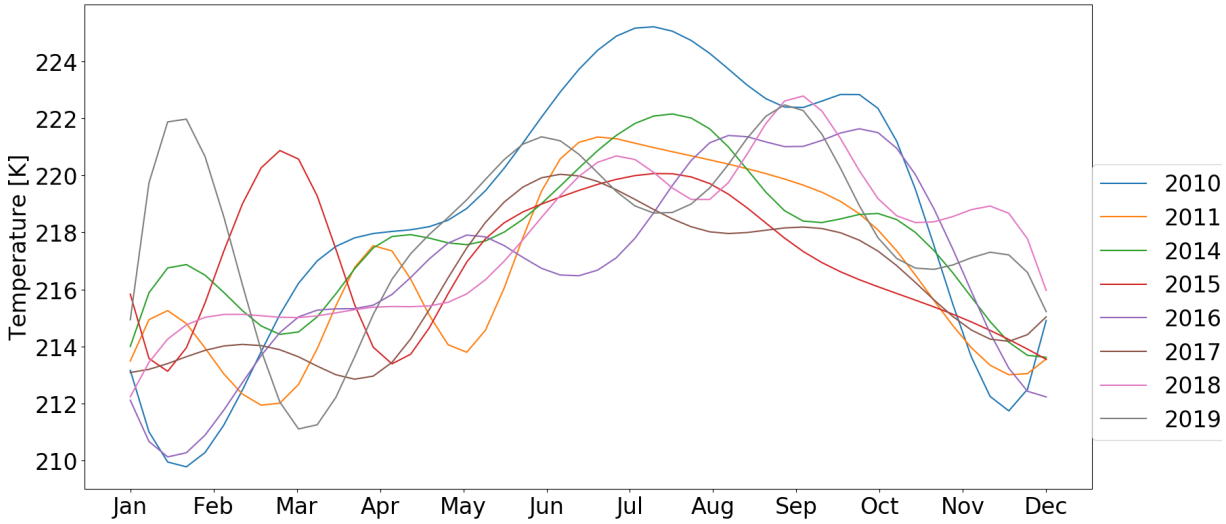

Figure 37: Temperature of ISSRs observed in the North Atlantic; showing variation throughout the year as well as over the years

In order to get a clearer idea of possible trends over the 10-year period, Figure 38 is plotted, showing the temperatures observed in ISSRs over the years. The data are separated by seasons, represented by January (winter), April (spring), July (summer), and October (autumn). The figures do not seem to indicate a clear trend in the temperatures of ISSRs.

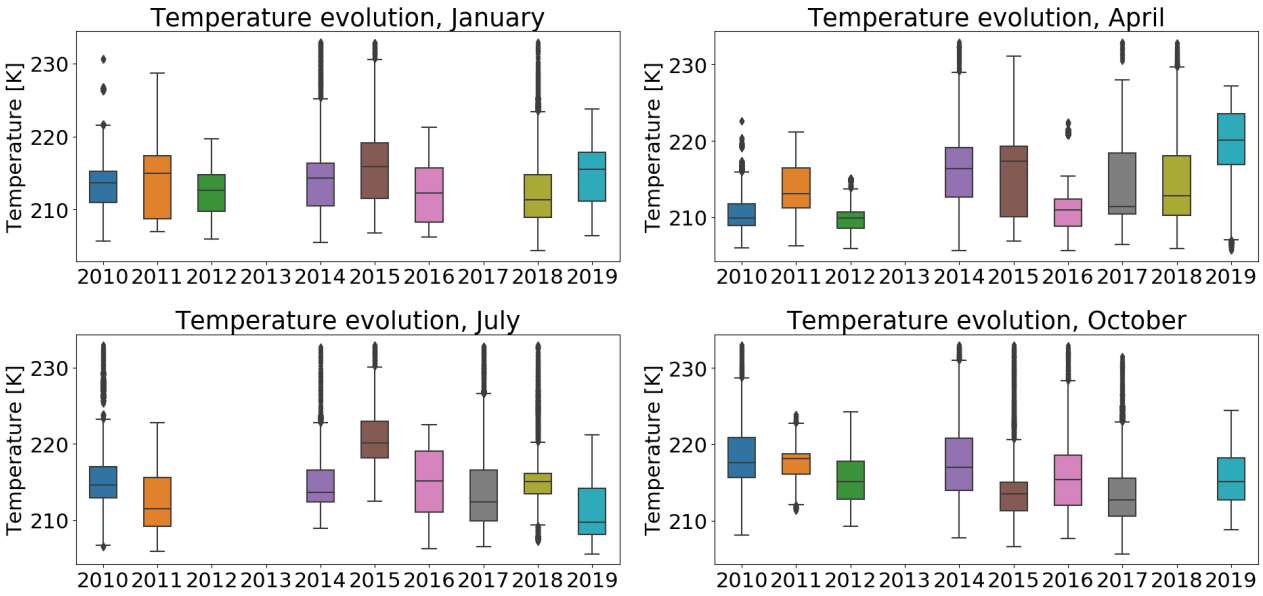

Figure 38: Temperature of ISSRs observed in the North Atlantic; showing variation over the span of several years for four months out of the year

7.2.3 Relative humidity of ISSRs

Figure 39 shows the RHI levels of the observed ISSRs. It appears that there is some seasonal variation in ISSR ice supersaturation levels, featuring slightly lower RHI values in summer months than in winter. This may be connected with the higher ISSR temperatures observed in summer time, given that temperature and relative humidity are inversely correlated. When looking at the trends over the years in Figure 40, it appears that RHI levels are relatively steady in summer (July) over the observed years. Other than that, no clear trends can be observed from these figures.

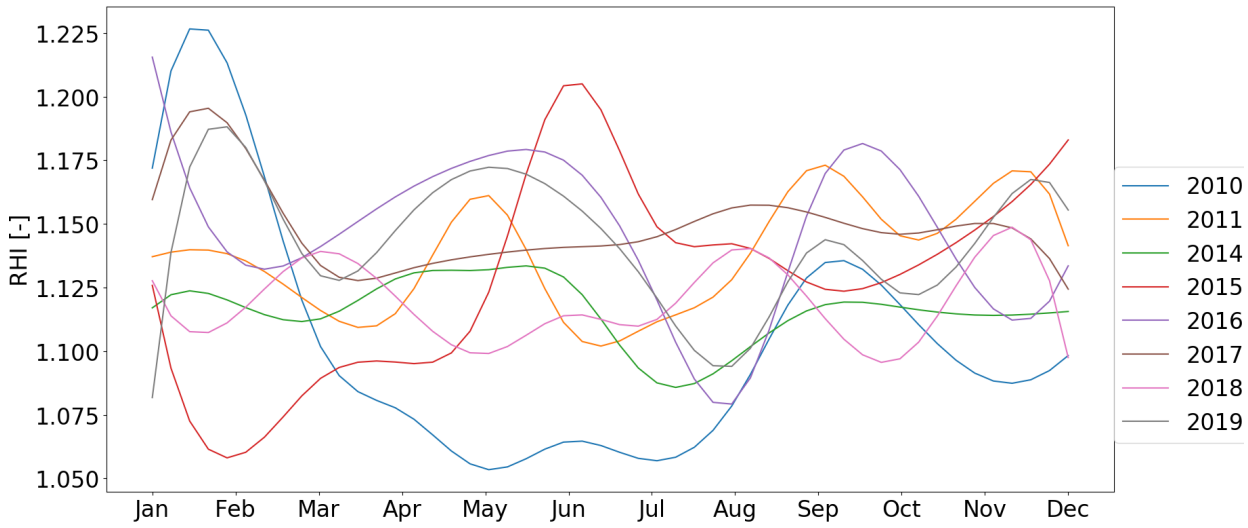

Figure 39: RHI values of ISSRs; showing variation throughout the year

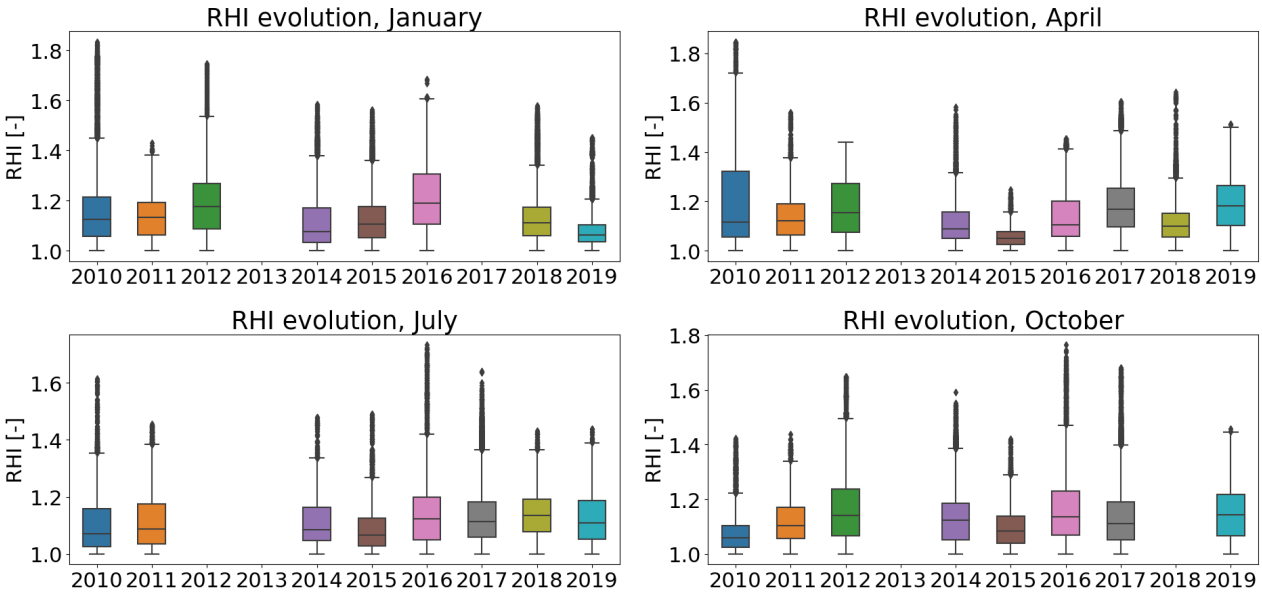

Figure 40: RHI of ISSRs observed in the North Atlantic; showing variation over the span of several years for four months out of the year

7.2.4 Pressure of ISSRs

From Figure 41, ISSRs generally appear to occur at higher altitudes (lower pressure levels) in summer than they do in winter. This is somewhat expected given that lower temperatures occur at lower altitudes (higher pressure levels) in winter than in summer, which would therefore make it more probable for ISSRs to occur at these altitudes. When plotting to observe trends over the years in Figure 42, a slight upwards trend is seen when it comes to the altitudes of ISSRs. The latter years (2017-2019) seem to show a more downward trend.

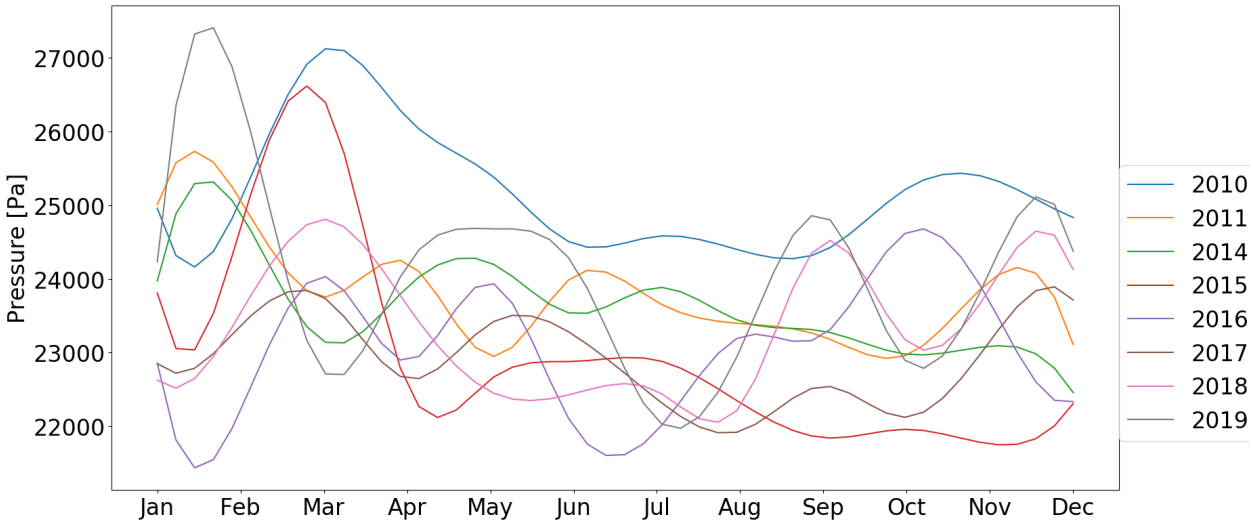

Figure 41: Pressures of ISSRs; showing variation throughout the year and over several years. Please note that this figure is plotted with increasing pressure (i.e. decreasing altitude) on the y-axis.

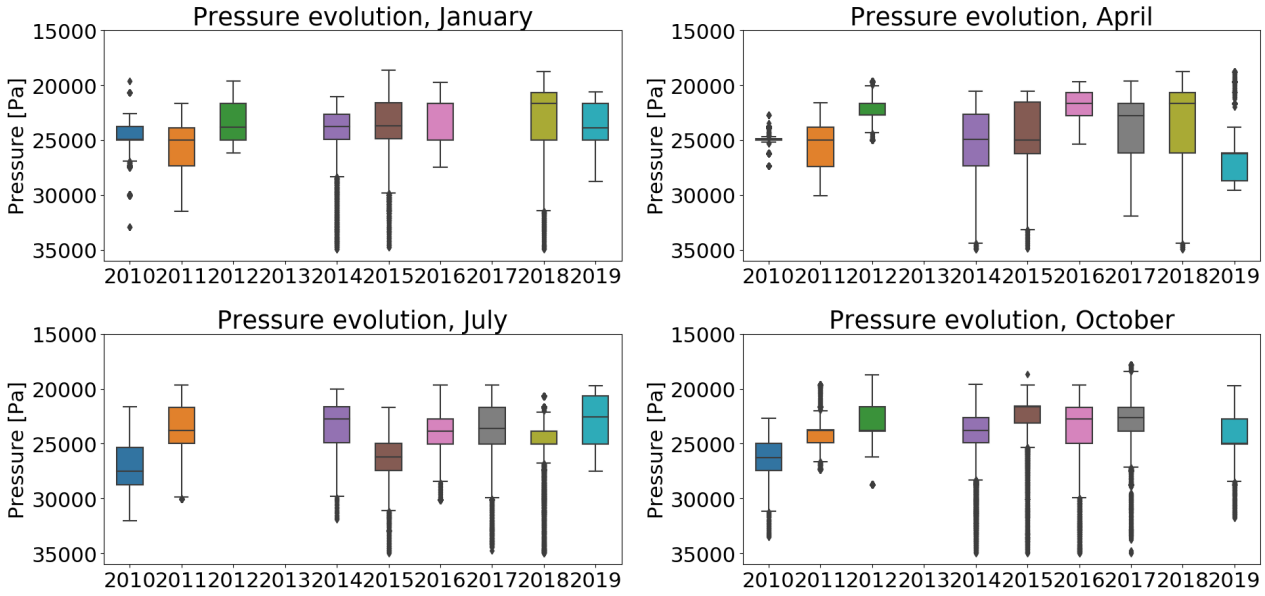

Figure 42: Pressure of ISSRs observed in the North Atlantic; showing variation over the span of several years for four months out of the year

Verification of the results

To place the findings of this section into a larger perspective as well as for the purpose of verification, one can look at other research with a similar scope as this part of the project. One study observed the distribution and seasonal variation of ice-supersaturated regions at mid-latitudes above Eastern North America, the North Atlantic and Europe from 1995 until 2010. This study also used observational data from the MOZAIC project. The study observed seasonality in contrail occurrence in the upper troposphere, featuring minimum values in summer (30% over

the ocean, 20 - 25% over land), and maximum values in late winter (35 - 40% over both land and ocean)[47]. No clear trends were observed when investigating the full timespan of the data, similar to this project.

A radiosonde study over Reading (UK) found that ISSR occurrence rates over the year varied in a similar way to what this project found, but at slightly different rates of occurrence: frequencies of 17.3% in winter and 9.4% in summer were found. The winter occurrence is highly similar to what was found in this project, but the summer occurrence is slightly lower. The difference is possibly due to a more limited geographical coverage. The study found that the higher rate of ISSR occurrence is mostly due to thicker layers[54]. It also found a mean ISSR height of about 10 km, which is slightly below the findings of this project.

8 Conclusion

A study was performed with the objective to better understand the nature of ice-supersaturated regions (ISSRs), the regions in which aircraft are known to be able to cause persistent contrails and their resulting contrails cirrus, both of which cause a positive radiative forcing and thus contribute to anthropogenic climate change. The study was divided into three parts, each of which attempted to address a particular gap in the understanding of ISSRs and the ability to recreate them within atmospheric simulations and reanalysis. Filling in the knowledge gaps in the understanding of ISSRs could eventually contribute to a better ability to avoid the formation of persistent contrails and contrail cirrus by aircraft, by avoiding flying through ISSRs, which would ultimately contribute to the mitigation of aviation climate impacts. For each part of the project, in-situ data from the IAGOS project were used.

The first part of the project looked into the current ability to simulate ISSRs, by evaluating data from ECHAM5 compared to in-situ measurements from IAGOS-CORE over the year 2018. It was found that ECHAM5 tends to underestimate temperature by 3.4 K on average. This cold bias is not found to impact ISSR simulation abilities very much. More impactful is the RHI distribution compared to the real RHI values measured, which is found to exhibit large differences. ECHAM5 is found to overestimate RHI when the real RHI lies below saturation, however it somewhat flattens out at around 100% and has difficulty simulating (high levels of) ice supersaturation. Overall, ECHAM5 appears to struggle to simulate the 'extremes' of RHI the values sampled, in particular when it come to ice supersaturation. The overestimation of RHI values which in reality lie (far) below 100%, results in some cases where IAGOS does not indicate contrail formation conditions, but ECHAM5 does. When sampling specifically for measured contrail conditions and using an ice supersaturation threshold of 90%, a success rate of 68.9% is found for simulating contrail formation conditions. In all cases of discrepancies, the RHI value is to blame (i.e. ECHAM5 produced a too low RHI to indicate contrail formation, but its simulated temperature was low enough). The fact that the temperature is never the cause of a discrepancy is thought to be due to the previously mentioned cold bias within ECHAM5.

ERA5 data is used to evaluate the ability of reanalysis to recreate contrail formation conditions. ERA5 does not seem to show a temperature bias the way ECHAM5 does, and shows good agreement between reanalysis data and IAGOS measurements when it comes to temperature. RHI values are more scattered, but show better agreement than ECHAM5. ERA5 does not seem to have the same tendency as ECHAM5 to overestimate subsaturation RHI values, rather it shows quite a good agreement between measurement and simulation at this RHI range. ERA5 shows better ability to recreate supersaturated values, however it has difficulty with the very high values of RHI, above 130% or so. When sampling for contrail conditions specifically (and again using a supersaturation threshold of 90%), a success rate of 70.1% is found. The vast majority of cases in which there is a discrepancy, it is due to a too low simulated RHI value. Interestingly, and different to ECHAM5, there are cases (albeit few) where the discrepancy is due to a temperature value within ERA5 which is too high to indicate contrails.

The third part looked into the temporal evolution of ISSRs over a period of 10 years (2010-2019), over the North Atlantic region. In-situ data from IAGOS-CORE as well as its predecessor, MOZAIC, was used for the analysis. ISSR occurrence rates show some variation throughout the year. ISSRs appear to occur more commonly in winter months versus summer, which is also seen in other studies and thought to be due to thicker layers during winter. ISSR temperatures show clear seasonality and reach highs from June to September, and lows from about December until February. No clear trend is observed over the yearly means over the 10-year period. ISSR

ice supersaturation levels vary throughout the year, with slightly lower RHI values in summer months than in winter. No clear trend is observed over the years. ISSRs appear to occur at higher altitudes (lower pressure levels) in summer than they do in winter, which is expected given the fact that lower temperatures occur at lower altitudes (higher pressure levels) in winter than in summer. Over the years, an upwards trend is seen when it comes to the altitudes of ISSRs, however in the latter years of the analysis (2017-2019), a downward trend is seen.

9 Discussion and recommendations

This section aims to discuss some problems encountered during the project, some aspects of the project work which did not result in the desired results, as well as some recommendations for further research work.

Several attempts were made to investigate more aspects of the variation in RHI and temperature simulation. For instance, a preliminary analysis was performed into the spatial (in terms of longitude, latitude and altitude) variation in the ability of ECHAM5 and ERA5 to simulate RHI and temperature. The limited geographical coverage of the IAGOS data proved to be a challenge in accomplishing this. Any trends observed were believed to be due to the flight coverage patterns in IAGOS, moreso than a trend within the ECHAM5 or ERA5 models. The limited or completely lacking data points in some regions was an obstacle in setting up a meaningful analysis. The geographical analysis was therefore left out of the report. More progress in this regard could be made by possibly incorporating data from other sources to complement the geographical coverage of IAGOS, if possible.

The geographical limitations from the IAGOS flight coverage also have consequences for the conclusions drawn for ECHAM5 and ERA5: it should be acknowledged that these models were not evaluated over their full spatial coverage (in terms of longitude, latitude and altitude), but just over those regions sampled from the IAGOS datasets.

A beginning was made into analysing the ECHAM5 and ERA5 simulation abilities over the year. An effort was made to observe variations throughout the months of the year, as well as looking over the seasons to investigate whether trends occurred. Due to time limitations, this was not included in the report.

The temporal evolution analysis of ISSRs did not produce any strong trends over the course of the years. This is thought to be due to limitations in the number of years covered. It is recommended that an analysis is performed using a larger temporal span, possibly using atmospheric data from several sources to deal with the issues resulting from a lack of good-quality data that could be used for the analysis, as mentioned in the section.

References

[1] Timothy Andrews, Christopher J. Smith, Gunnar Myhre, Piers M. Forster, Robin Chadwick, and Duncan Ackerley. Effective radiative forcing in a gcm with fixed surface temperatures. *Journal of Geophysical Research: Atmospheres*, 126(4):e2020JD033880, 2021. e2020JD033880 2020JD033880.

[2] D. Avila, L. Sherry, and T. Thompson. Reducing global warming by airline contrail avoidance: A case study of annual benefits for the contiguous united states. *Transportation Research Interdisciplinary Perspectives*, 2, 2019.

[3] Niklas Boers. Observation-based early-warning signals for a collapse of the atlantic meridional overturning circulation. *Nature Climate Change*, 11:680–688, 08 2021.

[4] Ulrike Burkhardt and Bernd Kärcher. Global radiative forcing from contrail cirrus. *Nature Climate Change*, 1(1):54 – 58, 2011.

[5] Katie Camero. Aviation's dirty secret: Airplane contrails are a surprisingly potent cause of global warming. *Science.org*, 2019.

[6] Neil Chen, Banavar Sridhar, and Hok Ng. Contrail reduction strategies using different weather resources. *AIAA Guidance, Navigation, and Control Conference 2011*, 08 2011.

[7] Matt Christensen, David Neubauer, C. Poulsen, Gareth Thomas, Gregory McGarragh, Adam Povey, Simon Proud, and Roy Grainger. Unveiling aerosol–cloud interactions – part 1: Cloud contamination in satellite products enhances the aerosol indirect forcing estimate. *Atmospheric Chemistry and Physics*, 17:13151–13164, 11 2017.

[8] D.P. Duda, R. Palikonda, and P. Minnis. Relating observations of contrail persistence to numerical weather analysis output. *Atmospheric Chemistry and Physics*, 9(4):1357 – 1364, 2009.

[9] University Corporation for Atmospheric Research. wrf.interplevel. *readthedocs.io*, 2016. https://wrf-python.readthedocs.io/en/latest/user$_a$pi/*generated*/*wrf.interplevel.html*.

[10] European Centre for Medium-Range Weather Forecasts. Who we are. *ECMWF*, 2022. https://www.ecmwf.int/en/about/who-we-are.

[11] L. Frey, F. A.-M. Bender, and G. Svensson. Cloud albedo changes in response to anthropogenic sulfate and non-sulfate aerosol forcings in cmip5 models. *Atmospheric Chemistry and Physics*, 17(14):9145–9162, 2017.

[12] K. Gierens, L. Wilhelm, S. Hofer, and S. Rohs. The effect of ice supersaturation and thin cirrus on lapse rates in the upper troposphere. *Atmospheric Chemistry and Physics*, 22(11):7699–7712, 2022.

[13] Klaus Gierens, Ling Lim, and Kostas Eleftheratos. A review of various strategies for contrail avoidance. *The Open Atmospheric Science Journal*, 2:1–7, 02 2008.

[14] Klaus Gierens, Sigrun Matthes, and Susanne Rohs. How well can persistent contrails be predicted? *Aerospace*, 7(12):1 – 18, 2020.

[15] Klaus Gierens, Peter Spichtinger, and Ulrich Schumann. *Ice Supersaturation*, pages 135–150. Springer Berlin Heidelberg, Berlin, Heidelberg, 2012.

[16] Brandon Graver, Kevin Zhang, and Dan Rutherford. co_2 emissions from commercial aviation, 2018. *The International Council on Clean Transportation*, 9 2019.

[17] V. Grewe, T. Champougny, S. Matthes, C. Frömming, S. Brinkop, O.A. Søvde, E.A. Irvine, and L. Halscheidt. Reduction of the air traffic's contribution to climate change: A react4c case study. *Atmospheric Environment*, 94:616–625, 2014.

[18] O. Hoegh-Guldberg, D. Jacob, M. Taylor, M. Bindi, S. Brown, I. Camilloni, A. Diedhiou, R. Djalante, K.L. Ebi, F. Engelbrecht, J. Guiot, Y. Hijioka, S. Mehrotra, A. Payne, S.I. Seneviratne, A. Thomas, R. Warren, and G. Zhou. Impacts of 1.5^{o}c global warming on natural and human systems. *Global Warming of 1.5°C. An IPCC Special Report on the impacts of global warming of 1.5°C above pre-industrial levels and related global greenhouse gas emission pathways, in the context of strengthening the global response to the threat of climate change, sustainable development, and efforts to eradicate poverty*, pages 175–312, 2018.

[19] IAGOS. Iagos climate and air quality research by passenger aircraft. 2020.

[20] IAGOS. Data processing levels. *IAGOS*, 2023. https://iagos.aeris-data.fr/levels/.

[21] IAGOS. Data quality. *IAGOS*, 2023. https://iagos.aeris-data.fr/data-quality/.

[22] IAGOS. Fleet. *IAGOS*, 2023. https://www.iagos.org/iagos-fleet/.

[23] IAGOS. Iagos-caribic. *IAGOS*, 2023. https://www.iagos.org/iagos-caribic/.

[24] IAGOS. Iagos-core. *IAGOS*, 2023. https://www.iagos.org/iagos-core-instruments/.

[25] IAGOS. Iagos-humidity sensor (ich, part of package1). *IAGOS*, 2023. https://www.iagos.org/iagos-core-instruments/h2o/.

[26] IAGOS. Iagos-in-service aircraft for a global observing system. *IAGOS*, 2023. https://www.iagos.org/.

[27] IAGOS. Instrumentation. *IAGOS*, 2023. https://iagos.aeris-data.fr/instrumentation/.

[28] MESSy interface. Framework - what is messy? 2023.

[29] National Atmospheric Emissions Inventory. Overview of greenhouse gases. *UK NAEI*, 2022. https://naei.beis.gov.uk/overview/ghg-overview.

[30] IPCC. *Annex VII: Glossary [Matthews, J.B.R., V. Möller, R. van Diemen, J.S. Fuglestvedt, V. Masson-Delmotte, C. Méndez, S. Semenov, A. Reisinger (eds.)]*, page 2215–2256. Cambridge University Press, Cambridge, United Kingdom and New York, NY, USA, 2021.

[31] IPCC. *Summary for Policymakers*, page 332. Cambridge University Press, Cambridge, United Kingdom and New York, NY, USA, 2021.

[32] E. A. Irvine, B. J. Hoskins, and K. P. Shine. A lagrangian analysis of ice-supersaturated air over the north atlantic. *Journal of Geophysical Research: Atmospheres*, 119(1):90–100, 2014.

[33] P. Jeßberger, C. Voigt, U. Schumann, I. Sölch, H. Schlager, S. Kaufmann, A. Petzold, D. Schäuble, and J.-F. Gayet. Aircraft type influence on contrail properties. *Atmospheric Chemistry and Physics*, 13(23):11965 – 11984, 2013.

[34] Utpal Kumar. Reading netcdf4 data in python. *Earth Inversion*, 2020. https://www.earthinversion.com/utilities/reading-NetCDF4-data-in-python/.

[35] B. Kärcher. The importance of contrail ice formation for mitigating the climate impact of aviation. *Journal of Geophysical Research: Atmospheres*, 121(7):3497–3505, 2016.

[36] Bernd Kärcher. Formation and radiative forcing of contrail cirrus. *Nature Communications*, 9, 12 2018.

[37] Nicolas Lamquin, Claudia Stubenrauch, K. Gierens, U. Burkhardt, and Herman Smit. A 6-year global climatology of occurrence of upper tropospheric ice supersaturation inferred from the atmospheric infrared sounder and its synergy with mozaic. *Atmospheric Chemistry and Physics*, pages 381–405, 01 2012.

[38] D.S. Lee. The contribution of global aviation to anthropogenic climate forcing for 2000 to 2018. *Atmospheric Environment*, 244, 1 2021.

[39] D.S. Lee, G. Pitari, V. Grewe, K. Gierens, J.E. Penner, A. Petzold, M.J. Prather, U. Schumann, A. Bais, T. Berntsen, D. Iachetti, L.L. Lim, and R. Sausen. Transport impacts on atmosphere and climate: Aviation. *Atmospheric Environment*, 44(37):4678–4734, 2010. Transport Impacts on Atmosphere and Climate: The ATTICA Assessment Report.

[40] D.K. Lynch. Cirrus clouds: Their role in climate and global change. *Acta Astronautica*, 38(11):859–863, 1996.

[41] Michael E. Mann. Radiative forcing. *Encyclopedia Britannica*, 2022.

[42] Hermann Mannstein, Peter Spichtinger, and Klaus Gierens. A note on how to avoid contrail cirrus. *Transportation Research Part D: Transport and Environment*, 10(5):421 – 426, 2005.

[43] Vincent R. Meijer, Luke Kulik, Sebastian D. Eastham, Florian Allroggen, Raymond L. Speth, Sertac Karaman, and Steven R. H. Barrett. Contrail coverage over the united states before and during the covid-19 pandemic. *Environmental Research Letters*, 17(3), 2022.

[44] G. Myhre, D. Shindell, F.-M. Bréon, W. Collins, J. Fuglestvedt, J. Huang, D. Koch, J.-F. Lamarque, D. Lee, B. Mendoza, T. Nakajima, A. Robock, G. Stephens, T. Takemura, and H. Zhang. Anthropogenic and natural radiative forcing. *Climate Change 2013: The Physical Science Basis. Contribution of Working Group I to the Fifth Assessment Report of the Intergovernmental Panel on Climate Change*, 2013.

[45] DLR Institute of Atmospheric Physics. Emac. 2020.

[46] World Meteorological Organization. Aircraft-based humidity measurement. 2019.

[47] Andreas Petzold, Patrick Neis, Mihal Rütimann, Susanne Rohs, Florian Berkes, Herman Smit, Martina Krämer, Nicole Spelten, Peter Spichtinger, Philippe Nedelec, and Andreas Wahner. Ice-supersaturated air masses in the northern mid-latitudes from regular in-situ observations by passenger aircraft: vertical distribution, seasonality and tropospheric fingerprint. 10 2019.

[48] Johannes Quaas. Evaluating the "critical relative humidity" as a measure of subgrid-scale variability of humidity in general circulation model cloud cover parameterizations using satellite data. *Journal of Geophysical Research: Atmospheres*, 117(D9), 2012.

[49] P. Reutter, P. Neis, S. Rohs, and B. Sauvage. Ice supersaturated regions: properties and validation of era-interim reanalysis with iagos in situ water vapour measurements. *Atmospheric Chemistry and Physics*, 20(2):787–804, 2020.

[50] Hannah Ritchie. Atmospheric concentrations. *Our World in Data*, 2020. https://ourworldindata.org/atmospheric-concentrations.

[51] Hannah Ritchie. Climate change and flying: what share of global co2 emissions come from aviation? *Our World in Data*, 2020. https://ourworldindata.org/co2-emissions-from-aviation.

[52] Hannah Ritchie. Co and greenhouse gas emissions. *Our World in Data*, 2022. https://ourworldindata.org/co2-and-greenhouse-gas-emissions.

[53] Hannah Ritchie, Max Roser, and Pablo Rosado. Greenhouse gas emissions. *Our World in Data*, 2022. https://ourworldindata.org/greenhouse-gas-emissions.

[54] G. Rädel and K.P. Shine. Evaluation of the use of radiosonde humidity data to predict the occurrence of persistent contrails. *Quarterly Journal of the Royal Meteorological Society*, 133(627):1413 – 1423, 2007.

[55] Holly Shaftel. The causes of climate change. *NASA*, 2023. https://climate.nasa.gov/causes/.

[56] Holly Shaftel. The effects of climate change. *NASA*, 2023. https://climate.nasa.gov/effects/.

[57] Holly Shaftel. Global climate change - vital signs of the planet. *NASA*, 2023. https://climate.nasa.gov/.

[58] Holly Shaftel. How do we know climate change is real? *NASA*, 2023. https://climate.nasa.gov/evidence/.

[59] Banavar Sridhar, Neil Chen, and Hok Ng. Fuel efficient strategies for reducing contrail formations in united states airspace. *AIAA/IEEE Digital Avionics Systems Conference - Proceedings*, 10 2010.

[60] Banavar Sridhar, Hok K. Ng, and Neil Chen. Uncertainty quantification in the development of aviation operations to reduce aviation emissions and contrails. volume 6, page 4830 – 4839, 2012.

[61] Nicola Stuber, Piers Forster, Gaby Rädel, and Keith Shine. The importance of the diurnal and annual cycle of air traffic for contrail radiative forcing. 441(7095):864 – 867, 2006.

[62] Roger Teoh, Ulrich Schumann, and Marc E.J. Stettler. Beyond contrail avoidance: Efficacy of flight altitude changes to minimise contrail. *Aerospace*, 7(9), 2020.

[63] A.M. Tompkins, K. Gierens, and G. Rädel. Ice supersaturation in the ecmwf integrated forecast system. *Quarterly Journal of the Royal Meteorological Society*, 133(622):53 – 63, 2007.

[64] Feijia Yin, Volker Grewe, Christine Frömming, and Hiroshi Yamashita. Impact on flight trajectory characteristics when avoiding the formation of persistent contrails for transatlantic flights. *Transportation Research Part D: Transport and Environment*, 65:466–484, 2018.

[65] J. Zhang, K. Furtado, S. T. Turnock, J. P. Mulcahy, L. J. Wilcox, B. B. Booth, D. Sexton, T. Wu, F. Zhang, and Q. Liu. The role of anthropogenic aerosols in the anomalous cooling from 1960 to 1990 in the cmip6 earth system models. *Atmospheric Chemistry and Physics*, 21(24):18609–18627, 2021.

[66] Ying Zhang, Andreas Macke, and Frank Albers. Effect of crystal size spectrum and crystal shape on stratiform cirrus radiative forcing. *Atmospheric Research*, 52(1):59–75, 1999.

[67] Alcide Zhao, David Stevenson, and Massimo Bollasina. The role of anthropogenic aerosols in future precipitation extremes over the asian monsoon region. *Climate Dynamics*, 52:6257–6278, 05 2019.

[68] Liuhua Zhu, Yansong Bao, George P. Petropoulos, Peng Zhang, Feng Lu, Qifeng Lu, Ying Wu, and Dan Xu. Temperature and humidity profiles retrieval in a plain area from fengyun-3d/hiras sensor using a 1d-var assimilation scheme. *Remote Sensing*, 12(3), 2020.